Engineering Journal

American Institute of Steel Construction

Third Quarter 2014 Volume 51, No. 3

www.aisc.org

ENGINEERING JOURNAL

AMERICAN INSTITUTE OF STEEL CONSTRUCTION

Dedicated to the development and improvement of steel construction, through the interchange of ideas, experiences and data.

ENGINEERING JOURNAL (ISSN 0013-8029) is published quarterly. Subscriptions: Members: one subscription, $40 per year, included in dues; Additional Member Subscriptions: $40 per year. Non-Members U.S.: $160 per year. Foreign (Canada and Mexico): Members $80 per year. Non-Members $160 per year. Published by the American Institute of Steel Construction at One East Wacker Drive, Suite 700, Chicago, IL 60601.

Periodicals postage paid at Chicago, IL and additional mailing offices. **Postmaster:** Send address changes to ENGINEERING JOURNAL in care of the American Institute of Steel Construction, One East Wacker Drive, Suite 700, Chicago, IL 60601.

Message from the Editor

This issue of *Engineering Journal* is the second of two issues highlighting the SDCL (simple for dead load–continuous for live load) approach to steel bridge design. The SDCL concept allows bridges to be constructed as simple spans with a unique field connection between girders to provide continuous-span behavior under live loads. We hope you found the coverage in the second and third quarter issues informative. For more information on SDCL steel bridge solutions, visit the National Steel Bridge Alliance at www.steelbridges.org.

Those of you who read *Engineering Journal* online will have noticed a change in our digital edition format. Rather than using a proprietary digital edition reader, each new issue will be available for downloading and viewing as a single PDF. As always, we will also post the articles individually in our searchable archives. We hope you find this change useful, and we welcome your feedback.

Sincerely,

Keith A. Grubb, P.E., S.E.
Editor

HSS Truss Connections With Three Branches

JEFFREY A. PACKER

ABSTRACT

Hollow structural section (HSS) three-branch (or KT) connections frequently occur in modified Warren trusses, but the design of these planar welded connections is beyond the scope of Chapter K of the 2010 AISC *Specification for Structural Steel Buildings*. Such connections are also not covered by other contemporary HSS design guides and standards. This paper reviews the many potential member and loading arrangements, for both gapped and overlapped KT connections, and offers some design guidance. A worked example for an overlapped square HSS KT connection is then given, in both LRFD and ASD formats, in accordance with the 2010 AISC *Specification for Structural Steel Buildings*.

Keywords: hollow structural sections, trusses, connections, KT, welded joints, overlapping branches.

INTRODUCTION

Hollow structural section (HSS) Warren trusses with K connections, which have two diagonal branch members, are frequently modified by the introduction of a third vertical branch to form a so-called KT connection, as shown in Figure 1. The vertical branch may be added to support an applied load between panel points or to reduce the effective length of a chord member, but in general, this vertical member is often lightly loaded. The design of statically loaded, planar, HSS KT connections is beyond the scope of the AISC 360 *Specification* (AISC, 2010), and AISC *Design Guide 24* (Packer et al., 2010), nor are they covered in the latest HSS design guidance from CIDECT (Packer et al., 2009; Wardenier et al., 2008; Wardenier et al., 2010), the International Institute of Welding (2012) or the International Organization for Standardization (2013). AWS D1.1 (2010) does not specifically address this type of connection either, although the American Welding Society method for handling overlapped tubular connections (Clause 2.25.1.6)—on a branch-by-branch basis—might be applied to overlapped KT connections between round HSS. The reason for this lack of contemporary coverage is the realization that there are a very large number of possible configurations for members in KT connections, combined with a large number of possible loading arrangements for the members. Very little research exists on HSS KT connections, so a synthesis of "best practice" guidance is offered in this paper, which serves to extend the scope of AISC *Specification* Chapter K (2010).

Jeffrey A. Packer, Bahen/Tanenbaum Professor of Civil Engineering, University of Toronto, Toronto, Ontario, Canada. E-mail: jeffrey.packer@utoronto.ca

METHODS OF ANALYSIS

Some of the possible load combinations on the three branch members of a KT connection are shown in Figure 2. Parts (a) through (d) of this figure illustrate combinations where the three branch member forces are in vertical equilibrium (i.e., normal to the chord direction), with the two diagonals either having the opposite or the same force sense. Parts (e) through (h) of this figure have the same branch member force sense as in parts (a) through (d), but some load is additionally transferred through the chord member. Parts (i) and (j) of Figure 2 have all of the load on one side of the connection transferred through the chord member to the other side; thus, these connections can be analyzed as cross (or X) connections.

Fig. 1. HSS KT connection.

Gapped KT Connections

When all three branches have gaps between them, at the junction with the chord connecting face, a suggested method of connection analysis is as follows:

1. In Figures 2(a) and 2(b), the force in branch 3 can be apportioned into two parts, each of which balances the vertical components of the forces in branches 1 and 2. Thus, the total connection can be subdivided into two K connections (bearing in mind that N connections are a special case of the general K connection), consisting of branches 1 and 3 and branches 2 and 3. The two K connections can then be checked using the procedures in Section K2 of the AISC 360 *Specification* (AISC, 2010). The total utilization of branch 3 in each sub-K connection would also need to be checked in the manner outlined in the *Commentary* to Section K2 of the *Specification*. A calculation example of a K connection, where a branch participates in two separate subconnections (or free-body diagrams), is given in Example 8.5 of AISC *Design Guide 24* (Packer et al., 2010).

2. In Figures 2(e) and 2(f), the procedure is similar to that in case 1, but the total-force, free-body diagram now needs to be split into separate free-body diagrams consisting of a cross connection plus two K connections, with the vertical branch 3 being checked for its utilization in three subconnections, as shown in Figure 3(a).

3. In Figures 2(c) and Figure 2(d), two neighboring branches have the same force sense, and these two branches could be possibly considered to have a "combined action." This is the one case of a KT connection covered in EN 1993-1-8 (CEN, 2005), where all the branches are illustrated with gaps between each other at the chord-connecting face. In Eurocode 3, Table 7.15, the checking method (using AISC LRFD terminology) is to confirm that [with reference to Figure 2(c)],

$$P_1\sin\theta_1 + P_3\sin\theta_3 \le \phi P_{n1}\sin\theta_1 \quad (1a)$$

$$P_2\sin\theta_2 \le \phi P_{n1}\sin\theta_1 \quad (1b)$$

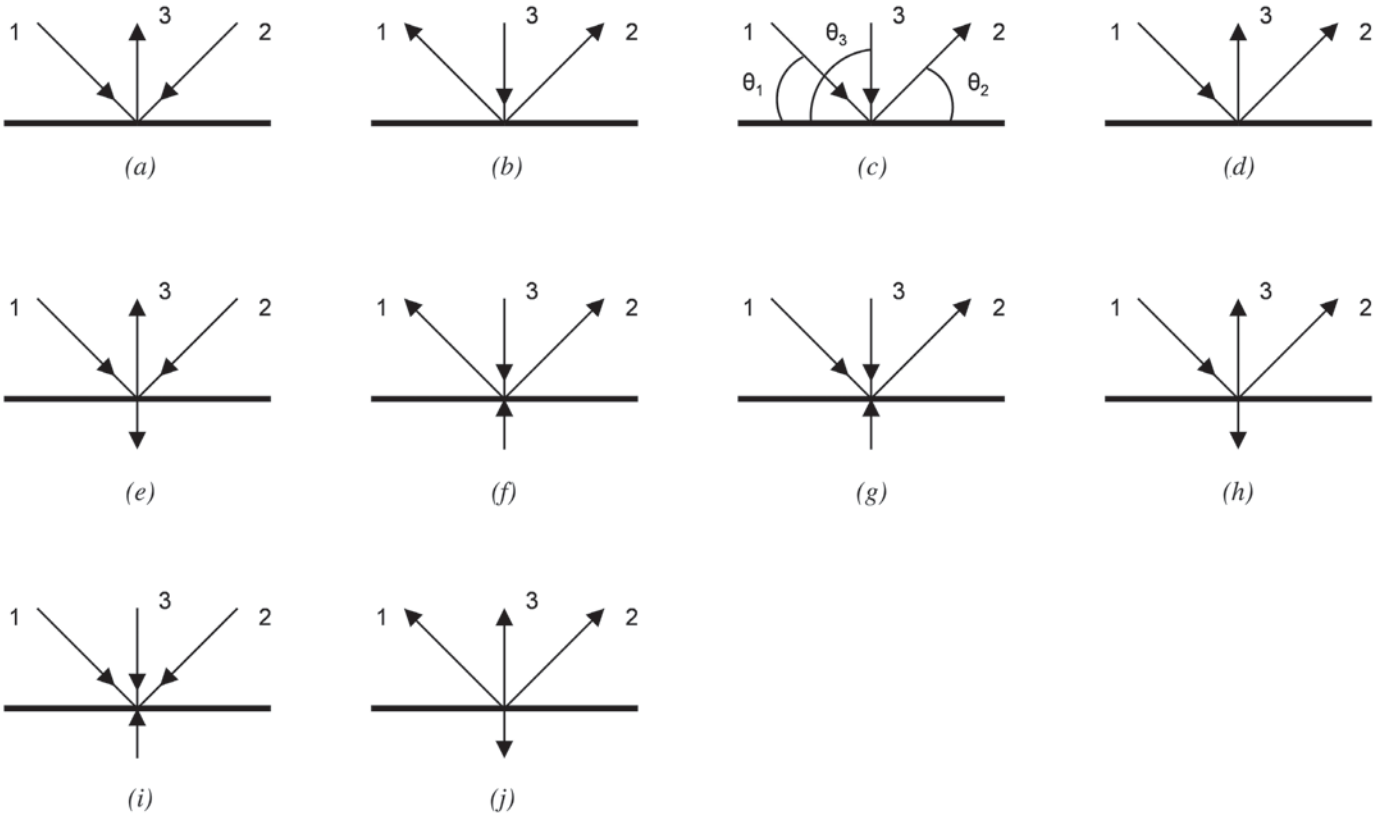

Fig. 2. Examples of load combinations on KT connections (after Tata Steel, 2011).

where P_1, P_2 and P_3 are the axial forces in branches 1, 2 and 3, respectively, and P_{n1} is the connection's available strength expressed as an axial force in branch 1, per *Specification* Equation K2-14. Also, it is stipulated that the value of β_{eff} in *Specification* Equation K2-24 be calculated by averaging over the three branches, as follows:

$$\beta_{eff} = [(B_b + H_b)_{branch\ 1} + (B_b + H_b)_{branch\ 2} + (B_b + H_b)_{branch\ 3}]/6B \quad (1c)$$

This method has the following drawbacks: (1) it is tailored to the limit state of chord-wall plastification, (2) it applies only to gapped KT connections with this unique pattern of branch loads, and (3) it presumes that the diagonal branches and their forces dominate. The EN 1993 (CEN, 2005) procedure has also been applied to round-to-round, gapped, HSS KT connections, pointing out that ($D_{b\ comp}/D$) in *Specification* Equation K2-4 should be replaced by ($D_{b1} + D_{b2} + D_{b3}$)/3D, where D_{b1}, D_{b2} and D_{b3} are the outside diameters of branches 1, 2 and 3, respectively. Very similar methods to this EN 1993 technique were cited earlier by Wardenier et al. (1991), Packer et al. (1992) and Packer and Henderson (1992, 1997), where the gap is recommended to be taken as "the largest gap between two [branches] having significant forces acting in the opposite sense" (Packer et al., 1992). Packer et al. (1992, 1997) also used a variant of Equation 1b, still with reference to Figure 2(c), as given in Equation 1d:

$$P_2 \sin\theta_2 \le \phi P_{n2} \sin\theta_2 \quad (1d)$$

where P_{n2} is the connection's available strength measured as a force in branch 2, per *Specification* Equation K2-14.

Despite all of the foregoing in case 3, it is much more logical, however, if the free-body diagram of KT connection forces is again broken into its constituent subconnections, as illustrated in Figure 3(b), and analyzed in this preferred manner.

4. In Figures 2(g) and 2(h), the procedure is similar to Figure 3(b), except an additional cross connection component will be introduced, thus making three separate subconnections (or free-body diagrams).

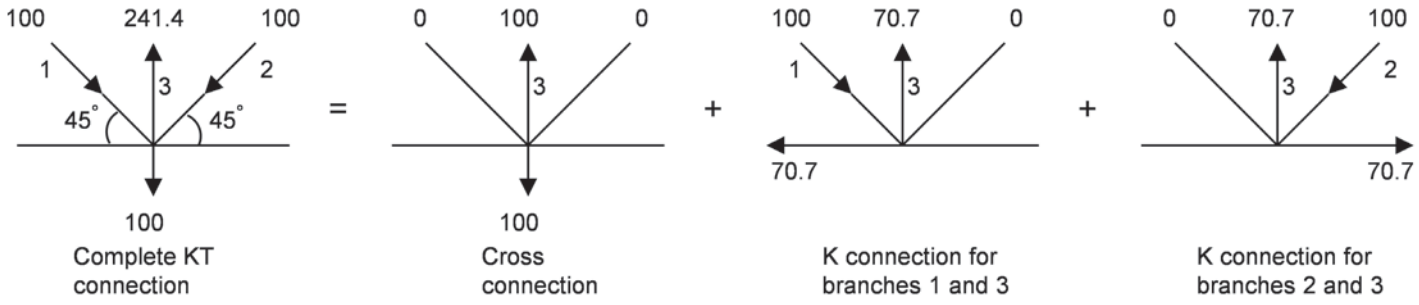

(a)

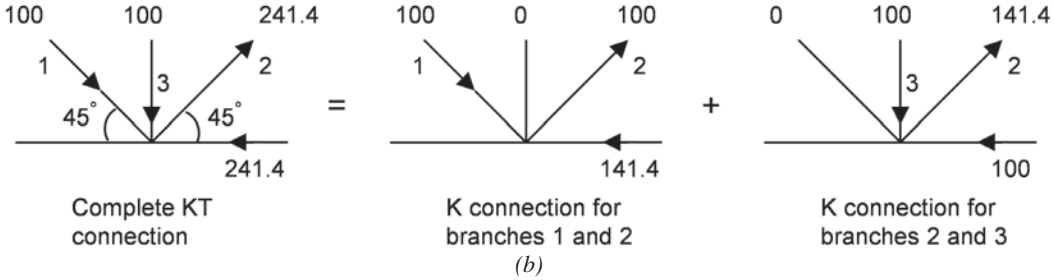

(b)

Fig. 3. Recommended analysis methods for gapped KT connections: (a) example of Fig. 2(e) broken into its constituent subconnections; (b) example of Fig. 2(c) broken into its constituent subconnections.

5. In Figures 2(i) and 2(j), the connection is a single cross connection—in both cases—because all branch-force components normal to the chord member are transferred through the chord. A calculation example of a very similar cross connection is given in Example 8.3 of AISC *Design Guide 24* (Packer et al., 2010).

If the vertical branch in a gapped KT connection has zero (or near-zero) force in it, then it can be ignored and the connection treated as a K connection, with the gap taken as the distance between the toes of branches 1 and 2 in Figure 2. This will be very conservative because the mere presence of additional steel (branch 3) welded to the gap region will stiffen the connection.

Overlapped KT Connections

Overlapped KT connections are much more probable than gapped KT connections because the latter produces a large positive noding eccentricity, which is likely to violate the limit of applicability for joint eccentricity in the AISC 360 *Specification* (AISC, 2010), Tables K2.1A or K2.2A. The common types of overlapped KT connections are shown in Figure 4. The sequence of overlapping should follow the basic premise that narrower branch members "sit on" (or frame into) wider members. If two overlapping branch members have the same width, then the thinner should sit on the thicker branch (i.e., the thicker branch should be the through member). As with overlapped K connections, overlapped KT connections should have (at least) one branch welded directly to the chord.

The resistance of round HSS overlapped KT connections can be handled in a similar way to cases 1 through 5, described for gapped KT connections, which involves splitting the free-body diagram of connection axial loads into subconnections involving K and cross connection types. Branch members participating in multiple subconnection types need to have their total utilization checked to ensure that it is less than unity by linear addition of their respective utilizations in each subconnection. As noted previously, refer to Example 8.5 of AISC *Design Guide 24* (Packer et al., 2010). The resistance of overlapped K connections between round HSS is based only on the limit state of chord plastification (Equations K2-4 and K2-5 of Table K2.1 of the *Specification*). The amount of overlap (O_v), or negative gap (g), to be used in Equation K2-6 pertains to the two branches under consideration in a particular subconnection. Again, if the vertical branch in an overlapped KT connection has zero (or near-zero) force in it, then it can be ignored and the connection treated as a K connection.

The resistance of rectangular and square HSS overlapped KT connections can be determined on a branch-by-branch basis, in a similar manner to overlapped K connections, using Equations K2-17 to K2-22 in Table K2.2 of the *Specification*. This is demonstrated in the following design example. This method of checking overlapped KT and K connections is different for square/rectangular HSS connections compared to round HSS connections (described previously) in the AISC *Specification*, but it is worth noting here that the most recent international design guidance for round HSS overlapped K connections (Wardenier et al., 2008; Wardenier et al., 2010; IIW, 2012; ISO, 2013) translates the round HSS branches into equivalent square HSS and then proceeds to use the square/rectangular HSS checking method.

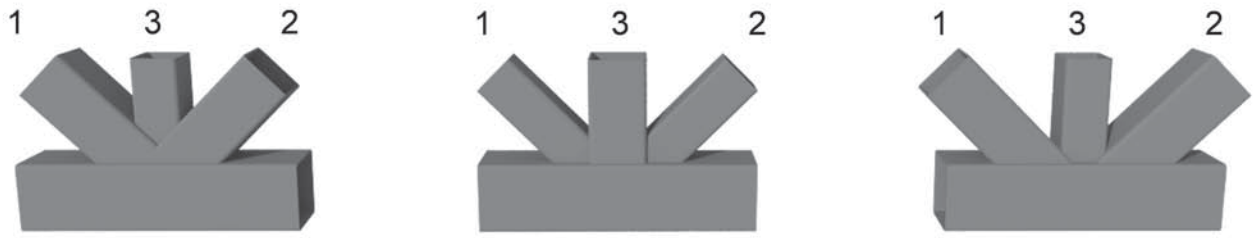

(a) *(b)* *(c)*

Fig. 4. Common types of overlapped KT connections.

DESIGN EXAMPLE FOR HSS OVERLAPPED KT CONNECTION

Figure 5 illustrates a KT connection using the new ASTM A1085 HSS (ASTM, 2013), with the branch member force arrangement being similar to Figure 3(b). The loads shown consist of live load (P_L) and dead load (P_D) in the ratio 3:1. Of the two diagonal HSS members, which are the largest branches and which are also of the same size, the branch with the largest force is welded directly to the chord member. The branches labeled 1 and 2 in Figure 5 have an overlap (O_v) of 50% at the chord connecting face. Thus, $l_{ov} = 0.50l_p = 0.50(5.774) = 2.89$ in. The aim is to determine the adequacy of this given connection.

Material Properties:

HSS chord member	ASTM A1085 Grade A steel	$F_y = 50$ ksi	$F_u = 65$ ksi
HSS branch members	ASTM A1085 Grade A steel	$F_{yb} = 50$ ksi	$F_{ub} = 65$ ksi

Geometric Properties:

HSS 10×10×⅜	$H = B = 10$ in.	$t = 0.375$ in.	$A = 14.1$ in.^{2}
HSS 5×5×5⁄16	$H_b = B_b = 5$ in.	$t_b = 0.313$ in.	$A_b = 5.61$ in.^{2}
HSS 4×4×¼	$H_b = B_b = 4$ in.	$t_b = 0.250$ in.	$A_b = 3.60$ in.^{2}

Note that the full nominal thickness is used as the design thickness for ASTM A1085 material.

Solution:

Check the limits of applicability of Specification Section K2, Table K2.2A.

The overlap length, l_{ov}, measured along the connecting face of the chord beneath branches 1 and 2, is 2.89 in., which implies a noding eccentricity, e, of –2.5 in. (negative because the branch centerlines intersect toward the branches, relative to the chord

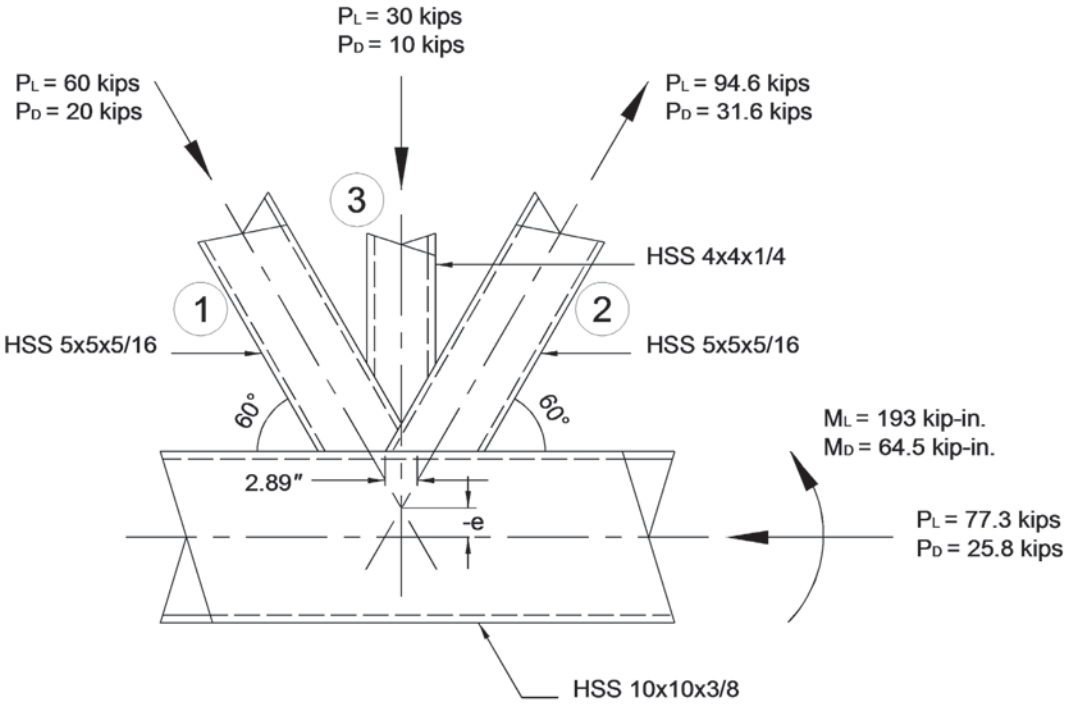

Fig. 5. Overlapped KT connection for design example.

centerline). A similar calculation example relating O_v, l_{ov} and e can be found in AISC *Design Guide 24* (Packer et al., 2010), page 111.

$-0.55 \le e/H = -0.25 \le 0.25$ **o.k.**

Branch angles, θ, are 60° and 90°, both of which are greater than 30° **o.k.**

B/t = (10.00 in./0.375 in.) = 26.7 ≤ 30 **o.k.**

H/t = (10.00 in./0.375 in.) = 26.7 ≤ 35 **o.k.**

For tension branch 2, $B_b/t_b = H_b/t_b$ = (5.00 in./0.313in.) = 16.0 ≤ 35 **o.k.**

For compression branch 1, $B_b/t_b = H_b/t_b$ = (5.00 in./0.313in.) = 16.0 ≤ 1.1 $(E/F_{yb})^{0.5}$ = 26.5 **o.k.**

For compression branch 3, $B_b/t_b = H_b/t_b$ = (4.00 in./0.250in.) = 16.0 ≤1.1 $(E/F_{yb})^{0.5}$ = 26.5 **o.k.**

For branches 1 and 2, $B_b/B = H_b/B$ = (5.00 in./10.00 in.) = 0.50 ≥ 0.25 **o.k.**

For branch 3, $B_b/B = H_b/B$ = (4.00 in./10.00 in.) = 0.40 ≥ 0.25 **o.k.**

$0.5 \le H_b/B_b$ = (5.00 in./5.00 in.) or (4.00 in./4.00 in.) = 1.00 ≤ 2.0 **o.k.**

$0.5 \le H/B$ = (10.00 in./10.00 in.) = 1.00 ≤ 2.0 **o.k.**

Between branches 1 and 2 only, 25% ≤ O_v = 50% ≤ 100% **o.k.**

Between branch 3 and the two diagonal branches, 25% ≤ O_v = 100% ≤ 100% **o.k.**

Between branches 1 and 2, B_{bi}/B_{bj} = (5.00 in./5.00 in.) = 1.00 ≥ 0.75 **o.k.**

Between branches 3 and 1, or branches 3 and 2, B_{bi}/B_{bj} = (4.00 in./5.00 in.) = 0.80 ≥ 0.75 **o.k.**

Between branches 1 and 2, t_{bi}/t_{bj} = (0.313 in./0.313 in.) = 1.00 ≤ 1.00 **o.k.**

Between branches 3 and 1, or branches 3 and 2, t_{bi}/t_{bj} = (0.250 in./0.313 in.) = 0.80 ≤ 1.00 **o.k.**

$F_y = F_{yb}$ = 50 ksi ≤ 52 ksi **o.k.**

$F_y/F_u = F_{yb}/F_{ub}$ = (50 ksi/65 ksi) = 0.77 ≤ 0.8 **o.k.**

Calculate the required strength.

From Chapter 2 of ASCE 7, the required connection strength, expressed as a force in each branch is:

LRFD	ASD
P_{r1} = 1.2(20 kips) + 1.6(60kips) = 120 kips	P_{r1} = 20 kips + 60 kips = 80 kips
P_{r2} = 1.2(31.6 kips) + 1.6(94.6kips) = 189 kips	P_{r2} = 31.6 kips + 94.6 kips = 126 kips
P_{r3} = 1.2(10 kips) + 1.6(30kips) = 60 kips	P_{r3} = 10 kips + 30 kips = 40 kips

Check the limit state of branch local yielding due to uneven load distribution (per Specification *Section K2, Table K2.2, with appropriate modifications where necessary to account for the actual overlapping of branch member walls).*

For branch 3 (which overlaps onto both branches 1 and 2), both transverse faces are represented by b_{eov} terms because both are welded to overlapped branches and not to the chord. Hence, Equation K2-19 of the *Specification* for overlapped K connections needs to be modified to:

$$P_{n,i} = F_{ybi}\, t_{bi}\, (2H_{bi} - 4t_{bi} + 2b_{eov}) \tag{2}$$

where

$$b_{eov} = [10/(B_{bj}/t_{bj})][F_{ybj}t_{bj}/(F_{ybi}t_{bi})]B_{bi} \le B_{bi} \qquad (\textit{Spec.}\ \text{Eq. K2-21})$$

and the subscript *i* refers to the overlapping branch 3 and the subscript *j* refers to the overlapped branch 1 or 2.

Thus,

b_{eov} = [10/(5.00 in./0.313 in.)][(50 ksi)(0.313. in.)/(50 ksi)(0.250 in.)](4.00 in.) ≤ 4.00 in.

= 3.14 in. ≤ 4.00 in.

and

P_{n3} = (50 ksi)(0.250 in.)[2(4.00 in.) − 4(0.250 in.) + 2(3.14 in.)]

= 166 kips < yield strength of branch = $(A_{b3}F_{yb3})$ = (3.60 in.^{2})(50 ksi) = 180 kips

LRFD	ASD
ϕ = 0.95	Ω = 1.58
ϕP_{n3} = 0.95(166 kips) = 158 kips	P_{n3}/Ω = 166 kips/1.58 = 105 kips
P_{r3} = 60 kips < ϕP_{n3} **o.k.**	P_{r3} = 40 kips < P_{n3}/Ω **o.k.**

For branch 1, checking can be performed as an overlapped K connection with branch 1 overlapping branch 2.

Thus, because O_v = 50%, and one transverse face of the overlapping branch is welded to the chord,

$P_{n,i} = F_{ybi}\, t_{bi}\, (2H_{bi} - 4t_{bi} + b_{eoi} + b_{eov})$ (*Spec.* Eq. K2-18)

where

$b_{eoi} = [10/(B/t)][F_y t/(F_{ybi} t_{bi})]B_{bi} \le B_{bi}$ (*Spec.* Eq. K2-20)

= [10/(10 in./0.375 in.)][(50 ksi)(0.375 in.)/(50 ksi)(0.313 in.)](5.00 in.) ≤ 5.00 in.

= 2.25 in. ≤ 5.00 in.

and

$b_{eov} = [10/(B_{bj}/t_{bj})][F_{ybj} t_{bj}/(F_{ybi} t_{bi})]B_{bi} \le B_{bi}$ (*Spec.* Eq. K2-21)

= [10/(5.00 in./0.313 in.)][(50 ksi)(0.313 in.)/(50 ksi)(0.313 in.)](5.00 in.) ≤ 5.00 in.

= 3.13 in. ≤ 5.00 in.

Hence,

P_{n1} = (50 ksi)(0.313 in.)[2(5.00 in.) − 4(0.313 in.) + 2.25 in. + 3.13 in.] = 221 kips

< yield strength of branch = $(A_{b1}\, F_{yb1})$ = (5.61 in.^{2})(50 ksi) = 281 kips

LRFD	ASD
ϕ = 0.95	Ω = 1.58
ϕP_{n1} = 0.95(221 kips) = 210 kips	P_{n1}/Ω = 221 kips/1.58 = 140 kips
P_{r1} = 120 kips < ϕP_{n1} **o.k.**	P_{r1} = 80 kips < P_{n1}/Ω **o.k.**

For branch 2, which is an overlapped member, the nominal available axial strength of this branch—as a proportion of its yield strength—is not to exceed the nominal available axial strength of the overlapping branch, as a proportion of its yield strength, which is the basis of the *Specification* Equation K2-22.

Thus, for two overlapping branches, $P_{n2}/(A_{b2}\,F_{y2}) \le P_{n1}/(A_{b1}\,F_{y1})$ and $P_{n3}/(A_{b3}\,F_{y3})$, i.e.,

$P_{n2}/(5.61 \text{ in.}^2)(50 \text{ ksi}) \le (221 \text{ kips})/(281 \text{ kips})$ and $(166 \text{ kips})/(180 \text{ kips})$

Hence,

$P_{n2} = 220$ kips

LRFD	ASD
$\phi = 0.95$	$\Omega = 1.58$
$\phi P_{n2} = 0.95(220 \text{ kips}) = 209 \text{ kips}$	$P_{n2}/\Omega = 220 \text{ kips}/1.58 = 139 \text{ kips}$
$P_{r2} = 189 \text{ kips} < \phi P_{n2}$ **o.k.**	$P_{r2} = 126 \text{ kips} < P_{n2}/\Omega$ **o.k.**

SYMBOLS

A	Gross cross-sectional area of chord member, in.
A_b	Gross cross-sectional area of branch member, in.
B	Overall width of rectangular HSS chord member, measured 90 degrees to the plane of the connection, in.
B_b	Overall width of rectangular HSS branch member, measured 90 degrees to the plane of the connection, in.
B_{bi}	Overall width of the rectangular HSS overlapping branch member, in.
B_{bj}	Overall width of the rectangular HSS overlapped branch member, in.
D	Outside diameter of round HSS chord member, in.
D_b	Outside diameter of round HSS branch member, in.
$D_{b\,comp}$	Outside diameter of round HSS compression branch member, in.
E	Modulus of elasticity of steel, 29,000 ksi
F_u	Tensile strength of the HSS chord member material, ksi
F_{ub}	Tensile strength of the HSS branch member material, ksi
F_y	Yield strength of the HSS chord member material, ksi
F_{yb}	Yield strength of the HSS branch member material, ksi
H	Overall height of rectangular HSS chord member, measured in the plane of the connection, in.
H_b	Overall height of rectangular HSS branch member, measured in the plane of the connection, in.
O_v	$l_{ov}/l_p \times 100$, %
P	Axial force in branch, kips
P_n	Nominal available axial strength of connection, expressed as a force in a branch, kips
P_r	Required axial strength of connection, expressed as a force in a branch, kips
b_{eoi}	Effective width of the rectangular HSS overlapping branch transverse face welded to the chord, in.
b_{eov}	Effective width of the rectangular HSS overlapping branch transverse face welded to an overlapped branch, in.
g	Gap between toes of branch members in a gapped K-connection, neglecting the welds, in. (negative $g = l_{ov}$ in an overlapped K-connection)
l_{ov}	Overlap length measured along the connecting face of the chord beneath two overlapping branches, in.
l_p	Projected length of the overlapping branch on the chord connecting face, in.
t	Design wall thickness of HSS chord member, in.
t_b	Design wall thickness of HSS branch member, in.
Ω	Safety factor
β_{eff}	Effective width ratio = $[(B_b + H_b)_{branch\ 1} + (B_b + H_b)_{branch\ 2}]/4B$, for two branches
θ	Acute angle between the branch and chord, degrees
ϕ	Resistance factor

REFERENCES

AISC (2010), *Specification for Structural Steel Buildings*, ANSI/AISC 360-10, American Institute of Steel Construction, Chicago, IL.

ASCE (2010), *Minimum Design Loads for Buildings and Other Structures*, SEI/ASCE 7-10, American Society of Civil Engineers, Reston, VA.

ASTM (2013), *Standard Specification for Cold-Formed Welded Carbon Steel Hollow Structural Sections (HSS)*, ASTM A1085-13, ASTM International, West Conshohocken, PA.

AWS (2010), *Structural Welding Code—Steel*, AWS D1.1/D1.1M–2010, American Welding Society, Miami, FL.

CEN (2005), *Eurocode 3: Design of Steel Structures—Part 1.8: Design of Joints*, EN 1993-1-8, European Committee for Standardization, Brussels, Belgium.

IIW (2012), *Static Design Procedure for Welded Hollow Section Joints—Recommendations*, 3rd ed., IIW Doc. XV-1402-12, International Institute of Welding, Paris, France.

ISO (2013), *Static Design Procedure for Welded Hollow Section Joints—Recommendations*, ISO 14346:2013(E), International Organization for Standardization, Geneva, Switzerland.

Packer, J.A. and Henderson, J.E. (1992), *Design Guide for Hollow Structural Section Connections*, Canadian Institute of Steel Construction, Toronto, Canada.

Packer, J.A. and Henderson, J.E. (1997), *Hollow Structural Section Connections and Trusses—A Design Guide*, 2nd ed., Canadian Institute of Steel Construction, Toronto, Canada.

Packer, J.A., Sherman, D.R. and Lecce, M. (2010), *Hollow Structural Section Connections*, AISC Steel Design Guide No. 24, American Institute of Steel Construction, Chicago, IL.

Packer, J.A., Wardenier, J., Kurobane, Y., Dutta, D. and Yeomans, N. (1992), *Design Guide for Rectangular Hollow Section (RHS) Joints under Predominantly Static Loading*, CIDECT Design Guide No. 3, CIDECT and Verlag TÜV Rheinland GmbH, Köln, Germany.

Packer, J.A., Wardenier, J., Zhao, X.L., van der Vegte, G.J. and Kurobane, Y. (2009), *Design Guide for Rectangular Hollow Section (RHS) Joints under Predominantly Static Loading*, CIDECT Design Guide No. 3, 2nd ed., CIDECT, Geneva, Switzerland.

Tata Steel (2011), "Design of Welded Joints—Celsius 355 and Hybox 355," Tata Steel Europe Ltd., Corby, United Kingdom.

Wardenier, J., Kurobane, Y., Packer, J.A., Dutta, D. and Yeomans, N. (1991), *Design Guide for Circular Hollow Section (CHS) Joints under Predominantly Static Loading*, CIDECT Design Guide No. 1, CIDECT and Verlag TÜV Rheinland GmbH, Köln, Germany.

Wardenier, J., Kurobane, Y., Packer, J.A., van der Vegte, G.J. and Zhao, X.L. (2008), *Design Guide for Circular Hollow Section (CHS) Joints under Predominantly Static Loading*, CIDECT Design Guide No. 1, 2nd ed., CIDECT, Geneva, Switzerland.

Wardenier, J., Packer, J.A., Zhao, X.L. and van der Vegte, G.J. (2010), *Hollow Sections in Structural Applications*, 2nd ed., CIDECT, Geneva, Switzerland.

Field Application Case Studies and Long-Term Monitoring of Bridges Utilizing the Simple for Dead—Continuous for Live Bridge System

AARON YAKEL and ATOROD AZIZINAMINI

ABSTRACT

The performance of three bridges constructed using the simple for dead load and continuous for live load (SDCL) bridge system for steel girders was monitored during and after construction to compare actual performance with predicted performance. The structure types were a box-girder bridge, an I-girder bridge and a box-girder bridge built using accelerated construction details. During construction, strains and deflections were monitored so that the degree of continuity over the pier could be determined. The design concept assumes that a simply supported condition exists during casting of the concrete deck. However, to provide lateral bracing, the concrete diaphragm—or turndown—over the pier is cast and cured prior to casting the deck. As expected, encasement of the girders provides some continuity over the pier during casting of the deck. The degree of continuity over the pier can be reduced by lowering the height of the construction joint and through the use of crack-inducing details. Long-term monitoring of the structures showed the behavior to be consistent over time with no significant deviations from the predicted bridge behavior. During the initial time period of approximately 18 months, a slight overall change in strain values was observed in concrete elements. The rate of change slowed during this period and eventually ceased. Subsequently, the response of the structure has been consistent with only small seasonal fluctuations observed. These fluctuations are expected and are generally attributable to changes in ambient temperature, relative humidity, incident solar radiation and ground freeze/thaw conditions.

Keywords: steel bridges, steel girders, SDCL, simple for dead load–continuous for live load.

INTRODUCTION

This paper presents the field application and long-term monitoring of the simple for dead load and continuous for live load (SDCL) bridge system for steel girders. The SDCL bridge system utilizes a joint detail at the interior supports that does not become continuous until after the dead loads have been applied. Prior to attaining this final continuity, the girders within the individual spans are simply supported.

This paper is one of five that describes the development and implementation of the SDCL system and provides the theoretical foundations of the system. An overview and general information regarding the behavior and design of the SDCL system can be found in Azizinamini (2014). After completion of laboratory testing (Lampe et al., 2014) and numerical modeling (Farimani et al., 2014), the concepts were utilized in three demonstration structures. The performance of these structures was monitored during and after construction to compare the actual performance with the predicted performance. The structure types were a box-girder bridge (N-2 over I-80), an I-girder bridge (Sprague Street over I-680) and a box-girder bridge built using accelerated construction details (262nd Street over I-80). The most important aspect of SDCL bridges is the detail used to connect the girders over the pier. Photos of the connection details used in each of the three case studies are shown in Figure 1.

The design concept of the SDCL system assumes that a simply supported condition exists during casting of the concrete deck. However, to provide lateral bracing, the concrete diaphragm, or turndown, over the pier is cast and cured prior to casting the deck. Encasement of the girders is expected to provide some continuity over the pier during casting of the deck. One goal of the research presented in this paper was to quantify the degree of continuity developed by the construction details. Two additional, and more general, goals were to ensure the actual behavior of the system in the final condition was consistent with the assumed behavior and also to ensure that the behavior did not change over time.

The following section describes general instrumentation details and data collection procedures that are common to all three projects. The remainder of the paper is broken into three sections, one for each case study.

Aaron Yakel, Ph.D., Research Associate, Civil and Environmental Engineering Department, Florida International University, Miami, FL. Email: ayakel@fiu.edu

Atorod Azizinamini, Ph.D., P.E., Professor and Chair, Civil and Environmental Engineering Department, Florida International University, Miami, FL (corresponding). Email: aazizina@fiu.edu

INSTRUMENTATION AND DATA COLLECTION

The instrumentation and long-term monitoring practices were similar for all three structures. Vibrating-wire type gages were used to monitor strains both on the surface of the steel and within the concrete. Vibrating-wire gages rely on the frequency of vibration of a wire within the gage. The tension in the wire, and therefore the frequency of vibration, varies with the strain of the component to which it is attached. This design results in a stable device, the zero and response characteristics of which do not vary over time. Additional instrumentation monitored displacements, rotations and weather. The long-term data were collected hourly using a data acquisition system. The collection interval was reduced during construction events such as casting of the concrete slabs. Additional details pertaining to the instrumentation and data collection can be found in the research reports for the individual structures (Ala et al., 2009; Yakel and Azizinamini, 2009; Yakel and Azizinamini, 2012).

SDCL SYSTEM USING BOX-GIRDER AND CONVENTIONAL CONSTRUCTION

Replacement of the N-2 over I-80 overpass near Grand Island, Nebraska, provided an opportunity to construct a bridge using the SDCL detail. The first bridge to use this detail, it was also the first bridge in the United States to use HPS-100W high-performance weathering steel. The bridge utilized a box-girder configuration. The bridge was instrumented and then monitored during and after its construction. During construction, the bridge behavior was monitored to verify the simple connection behavior and also to determine the amount of possible continuity before the concrete was cast. A live load test using loaded dump trucks was also carried out prior to opening the bridge to traffic. The results of the monitoring and live load testing were used to validate finite element modeling, which allowed further investigation into the behavior of the structure and the connection detail.

Structure Description and Design Details

The construction of the bridge was part of the 2002 FHWA Innovative Bridge Research and Construction (IBRC) initiative. The bridge is a two-span steel box bridge, with each span being 139 ft long. The bridge is a grade crossing over the I-80 highway, so minimizing the interruption to traffic was a major concern for the Nebraska Department of Roads. The bridge incorporated several unique and innovative design features that facilitated both fabrication and construction. Following is a summary of the design, fabrication and construction, including solutions to challenges that faced the designer, fabricator and contractor.

Steel boxes are typically assumed best suited for spans longer than 250 ft. However, preliminary designs indicated that use of high-performance steel (HPS) and steel boxes in conjunction with the new system would result in an economical bridge. A prior study indicated that the best way to use HPS in steel bridges using I-girders is a hybrid arrangement where 50- and 70-ksi steels are used in combination (Horton et al., 2000). Preliminary designs indicated that the same conclusions also apply to the case of steel boxes. Therefore, the design of the box girders was based on the assumption that the girders will use a hybrid arrangement, with bottom flanges of the box sections using 70-ksi HPS and webs and top flanges utilizing conventional 50-ksi steel. Additional parametric studies carried out during design indicated that this hybrid arrangement is the most ideal for the bridge under consideration.

During the design phase of the bridge, 100-ksi HPS was just becoming available in the market, and there was no experience with using 100-ksi HPS in bridge construction. After the design was completed, using 70-ksi HPS in hybrid form, a decision was made to substitute the 100-ksi HPS for all webs and flange materials. This conservative replacement allowed evaluating the fabrication processes using 100-ksi HPS materials without relying on the additional strength provided.

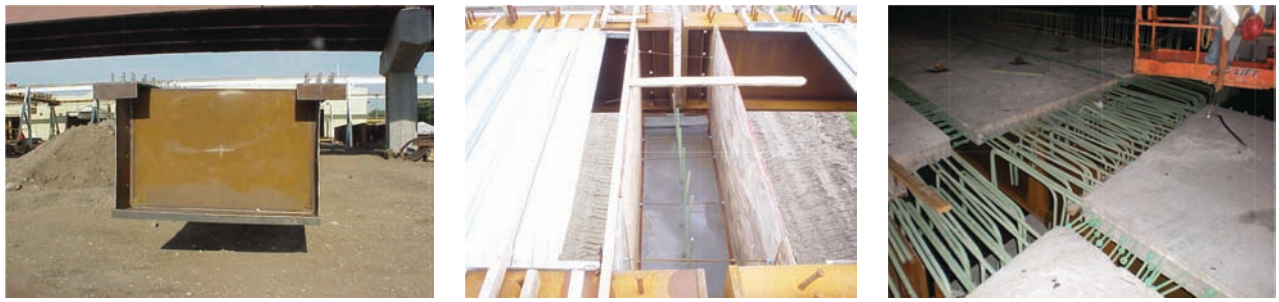

(a) *(b)* *(c)*

Fig. 1. Bridge pier details: (a) N-2 over I-80 (box); (b) Sprague Street (I-girder); (c) 262nd Street (accelerated).

Use of HPS resulted in keeping the maximum weight of each girder under 60,000 lb, the maximum crane capacity of the local fabricators, while increasing the girder lengths to 139 ft from traditional 120-ft values. Use of HPS plates permitted using thinner plates for the bottom flange and a reduction in web depth.

General Structure Information: Location, Spans, Cross-Section, Materials

The N-2 over I-80 overpass is a two-span structure, each span being 139 ft in length. It replaces a four-span, prestressed concrete girder bridge. There are three lines of girders, spaced 16 ft 1 in. on center. The girders are steel box girders fabricated from HPS-100W high-performance weathering steel. The system utilizes the SDCL connection detail at the pier. The cast-in-place concrete deck is 46 ft 4 in. wide and 7.5 in. thick, which includes a 0.5-in. integral wearing surface. Figure 2 shows a cross-section of the structure.

The top flanges are made from ⅞ in. × 1 ft 4 in. plate. The webs are made from ⅜ in. × 4 ft 2 in. plate. The bottom flange is made from ¾ in. × 6 ft plate. These plate thicknesses remain constant throughout the entire bridge length. Cross-frames were located inside of each girder at a spacing of 25 ft.

Longitudinal reinforcement consisted of #4 bars at 12 in. on center in the top layer and #5 bars at 12 in. on center in the bottom layer. Transverse reinforcement consisted of #5 bars at 12 in. on center in both the top and bottom layers. Additional reinforcement was placed in the deck over the pier to provide the tensile continuity. Two #7 bars were placed between each #4 bar in the top layer, and a #7 bar was placed between each #5 bar in the bottom layer.

SDCL Details: Bearing Plate, Double Composite, Reinforcement

The pier connection detail is shown in Figure 3; extraneous details have been omitted for clarity. Each girder was set on two 12-in.-long steel tubes that were filled with epoxy grout. To prevent interruption to the diaphragm face steel, #4 bars were placed through the holes in the girder webs and tied with #4 stirrups. The bulkheads served as formwork for when the diaphragm was poured.

Steel bearing blocks welded to the bottom flange of the

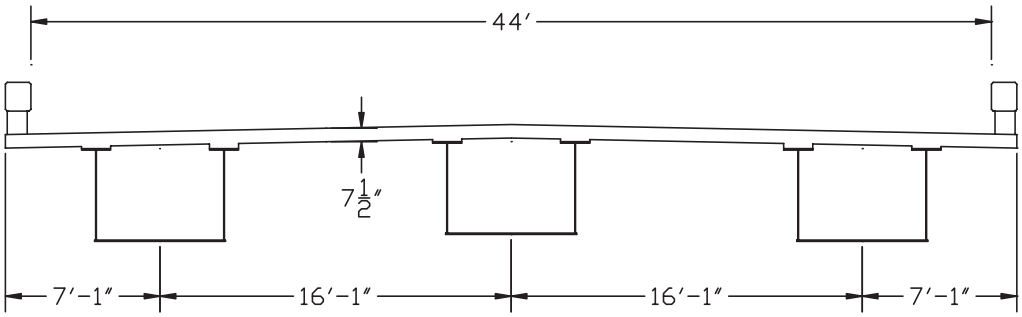

Fig. 2. Bridge cross-section.

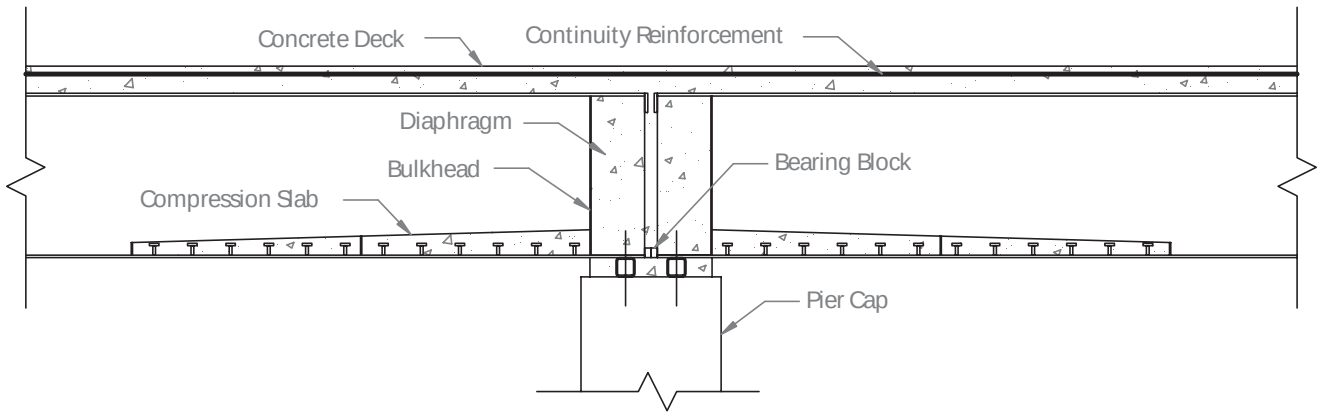

Fig. 3. Pier connection detail.

boxes transfer the compressive force from one girder to the adjacent girder directly, eliminating possibility of crushing of the concrete in the concrete diaphragm. This plate can be seen in Figure 4. Also seen in Figure 4 are small plates welded to the top flanges of the box girder. These welded plates are intended to prevent pull-out of the tension flanges from the concrete diaphragm.

Another unique feature of the bridge is the use of a new concept that allowed keeping the thickness of the bottom flange constant over the entire span length without the use of longitudinal stiffeners near the pier. Buckling capacity of the compression flange near the pier demanded either welding longitudinal stiffener to the bottom flange or increasing the thickness of the bottom flange plate in the vicinity of the pier. Besides the obvious cost issues, this option would have added to the total weight of the girder to be shipped to the job site, which was undesirable. The solution was to keep the thickness of the bottom flange constant over the entire girder length and increase the compressive capacity of the bottom flange by placing concrete inside the box, on top of the bottom flange, near the pier. This detail can be seen in Figure 3. This concrete was intended to prevent the buckling of the compression flange and allow it to reach the full yield strength of the plate. This concrete was added after the girders were placed on the support. Figure 5 shows the inside of the box, near the pier, after casting this concrete. The effect of this concrete in enhancing the strength of the cross-section near the pier was conservatively ignored.

Although the strength contribution was ignored, the stiffening effect of this additional concrete was considered in the analysis as the additional stiffness will result in increased stresses. This was accomplished by carrying out two different analyses—one with the additional concrete and one without—and using the maximum moment obtained from both analyses for design. This conservative approach was undertaken due to lack of precise knowledge about the level of the composite action that could develop between the bottom flange of the box near the pier and the concrete placed over it. This concrete was attached to bottom flange of the box using shear studs placed at the relatively large spacing of 24 in.

Bridge Construction and Monitoring

Construction of the N-2 over I-80 overpass began in May 2003. Girder fabrication began in June 2003. The construction sequence and the girder fabrication sequence are outlined in the following sections.

Girder Fabrication

As can be seen in Figure 6, the webs of the girder were perpendicular to the bottom flange. Traditionally, the webs of box girders are sloped. Making the webs perpendicular to the bottom flange significantly reduced the fabrication time and cost because this allowed the fabricator to use equipment and procedures commonly used for fabricating I-shapes.

A semi-integral abutment detail, with limited rotational stiffness, was used at each end of the two spans. Three sets of four piles were connected at the top with a steel channel, which the girders would bear on.

Girder Placement

Use of the SDCL steel bridge system significantly reduced the time required to place the girders over the supports compared to a typical arrangement that would have required a field splice within the span. In the SDCL system, each field section spans between the abutment and pier and, therefore, can be set in its final position and immediately released. Temporary shoring is not required. The bridge is a grade crossing over I-80, which was closed for only 90 minutes to place the three girders for each span. The SDCL system allowed accelerating the process of setting the girders and

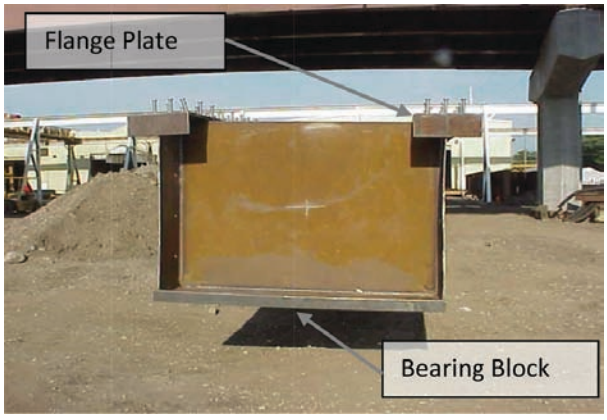

Fig. 4. Girder end to be embedded in concrete diaphragm.

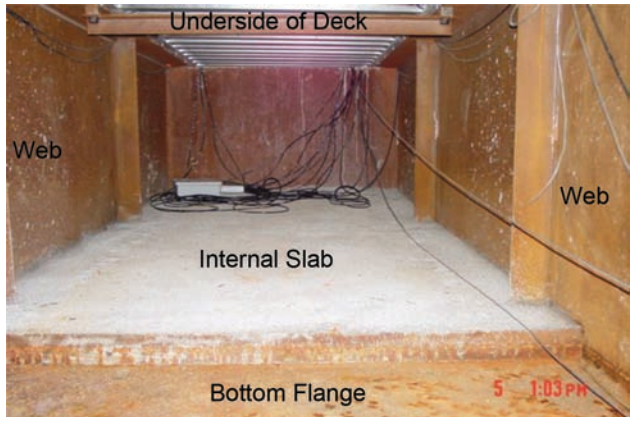

Fig. 5. Inside the box girder near the pier.

reduced the interruption to traffic. Figure 6 shows one of the 129-ft box girders being maneuvered for placement on the supports.

Installation of a box girder with the traditional construction method could exceed 4 days considering the time needed for erecting the temporary shoring and fastening of the field splices.

Global Stability Issues Related to the N-2 over I-80 Bridge

As shown in Figure 2, there were no cross-frames between the box girders. This provided an aesthetically pleasing bridge configuration while reducing the cost. However, this necessitated the detailed investigation of the global stability issue.

Designers need to be very cautious about global stability issues during construction. The AASHTO *LRFD Bridge Design Specification* (1998) does not provide any check or guideline for checking the global stability of I- or box girders during construction. The AASHTO specification only provides design provisions for checking the stability issues related to local flange, web or lateral torsional buckling of single girder. It does not, however, provide any checks for global stability. Global stability is where one box as a whole or the all girders in the cross-section move in a lateral direction, causing catastrophic collapses during construction. The global stability analysis was carried out using detailed nonlinear finite element analyses. The target factor of safety was 2.7 against collapse due to construction loads. Further, the analyses checked for adequate ductility to provide warning prior to collapse.

Evaluation of Continuity for Dead Load

In the SDCL system, the connection of the girders over the pier is assumed to not transfer moment from one span to the other during the construction phase (simple span behavior). However, due to the partially filled concrete diaphragm and reinforcement, particularly the dowels passing through the web, some amount of continuity was anticipated. Data obtained during casting of the deck from strain gages located near the pier and displacement gages placed within each span can be used to evaluate the degree of continuity over the pier. Note that the degree of continuity may vary during the course of casting the concrete in response to changes within the system, such as cracking in the concrete diaphragm.

Fig. 6. One of the girders during placement over the support.

Figure 7 shows the strain at the mid-span of both spans at the top flange, bottom flange, and web. In this chart, the first letter (S or N) indicates the span (south or north) and the second letter (B, W or T) indicates bottom flange, web and top flange, respectively. Key events are listed here, and their effect can be readily seen in the resulting strains.

1. Concrete casting began at 8:00 a.m. moving from north to south.
2. Casting entered the south span at 9:30 a.m.
3. Casting was completed at 11:45 a.m.

Moment

Figure 8 shows a comparison of the moment diagrams for a two-span bridge with a simple connection assumption, full continuity over pier assumption and experimental observation in the practice. The experimental value was obtained by examining the strain through the depth of the section at several locations and calculating the resulting moment. The resulting values at these locations allowed a curve, whose shape is consistent with the loading pattern, to be obtained. The details of this procedure can be found in the full project report (Ala et al., 2009).

As was expected, the behavior of the connection indicates partial continuity. If the transition from a simple connection to a fully continuous connection is assumed to be linear, then the percentage of continuity is given by Equation 1.

$$\text{Percent continuity} = \frac{\text{Observed} - \text{Simple}}{\text{Continuous} - \text{Simple}} \times 100 \qquad (1)$$

where

Observed = value of response variable from monitoring
Simple = value of response assuming simply supported conditions
Continuous = value of response assuming full fixity

For the response variable of positive moment at the midspan of the first span, Equation 1 indicates that 44% continuity was observed.

Table 1 shows the summary of the continuity percentage for positive and negative moments in both spans. It should be mentioned that for this bridge, no measures were taken to reduce the level of continuity over the pier during deck casting. A number of details could be used to reduce this level of continuity (Azizinamini, 2014).

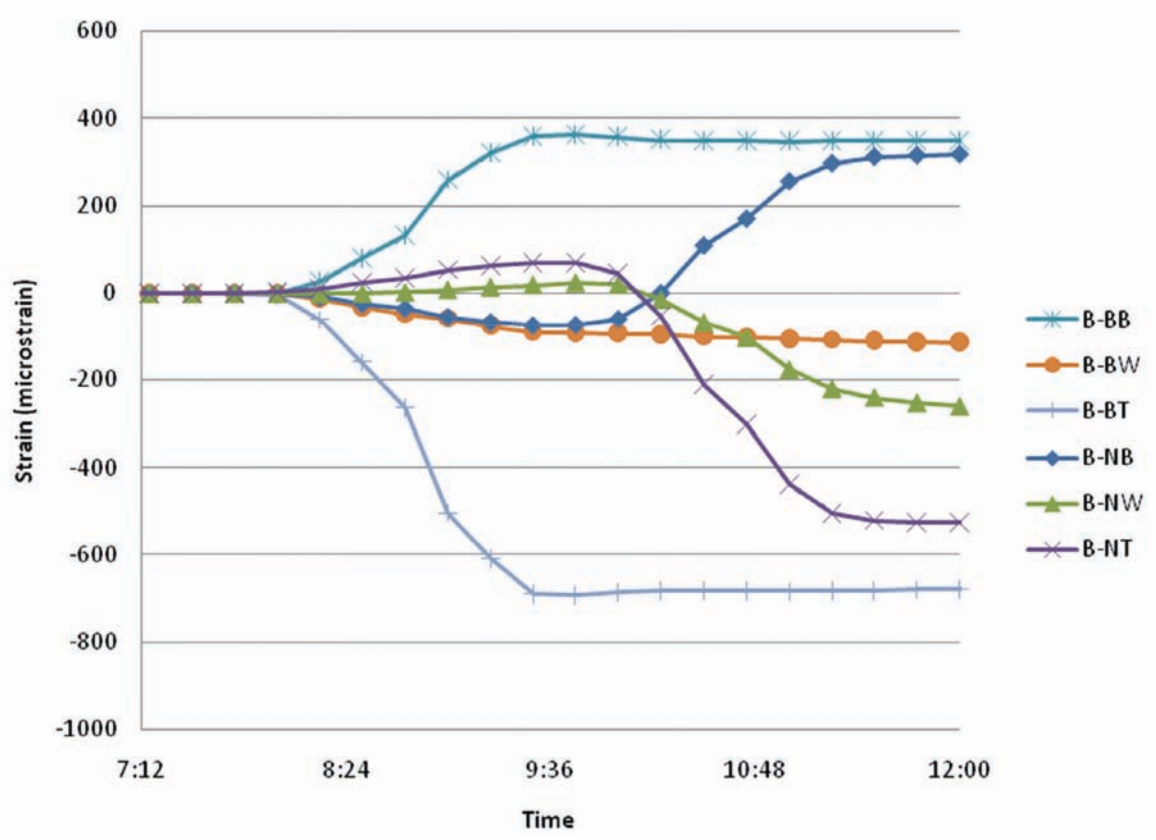

Fig. 7. Strain changes at the mid-span on both internal girders during pouring of the north and south spans.

Deflection

The amount of continuity over the pier also affects deflection. Determination of the deflection during construction is important because it will be used to specify the amount of camber during fabrication.

Figure 9 shows the observed deflection during concrete casting on the deck. Observe that the north began deflecting downward until the casting reached the pier, at which point the deflection remained relatively constant. The south span did not begin to deflect until the casting operation entered the south span. In fact, the south span initially deflected upward as casting was occurring in the north span, as would be expected of a continuous girder. This small upward deflection is a reflection of the fact that some level of continuity existed as a result of casting the concrete diaphragm first. Solutions to minimize this continuity are provided in Azizinamini (2014).

Table 2 reports the observed bridge deflections in addition to the predicted deflections obtained assuming both a simple connection and fully continuous connection.

Based on the comparisons carried out for deflections from the field measurements and the analytically calculated deflections for a simple connection and a fully continuous connection, there was 29.5% and 19% continuity for the constructed connection for deflection in the north and south spans, respectively. Note that the level of continuity based on deflection uses a single point of deflection observation while the moment-based approach uses a curve fit obtained from strain data throughout the length. These two methods are not expected to yield the same results because deflections can occur that do not cause strain in the girder. The deflection-based method is specifically used to help determine camber. The moment-based result is used for evaluating the structural behavior and validity of the assumptions. However, the strains are a result of continuity provided by the young concrete of the pier diaphragm, the effects of which will rapidly diminish. Further, once the deck has hardened, the presence of these strains will be of little consequence with regard to the strength and behavior of the system.

The degree of continuity over the pier can be reduced by lowering the height of the construction joint and through the use of crack-inducing details. One such option is shown in Figure 10, a solution used on a similar bridge system and constructed in Montana, which uses a strip of sheet metal to induce a crack to form between the ends of the two girders.

Live Load Testing

A live load test was performed to investigate several aspects of the bridge behavior. Three trucks filled with gravel were used to load the bridge. The behavior under the live load was recorded using both the long-term monitoring instrumentation and some additional sensors placed throughout

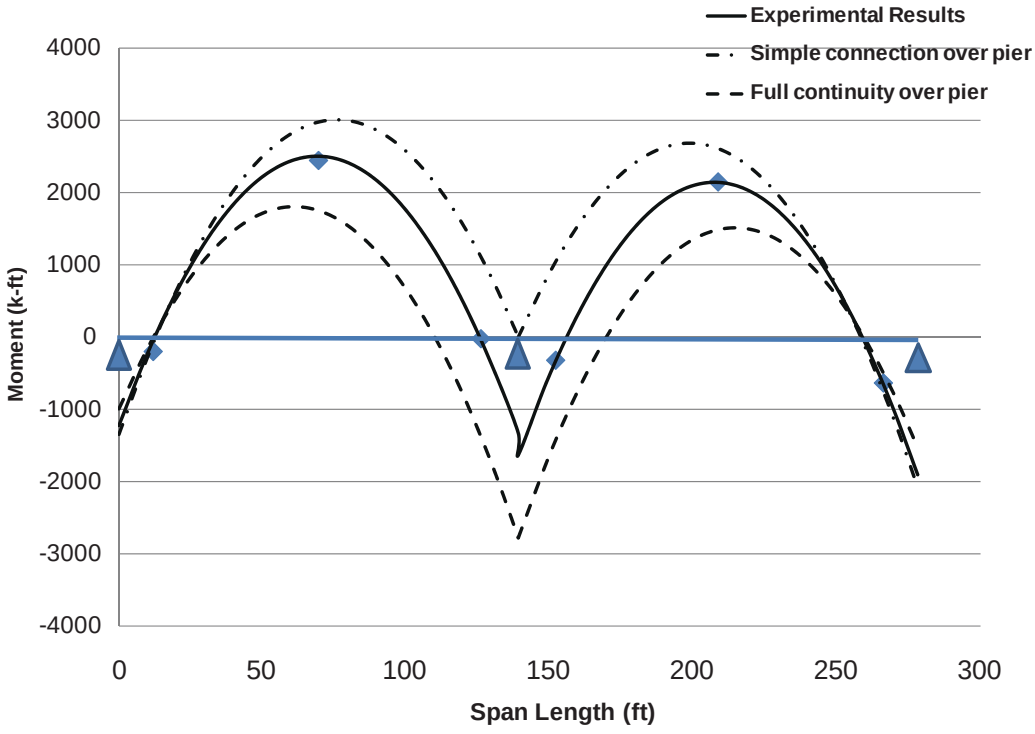

Fig. 8. Comparison among simple connection, fully continuous and experimental observations.

Table 1. Continuity Percentage for Positive and Negative Moment at Both Spans		
	North Span (%)	South Span (%)
Positive moment at midspan	44	42
Negative moment over pier	46	55

the structure. The location of the instrumentation and configuration of test vehicles were based on the objectives of the live load test, which are listed here. The observed distribution factors and load rating analysis are discussed in the following sections. More details of the live load test results are provided elsewhere (Ala et al., 2009). The objectives are as follows:

1. Compare distribution factors to AASHTO values.
2. Determine load rating according to AASHTO standards.
3. Verify the validity of assuming superposition in analysis.
4. Verify the accuracy of finite element modeling technique.
5. Investigate bottom flange slab behavior near pier.
6. Determine neutral axis locations.
7. Investigate continuity over the pier.

Experimental Determination of Distribution Factors

One of the objectives of the live load test was to determine the live load distribution factors for test data for comparison with code values. The strains used to calculate the distribution factors were taken from the bottom flange gages at the midspan section. The bottom flange tensile strains have the largest magnitude, making the resulting distribution factor less sensitive to error. Equation 2 gives the formula to calculate distribution factors from strain data (Stallings and Yoo, 1993):

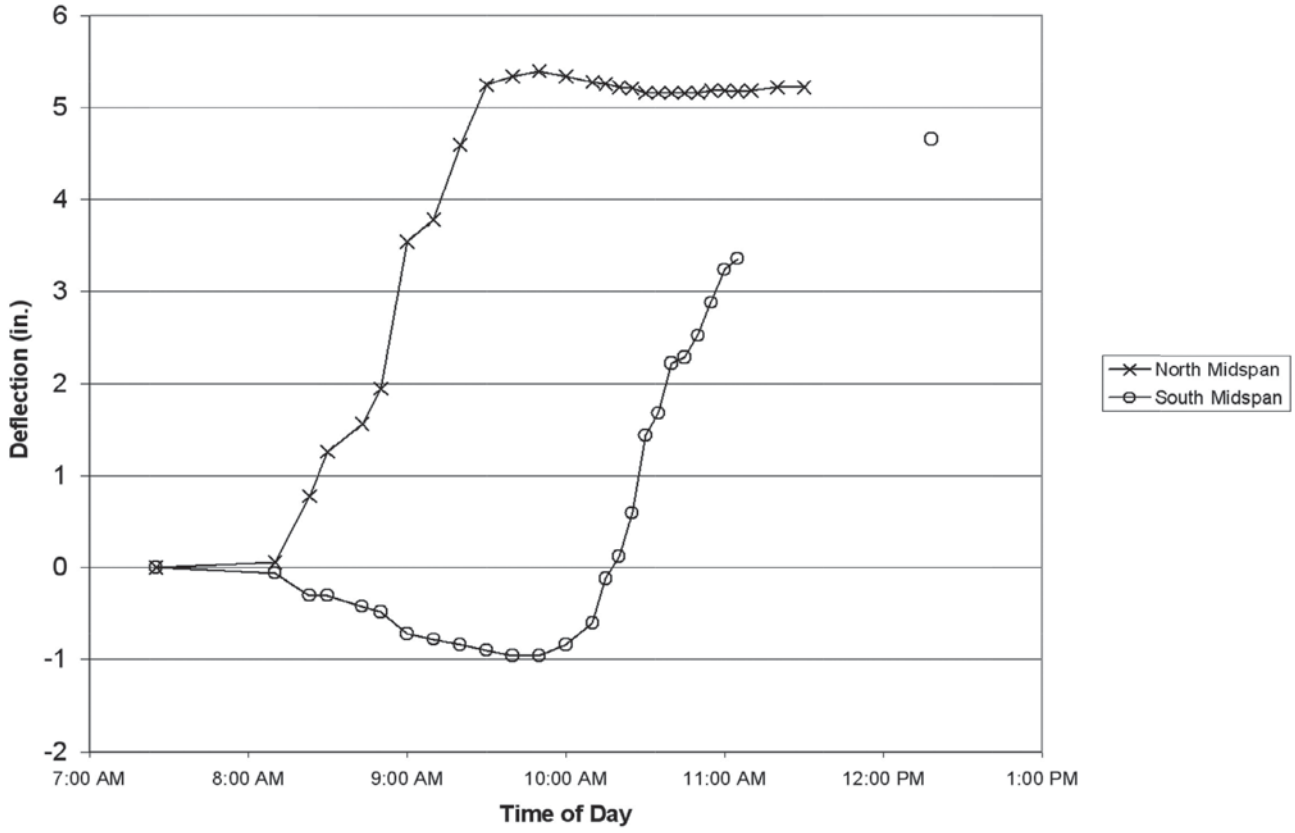

Fig. 9. Observed girder deflections during the deck pour.

Table 2. Deflection at Three Conditions for the Bridge		
	Deflection at Mid-North Span (in.)	Deflection at Mid-South Span (in.)
Simple connection over pier	6.15	5.20
Full continuity over pier	3.00	2.30
Field measurement	5.22	4.66

$$DF_i = \frac{mn\varepsilon_i}{\sum_{j=1}^{k} \varepsilon_j w_j} \quad (2)$$

where

DF_i = distribution factor for the ith girder
m = multiple presence factor
n = number of lanes loaded
k = number of girders
ε_j = bottom flange strain of jth girder
w_j = ratio of moment of inertia of jth girder to an interior girder

The weighting factor, w_j, was taken equal to 1, which means all girders are assumed to have equal stiffness. The multiple presence factor is included so the calculated values can be compared with the AASHTO values, which are given by Equation 3 (AASHTO Table 4.6.2.2.2b-1) for a concrete deck on multiple steel-box-section beams (AASHTO, 1998).

$$DF = 0.05 + 0.85\frac{N_L}{N_b} + \frac{0.425}{N_L}$$

$$\text{for } 0.5 \le \frac{N_L}{N_b} \le 1.5 \quad (3)$$

where

DF_i = distribution factor
N_L = number of lanes loaded
N_b = number of box girders

This equation was developed for simple spans but is also considered applicable to continuous-span bridges by the LRFD specifications. The distribution factor is used for both interior and exterior girders as well as for moment and shear.

Table 3 shows the calculated AASHTO distribution factors compared with the measured values for 1, 2 and 3 lanes loaded. The controlling experimental distribution factor was taken as the maximum observed value along the span for the moving load.

The difference between measured values and AASHTO values is within 15% for the three cases of number of lanes loaded. The AASHTO value compared with the measured value is slightly conservative for one lane loaded and slightly unconservative for two lanes loaded. The AASHTO distribution factor for three lanes loaded is conservative compared with the measured value. The observed result for the case of three lanes loaded is considered attributable to the conservative nature of the AASHTO equation and the particular geometry of the structure—and not a consequence of using the SDCL system.

Load Rating

Before opening a bridge to traffic, many state Departments of Transportations carry out rating calculations as part of the permanent documentation for the bridge. Consequently, rating calculations were carried out for the structure.

The bridge was load rated according to the procedure specified in the *Guide Manual for Condition Evaluation and Load and Resistance Factor Rating of Highway Bridges* (MCE) published by AASHTO (2003). This procedure is consistent with the LRFD bridge design philosophy. The purpose of this rating is to recognize any need for the posting of loads or the strengthening of the bridge. It is also a basis for determining the safe loading capacity. The basic load-rating equation is as follows:

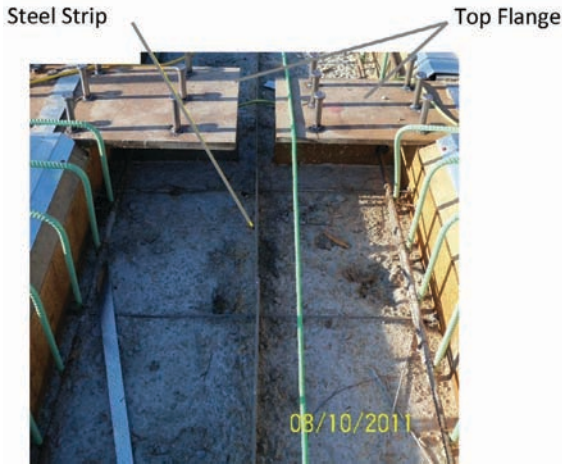

Fig. 10. Detail to induce cracking between girder ends, resulting in reduced continuity.

Table 3. Distribution Factors				
Lanes Loaded	Multiple Presence Factor	Distribution Factor		Measured/AASHTO
		AASHTO	Measured	
1	1.20	0.76	0.73	0.96
2	1.00	0.83	0.89	1.07
3	0.85	1.04	0.89	0.85
	Maximum	1.04	0.89	0.85

$$RF = \frac{C - (\gamma_{DC})(DC) - (\gamma_{DW})(DW) \pm (\gamma_P)(P)}{(\gamma_L)(LL + IM)} \quad (4)$$

where

RF = rating factor
C = capacity
DC = dead load effect due to structural components and attachments
DW = dead load effect due to wearing surface and utilities
P = permanent loads other than dead loads
LL = live load effect
IM = dynamic load allowance
γ_{DC} = LRFD load factor for structural components and attachments
γ_{DW} = LRFD load factor for wearing surface and utilities
γ_P = LRFD load factor for permanent loads other than dead loads
γ_L = evaluation live load factor

Consideration of the bending moment and shear capacity of an interior and exterior girder resulted in a calculated inventory design rating factor (RF_C) of 1.02, governed by the shear capacity. Because this factor is >1, the bridge has sufficient capacity for the HL-93 loading. This also implies that the bridge has adequate capacity for all AASHTO legal loads, so no load posting is required.

A refined rating calculation was also carried out using live load test results. The procedure for rating bridges using live load testing is provided in Chapter 8 of the MCE (AASHTO, 2003). Following is the equation to be used to obtain load rating using live load data:

$$RF_T = RF_C \times K \quad (5)$$

where

RF_T = load-rating factor for the live load capacity based on the load test result
RF_C = load-rating factor based on calculations prior to incorporating testing results
K = adjustment factor resulting from the comparison of measured test behavior with the analytical model

The K factor is calculated directly from load testing results using the following equation:

$$K = 1 + K_a K_b \quad (6)$$

where

K_a = accounts for both the benefit derived from the load test, if any, and consideration of the section factor resisting the applied test load
K_b = accounts for the understanding of the load test results when compared with those predicted by theory

Through diagnostic load testing, the K_a and K_b values were found to be 0.55 and 0.8 respectively. The K value from Equation 6 is, therefore, 1.44, resulting in an adjusted design load-rating factor (RF_T) of 1.47.

A rating factor was also calculated for each of the AASHTO legal loads, Type 3, Type 3S2 and Type 3-3. The results of this analysis are listed in Table 4.

Long-Term Monitoring

Performance of the bridge was evaluated by continuously monitoring the response of the bridge, with data taken once every hour. Monitoring began with casting of the deck on the morning of October 29, 2003, at 8:30 a.m. and continued for the next 6 years. This was used as a starting time for the long-term monitoring portion of the project. The readings of the gages at that time used as zero values.

Variations in the data were observed to occur on several different timescales. Many of the variations were cyclic in nature and were largely attributed to temperature or other meteorological phenomena, such as humidity. These were observed to occur on daily (solar heating), multi-day (weather fronts) and annual (seasonal) bases. Note that the hourly monitoring was not intended to pick up short-term transient responses due to traffic loading.

Given that the objective of the monitoring was to evaluate the long-term performance of the structure, a filtering technique was employed to filter out the noise of short-term effects. The goal of filtering was to isolate a quiescent period of time during the day and obtain the temperature and bridge responses for this period. The values are from

Table 4. Legal Truck Load Rating					
Loading	Weight (kips)	RF_C	K	RF_T	Capacity (tons)
Type 3	50	2.92	1.44	4.21	105
Type 3S2	72	2.16	1.44	3.11	112
Type 3-3	80	2.00	1.44	2.88	115

a period each day when the thermal gradient through the depth is at a minimum. Days during which the temperature is changing rapidly have been discarded, and central averaging over the day has been utilized to further smooth the response variables. The result of temperature filtering reduced the full data set into a single temperature and the corresponding response data for each day.

Observations

In order to assess the long-term bridge behavior from the strain gages, the general trend of the strain data is of interest. Specifically, in the case that the measured strains, or their periodic fluctuations, do not significantly change over the data-logging period, it can be concluded that the bridge responses to loading remain stationary.

Consider the data shown in Figure 11, which comes from a gage located within the diaphragm at the pier. Cyclic, seasonal fluctuations are quite evident, with peaks occurring near the start of each year. On top of this pattern can be seen a trend of decreasing values that is strongest at the beginning and diminishes over time. The trend is nearly indistinguishable after 2 years, and only the seasonal fluctuations remain. This initial downward trend can be attributed to concrete creep and shrinkage. The observed seasonal pattern can be attributed to thermal effects resulting from either partial restraint at the girder ends or differential expansion and contraction of the materials. All gages from similar locations showed similar behavior.

The long-term monitoring shows that the structure behavior becomes consistent over time, with no significant deviation from the predicted bridge behavior.

SPRAGUE STREET OVER I-680 I-GIRDER

The Sprague Street Bridge over I-680 is the second bridge to be constructed using the simple for dead load–continuous for live load pier connection detail developed at the University of Nebraska–Lincoln. Similar to the previous structure, the bridge was instrumented and then monitored during and after its construction.

Structure Description and Design Details

This bridge is located in Omaha, Nebraska, and replaces a four-span steel-girder bridge. The new bridge consists of two 97-ft spans. There are four lines of girders, spaced 10 ft 4 in. apart. The girders are HPS-50W high-performance weathering steel, W40×249 rolled sections. The overall width of the bridge is 41 ft 8 in., which includes a 7-ft pedestrian walkway on one side and a 3 ft 8 in. overhang on the other. A continuous composite bridge rail exists on both sides of the bridge. Figure 12 shows a cross-section of the bridge. Cross-frames, in the form of bent-plate separators (not shown), are located at each midspan and at the quarter points of each span.

SDCL Details: Bearing Plate, Reinforcement

The pier connection detail is shown in Figure 13. Each girder was set on a steel bearing plate. Transverse reinforcement, #4 bars, was placed through the holes in the webs at the end of girder. Each girder had a 1.5-in.-thick end plate over the full depth and an additional 2-in.-thick bearing block at the bottom of the end plate. The bearing blocks transfer the compression between the bottom flanges.

The cast-in-place concrete deck is a 7.5-in.-thick deck with an integral 0.5-in. wearing surface. The width of the deck is 41 ft 8 in. Longitudinal reinforcement consists of #4 bars at 12 in. on center in the top layer and #5 bars at 12 in. on center in the bottom layer. Transverse reinforcement consists of #4 bars at 12 in. on center in the top layer and #5 bars at 12 in. on center in the bottom layer. Additional longitudinal steel, #6 bars at 12-in. centers, was placed in the top layer over the pier to transfer the tensile component of the bending moment.

Construction Sequence

Construction of the bridge began in February 2004. The pier was constructed first, followed by the west abutment. Once finished, the west girders were placed on the night of May 5, 2004. They were set at night in order to minimize disruption to traffic, as Interstate 680, below the bridge, had to be closed during that time. After setting the west girders, the east abutment was constructed. The east girders were then erected on the night of June 3, 2004. Again, it was done at night to minimize traffic disruption.

The girders of the first span of the bridge were set independently (see Figure 14). This sequence would not have been possible with the typical method of practice, which would require a field splice within the span, away from the

support. Figure 15 shows the abutment end of the girders, which are set on channels spanning between piles.

After the east girders were set, the rest of the deck, diaphragm and abutment formwork were installed. The deck pour took place on July 10, 2004. The large overhang on the south side of the bridge was cast separately 6 days later to avoid placing excessive torsion on the exterior girder. The construction joint was located beneath the barrier. After the deck had cured, the barriers were slip-formed, and the pedestrian fence was installed. The bridge was opened to traffic the last week of July in 2004.

Construction Monitoring

The data acquisition system was installed and operational shortly after the girders were erected so that events such as deck pour, overhang pour and rail pours could be observed.

Casting of the deck presented an excellent opportunity to collect data to investigate the behavior of the structure during construction. Similar to what was shown in for the N-2 over I-80, the observed values obtained during the deck pour were compared with calculated values, assuming the structure behaved both as two simple spans and continuously. For the purposes of this investigation, the strains were assumed to be zero at the beginning of the deck pour so that the strains at the end of the pour were the result of the weight of the wet concrete being applied to the girders.

Strain

Figure 16 shows the strains in the top and bottom flanges along the length of the exterior girder at the end of the deck pour. Also shown are the strains predicted by assuming the system to behave as simple and continuous. In a simple-span condition, the entire top flange should show compressive strains, except at the supports, where the strains should be zero because there would be zero moment. However, Figure 16 shows tensile strains in the top flange near the abutments and near the pier. Additionally, the compressive strain in the top flange at both midspans is less than the expected value. This indicates that there is some degree of fixity at the abutments and at the pier. Similar observations can be made regarding the strains in the bottom flange.

While there is clearly some degree of continuity present, there is not enough to consider the system fully continuous. The actual degree of continuity was determined by fitting a curve with a shape prescribed by loading pattern through the observed data points. The curve is shown in Figure 16

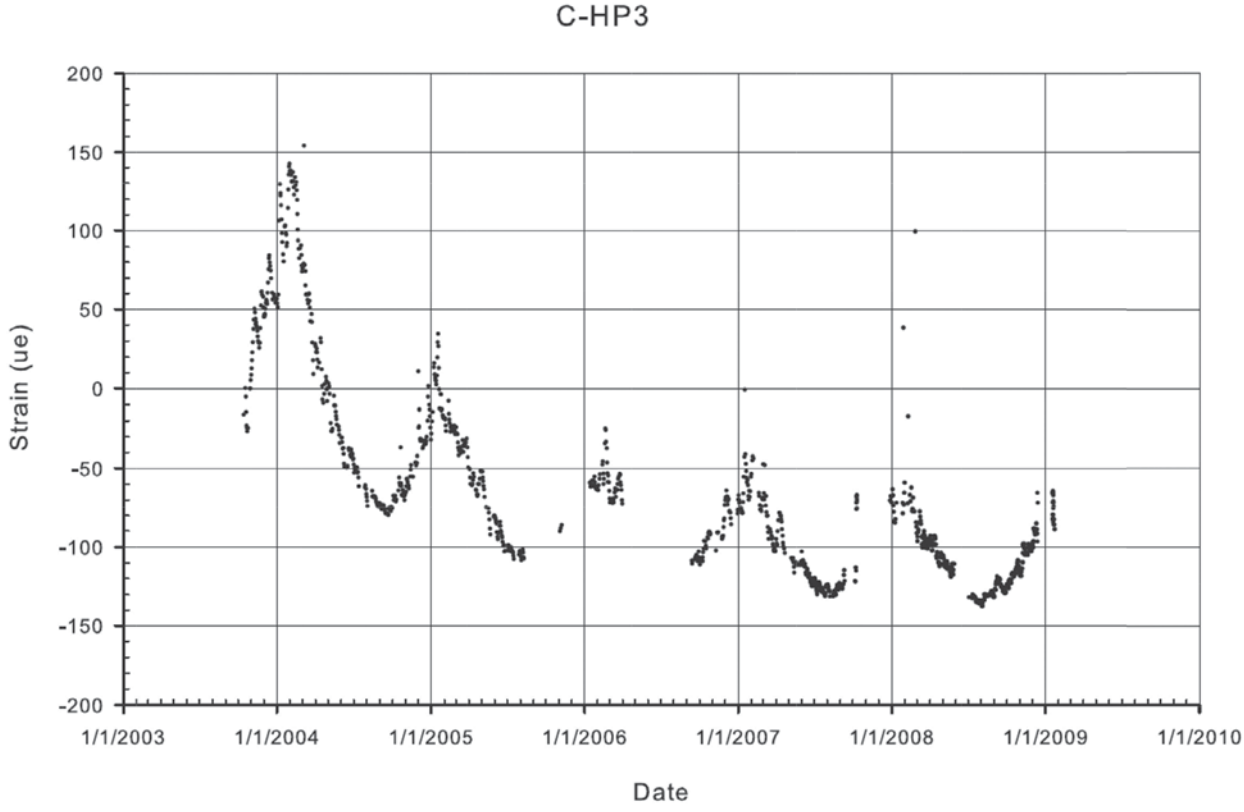

Fig. 11. Strain from concrete embedment gages located in concrete diaphragm between the girders over the pier near an exterior girder.

Table 5. Continuity Percentage for Positive and Negative Moment at Both Spans		
	South Span (%)	North Span (%)
Top flange stress—midspan	61	52
Bottom flange stress—midspan	58	49
Top flange stress—pier	8	17
Bottom flange stress—pier	46	42

as well. Table 5 summarizes the degree of fixity that was observed as calculated using Equation 1.

Deflection

During the deck pour, elevations of the screed rail at the midspans of all exterior girders were taken as concrete was placed along the length of the bridge in order to determine girder deflections and transverse structure rotation. The deflections were compared to calculated values to determine the difference. The expected deflection at midspan for the north exterior girders, points C and D, was 3.11 in., and for the south exterior girders, points A and B, was 2.04 in., assuming simply supported spans. The observed deflections at the south exterior girder at the conclusion of the deck pour were 1.32 in. at point A (west span) and 1.56 in. at point B (east span). These values are less than the expected values (2.04 in.), which is likely due to the restraining moments discussed earlier.

In the transverse direction, some rotation occurred due to the unbalanced loading from casting an overhang on the north side of the bridge, but not on the south side. There was

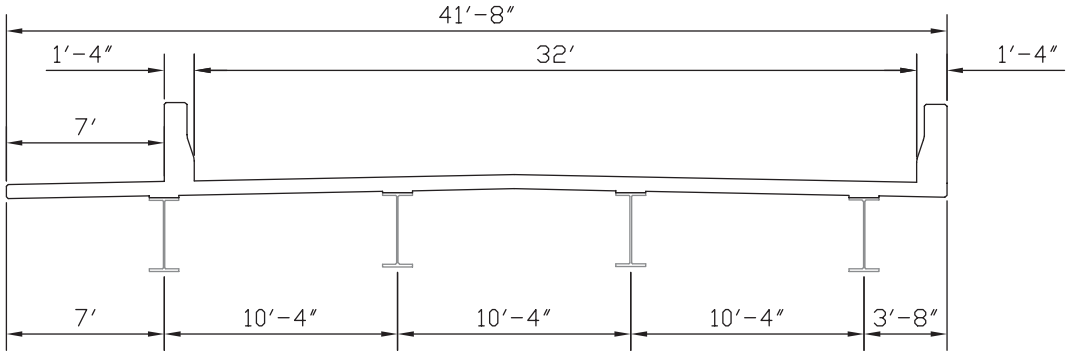

Fig. 12. Bridge cross-section.

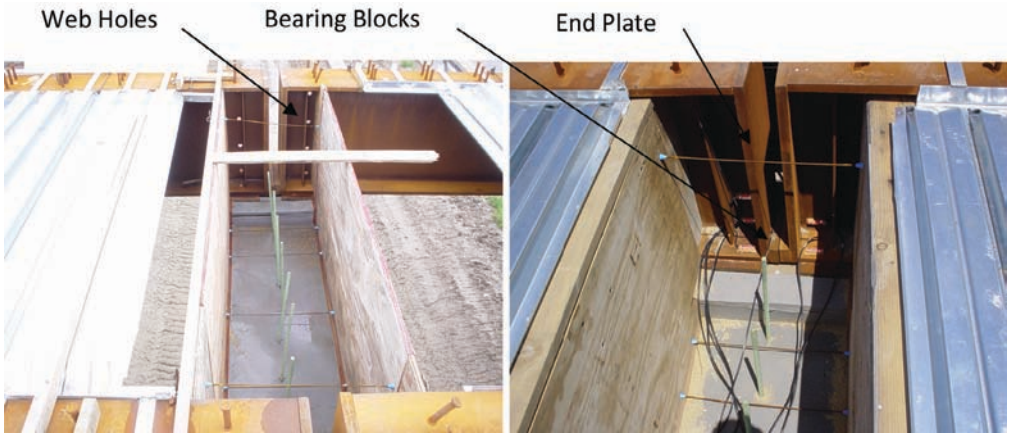

Fig. 13. Pier connection detail.

Fig. 14. Erection of first span of Sprague Street bridge over I-680.

Fig. 15. Erection of first span of Sprague Street bridge over I-680.

0.36 in. more deflection at point C than at point B, and there was 0.6 in. more deflection at point D than at point A.

The restraining moments obtained in the development of the curve fit shown in Figure 16, were used to predict deflections and resulted in values that were different from the observed by 2.9% at point A and 14.7% at point B. Note that the development assumed the end restraining moments are equal for both abutments, while in reality, they are not necessarily equal.

Girder Separation

Another item of interest during the deck pour was the data collected from crackmeters that were installed between the ends of the girders at the diaphragm. These were installed to measure the longitudinal separation between the girder ends during the deck pour. It can be seen in Figure 17 that as the pour progressed, the displacements increased, but at about 7:45 they leveled off and decreased briefly, then began increasing again. This is when the concrete placement crossed over the pier into the other span. The noted separation reduction is likely due to the finishing machine being directly supported by the pier for a period of time. The final displacements due to the deck pour were 0.19 in. at girder C and 0.17 in. at girder D. Note there was no sudden increase as would be expected if a large crack event had occurred.

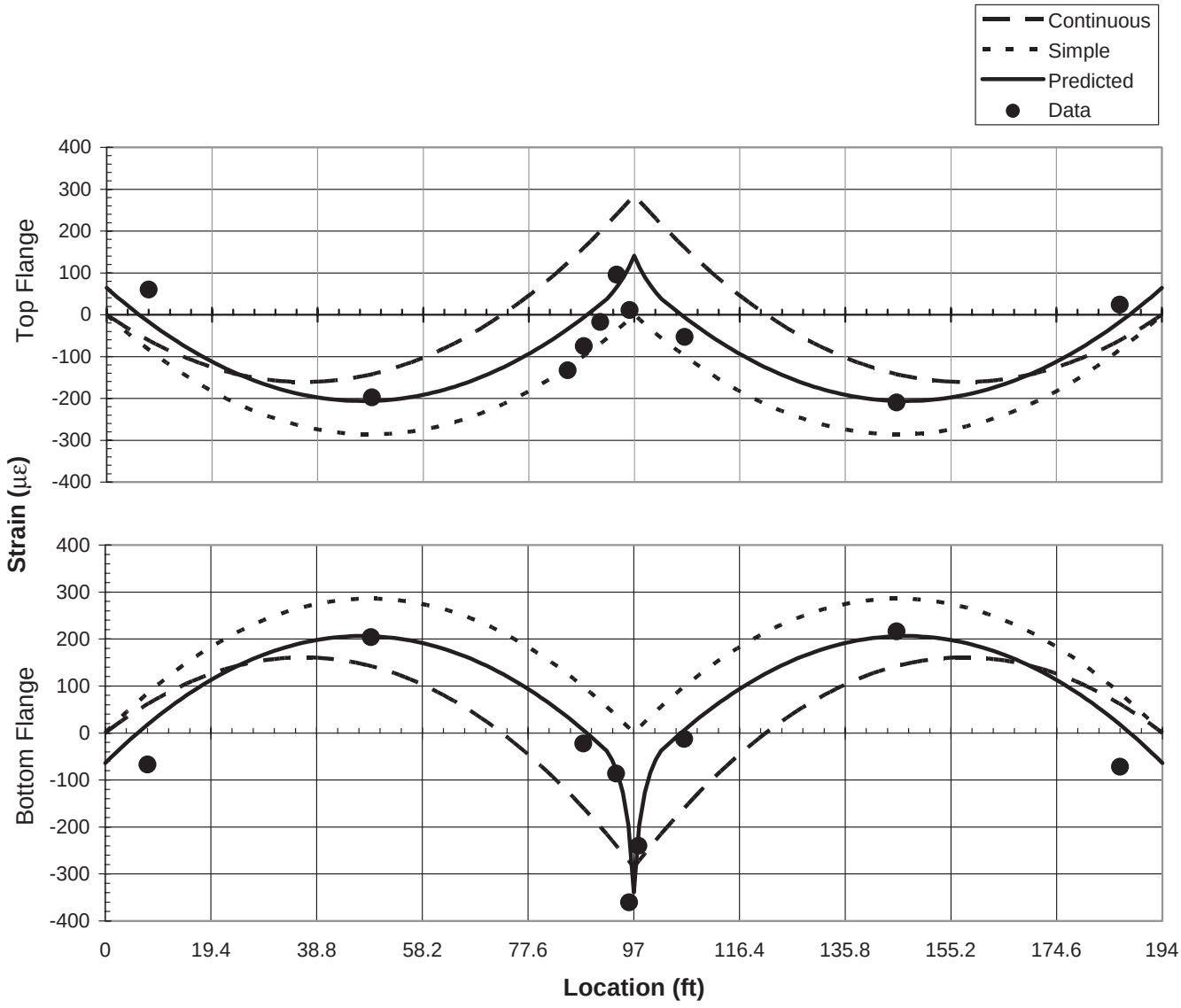

Fig. 16. Strains from analysis and measured values.

Long-Term Monitoring

The Sprague Street Bridge was continuously monitored for 5 years after completing construction. The long-term monitoring of the Sprague Street Bridge was very similar in nature and scope to the previous project. Casting of the deck began on the morning of July 10, 2004, at 6:00 a.m. This is used as a starting time for the long-term monitoring portion of the project. The readings of the gages at that time were used as zero values. Filter of the data to minimize the clutter caused by daily temperature fluctuations was again utilized. These procedures were briefly mentioned in the discussions for the N-2 over I-80 Bridge, described earlier. More detail information is provided elsewhere (Yakel and Azizinamini, 2009).

Observations

Note that the primary goal of performing the long-term monitoring of the structure was to ensure that the new, simple for dead load, continuous for live load design procedures did not exhibit unforeseen long-term performance issues. Therefore, the expected result is to see no change in gage responses other than possibly regular annual fluctuation attributable to seasonal variations in temperature, incident sunlight and relative humidity or precipitation levels. The results obtained from the gages were as expected.

A number of gages are embedded concrete. The responses of these gages display a logarithmic response characteristic of creep and shrinkage. This is most evident in the gages attached to sister bars located in the deck. The result from

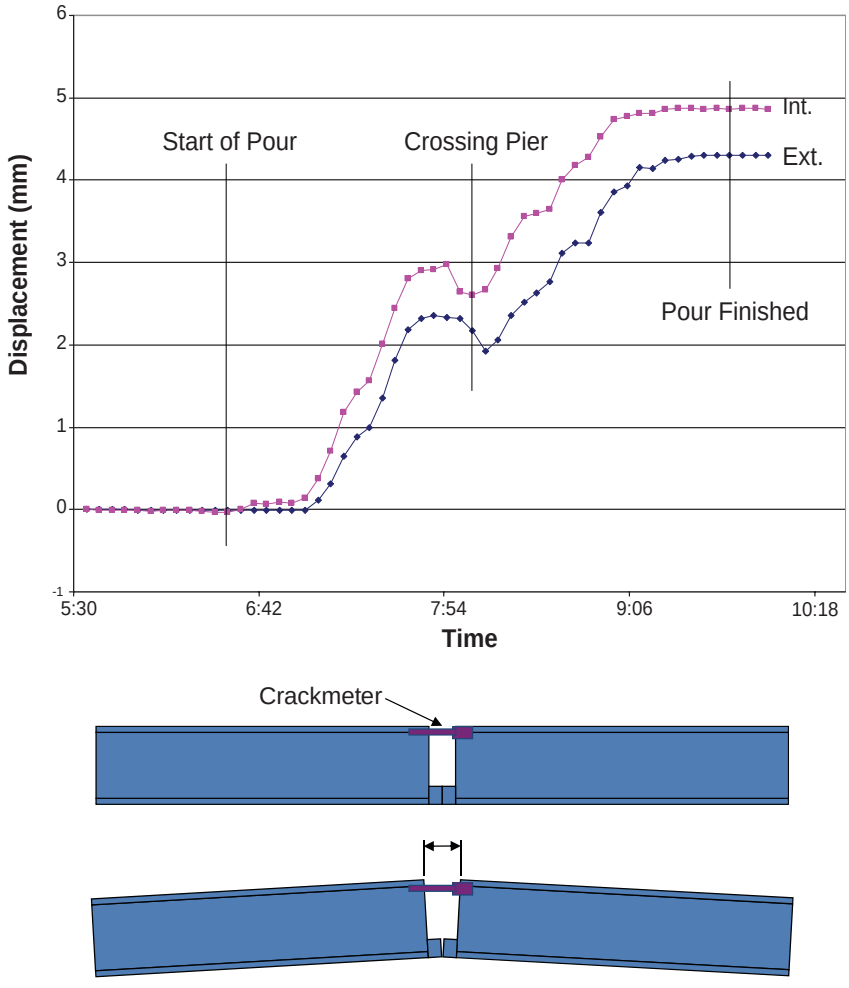

Fig. 17. Crackmeter displacements at diaphragm showing relative longitudinal movement of the top flanges.

one of the bars is shown in Figure 18 and is typical of the results observed in the other bars. After the first 2.5 years, the response had essentially flattened and remained fairly level, except for seasonal fluctuation, for the final 2 years.

A similar response can be seen in the results from the gages attached to the top flange directly over the pier. The strains are very low at this location due to the fact that the top flange is discontinuous over the pier. As a result, the response is more susceptible to influence of the concrete. In contrast, consider the bottom flange near the pier, which carries a significant compressive force and is not continuously connected to concrete. The strains from gages connected to the bottom flange nearest the pier do not show any changes in strain values other than seasonal fluctuations.

Summary

After an initial period of time when limited changes were observed, which have been attributed to creep and shrinkage of concrete, the response of the structure has been constant with only small, seasonal fluctuations. These fluctuations are expected and are generally attributable to changes in ambient temperature, relative humidity, incident solar radiation and ground freeze/thaw conditions.

262ND STREET OVER I-80—ACCELERATED CONSTRUCTION

The 262nd street bridge over I-80, located near Lincoln, Nebraska, incorporates several innovative concepts. The bridge utilizes a modular pre-top, steel, box-girder system, which allows much of the construction process to be performed prior to placing the girders and, therefore, reduces traffic disruptions. The bridge incorporates the simple for dead and continuous for live load system. The individual girders are simply supported while the pre-top deck is placed. Once in place, the modular units are joined together such that the resulting system is continuous for live load.

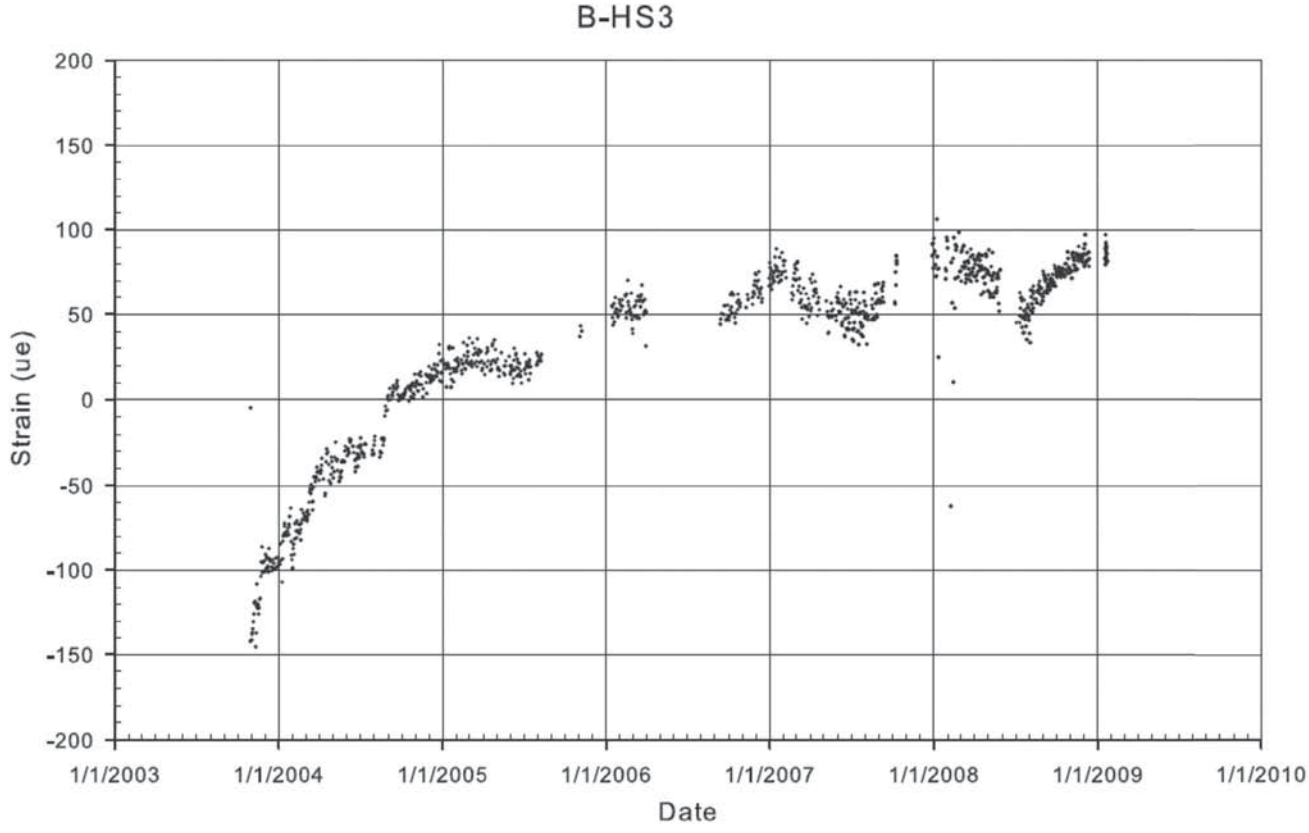

Fig. 18. Strain in concrete deck at pier (sister bar).

The steel box girders utilize high-performance steel in a hybrid configuration, 70 ksi in the bottom flange and 50 ksi in the top flanges and webs. The use of high-performance steel, combined with the simple for dead and continuous for live load system, allows eliminating plate-size transitions through the length of the structure.

The modular units must be joined in both the transverse and longitudinal directions. For the transverse direction, headed transverse reinforcement extends beyond the edges of the slab. The adjacent pre-top girders were then connected through the use of longitudinal closure strips. For the longitudinal connection at the pier, longitudinal reinforcement extends from the ends of the units and is bent downward to be cast into the concrete diaphragm. Both the transverse and longitudinal details can be seen in Figure 19.

The resulting system performs exactly as the original SDLC concept envisions and enjoys all of the accompanying benefits. Additional details and results of monitoring from that structure can be found in the paper describing the accelerated construction system (Javidi et al., 2014).

DESIGN COMPARISON OF N-2 AND SPRAGUE STREET BRIDGES

Design comparisons for the N-2 and Sprague Street bridges were carried out using two methods: (1) as a continuous beam for dead, live and superimposed loads (conventional method) and (2) as two simple beams for dead load and continuous for live loads according to the new proposed concept. A summary of the design results is given in Table 6. The variation of flange thickness was limited to two thicknesses along the girder length to include practical fabrication considerations. The web depth and thickness remained constant in both methods to satisfy the deflection requirements. In weight calculations, the weights of stiffeners and cross frames were ignored because they are similar in both alternatives. The values in the table are presented as ratios in the form of demand/resistance. The flange thickness was varied to obtain a demand-to-strength ratio for the section close to 1.00. Recall that the designs were optimized in terms of steel weight only. Note that for each case, the weight of additional steel using the new concept is about 4% for a box girder and 3% for the I-girder over the conventional option. This additional steel is provided in the positive section, which is beneficial in controlling the deflection under live loads.

Cost–Benefit Analysis

In the previous section, it was stated that application of the new construction method could result in a slight increase in weight of the steel girder. In return, the field splices were eliminated in each girder. Although each of the design parameters somewhat affected the cost of bridge construction, the major factors remain the weight of the steel girders and the cost of the field splices. Following is a summary of a cost–benefit analysis.

The cost of a steel girder consists of material, labor and facility costs. The assumed average bid unit price of fabrication for each steel girder is listed in Table 7, which was

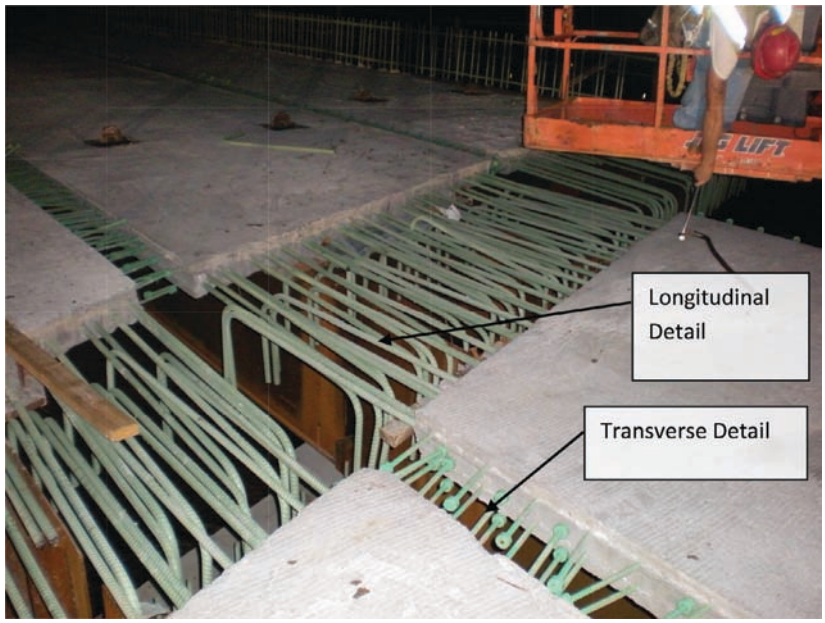

Fig. 19. Accelerated construction closure pier detail.

Table 6. Girder Sizing				
	N-2 (Box Girder)		Sprague (I-Girder)	
	Continuous for Dead and Live Loads	Simple for Dead Loads, Continuous for Live Loads	Continuous for Dead and Live Loads	Simple for Dead Loads, Continuous for Live Loads
Top flange sizes (in.)	16×0.64 16×1.3	16×0.7 16×0.8	15.8×0.5 15.8×2.6	15.8×0.5 15.8×2.6
Web sizes (in.)	50×0.375	50×0.375	36.56×0.75	36.56×0.75
Bottom flange sizes (in.)	72×0.64 72×1.3	72×0.7 72×0.8	15.8×0.5 15.8×2.6	15.8×0.5 15.8×2.6
Demand/strength ratio	1.00	1.00	1.00	1.00
Weight of one girder (kips)	52.47	54.63	21.46	22.07
Weight difference (percent)	4.13%		2.82%	

Table 7. Cost of Each Steel Girder				
	N-2 (Box Girder)		Sprague (I-Girder)	
	Continuous for Dead and Live Loads	Simple for Dead Loads, Continuous for Live Loads	Continuous for Dead and Live Loads	Simple for Dead Loads, Continuous for Live Loads
Weathering steel unit price per pound	$1.10	$1.10	$0.75	$0.75
Price of each steel girder	$57,712	$60,093	$15,627	$16,551
Splice cost (two per girder)	$12,800	$0	$4,000	$0
Splice schedule time	8 days	0 days	3 days	0 days
Total cost	$70,512	$60,093	$19,627	$16,661
Cost difference (percent)	15%		15%	

obtained from a local fabricator at the time of the study. The fabrication method—and, therefore, unit cost—is the same for both the SDCL and conventional systems. The increase in fabrication cost for the new concept is $923 for the I-girder and $2,380 for the box girder, as given in Table 7.

The cost of fabrication and installation of each field splice needs to be estimated in order to determine the extra cost of each girder when designed using the conventional method compared with the new concept. The cost of fabrication and erection consists of the cost of bolts, holes, plates, an extra crane and steel workers for installation and inspection. The unit price and required time for each item was obtained from RS Means, *Open Shop Building Construction Cost Data* (2003). A 55% surplus was added to the total cost of material, equipment and labor to consider the overhead, profit and indirect costs of the contractor. The typical field splice designed for the I-girder bridge is shown in Figure 20, and the splice cost is given in Table 7. Each girder will require two splices—a short section is first placed over the pier, and each of the span sections are then placed with one end supported on the abutment and the other spliced to the pier section. The splice geometry and construction sequence is similar for the box girder. Note that the span lengths for the I-girder bridge are such that one splice could be a welded shop splice, but this added complexity to the cost analysis and has been ignored. The information given in Table 7 indicates that although the SDCL requires slightly heavier girders, the additional cost of the steel is more than offset by the savings realized by eliminating the splices. For both cases, the net savings is approximately 15%.

The extra time for the fabrication and erection of each splice was evaluated based on a crew consisting of two steel

workers for fabrication and installation, one crane operator and one inspector. The total estimated time for the field splice of the I-girder is about 20 hours. This will extend the project time by approximately 3 days because the fabrication and erection of a steel girder is usually on the critical path of the project schedule. Similarly, the time estimation for the box girder indicates that using field splices can extend the project time by more than 8 days compared to the SDCL method.

OVERALL SUMMARY AND CONCLUSIONS FROM ALL THREE PROJECTS

Construction and long-term monitoring of three bridges provided an opportunity to monitor bridges constructed using three variations of the simple for dead, continuous for live load technique both during construction and beyond.

Monitoring of the strains and deflections during construction resulted in few surprises. The design concept assumes a simply supported condition exists during casting of the concrete deck. However, to provide lateral bracing, the diaphragm, or turndown, over the pier is cast and cured prior to casting the deck. As expected, encasement of the girders does provide some continuity over the pier during casting of the deck. The detail near the pier that utilizes a concrete slab cast onto the bottom flange to provide a stiffening effect to the compression flange behaved as expected.

Close observation of the construction activities allowed the overall constructability to be observed, and communication with the construction crews provided feedback and details on any challenges posed by the new type of construction. In general, the feedback was very positive. From a construction point of view, the system is very similar to that of a regular steel girder bridge.

Live load testing of the N-2 over I-80 bridge showed that the structure behaved as expected under real-life loading and that the simplified equations for distribution factors contained in AASHTO provide conservative results.

The long-term monitoring of the structures showed the behavior to be consistent over time with no significant deviations from the predicted bridge behavior. During the initial period of time of around 1.5 years, a slight overall change in strain values was observed. The rate of change slowed during this period and eventually ceased such that beyond this initial period of time, the responses of the structures have been constant with small seasonal fluctuations. These fluctuations are expected and are generally attributable to changes in ambient temperature, relative humidity, incident solar radiation and ground freeze/thaw conditions.

A cost–benefit analysis showed that although the SDCL system requires slightly heavier girders, the additional steel cost is offset by the savings realized due to elimination of the splices, resulting in a net savings of 15% over conventional construction.

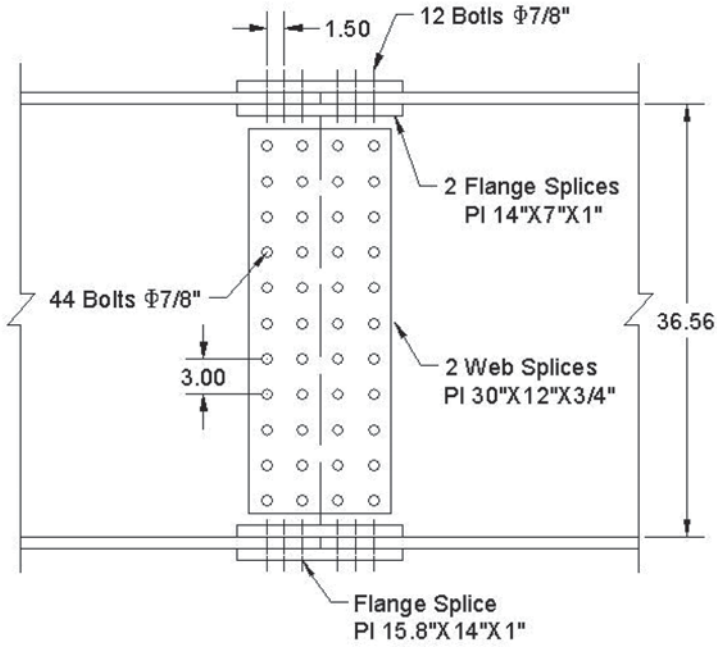

Fig. 20. I-girder field splice details.

ACKNOWLEDGMENTS

This paper presents details of a major undertaking to develop an economical steel bridge system. The initiative was directed by Atorod Azizinamini, Professor and Chair at Florida International University, and made possible by contributions by many current and former graduate students and research associates, as well as input from many in the bridge community. In particular, the contributions of the following individuals are acknowledged.

Graduate students earning degrees from the project were Nick Lampe, Nazanin Mahasebi, Reza Farimani, Saeed Javidi, Derek Kowalski and Mark Otte. The research study was conducted at the University of Nebraska–Lincoln. Dr. Aaron Yakel was the research associate assisting the project. Laboratory technicians Jeff Boettcher, John Dageford and Peter Hilsabeck assisted in conducting the experimental portion of the study. Graduate students who assisted with experimental testing include John Swendroski, J. Brian Hash, Patrick Mans, Luke Glaser and Nima Ala. The study was supported by the Federal Highway Administration and Nebraska Department of Roads. Several visionary engineers at NDOR were critical to the successful completion of the project: Lyman Freeman, Moe Jamshdi and Hussam "Sam" Fallaha. Steel fabrication and assistance during specimen preparation was provided by Capitol Contractors of Lincoln, Nebraska.

The opinions and conclusions presented in this paper are those of the authors and do not necessarily represent the viewpoints of the project sponsors.

REFERENCES

AASHTO (1998), *LRFD Bridge Design Specifications*, 2nd ed., American Association of State Highway and Transportation Officials, Washington, DC.

AASHTO (2003), *Manual for Condition Evaluation and Load and Resistance Factor Rating (LRFR) of Highway Bridges*, American Association of State Highway and Transportation Officials, Washington, DC.

Ala, N., Javidi, S.N., Glaser, L., Burner, K., Yakel, A.J. and Azizinamini, A. (2009), *Steel Box System Monitoring of N-2 over I-80 Bridge*, A Final Report Submitted to the Nebraska Department of Roads, National Bridge Research Organization.

Azizinamini, A. (2014), "Simple for Dead Load–Continuous for Live Load Steel Bridge Systems," AISC, *Engineering Journal*, Second Quarter, pp. 59–81.

Farimani, M.R., Javidi, S.N., Kowalski, D.T. and Azizinamini, A. (2014), "Numerical Analysis and Design Provision Development for the Simple for Dead Load–Continuous for Live Load Steel Bridge System," AISC, *Engineering Journal*, Second Quarter, pp. 109–126.

Horton, R., Power, E., Van Ooyen, K. and Azizinamini, A. (2000), "High performance Steel Cost Comparison Study," *Proceedings, Steel Bridge Design and Construction for the New Millennium with Emphasis on High Performance Steel*, Baltimore, MD, pp. 120–137.

Javidi, S.N., Yakel, A.J. and Azizinamini, A. (2014), "Experimental Investigation, Application and Monitoring of a Simple for Dead Load–Continuous for Live Load Connection for Accelerated Modular Steel Bridge Construction," AISC, *Engineering Journal*, Third Quarter, pp. 177–198.

Lampe, N.J., Mossahebi, N., Yakel, A.J., Farimani, M.R. and Azizinamini, A. (2014), "Development and Experimental Testing of Connections for the Simple for Dead Load–Continuous for Live Load Steel Bridge System," AISC, *Engineering Journal*, Second Quarter, pp. 83–108.

RS Means (2003), "Open Shop Building Construction Cost Data," Kingston, RS Means Company.

Stallings, J.M. and Yoo, C.H. (1993), "Tests and Ratings of Short-Span Steel Bridges," *Journal of Structural Engineering, ASCE*, 119(7), pp. 2150–2168.

Yakel, A.J. and Azizinamini, A. (2009), *Monitoring of a Steel Bridge: Sprague Street over I-680*, A Final Report Submitted to the Nebraska Department of Roads, National Bridge Research Organization.

Yakel, A.J. and Azizinamini, A. (2012), *Side by Side Steel Box System for Accelerated Construction: Monitoring of 262nd Street over I-80*, A Final Report Submitted to the Nebraska Department of Roads, National Bridge Research Organization.

Experimental Investigation, Application and Monitoring of a Simple for Dead Load–Continuous for Live Load Connection for Accelerated Modular Steel Bridge Construction

SAEED JAVIDI, AARON YAKEL and ATOROD AZIZINAMINI

ABSTRACT

The inherently modular nature of the simple for dead–continuous for live load system (SDCL) makes it a natural fit for the accelerated construction paradigm. A detail capable of connecting pre-topped girders over the middle supports is developed and described in this paper. To evaluate the performance of the proposed connection, a full-scale specimen was built and subjected to cyclic and ultimate load testing. The connection showed very little change during cyclic loading equivalent for 70 years of traffic. During the ultimate load test, the connection demonstrated large displacement ductility, reaching its ultimate capacity after complete yielding of the longitudinal reinforcement. After the successful experimental test, a field application bridge was constructed utilizing a modular pre-topped steel box girder system, which allows much of the construction process to be performed prior to placing the girders. The bridge consisted of three pre-topped steel box units placed side by side and connected using longitudinal joints between pre-topped units. The steel box girders used 70-ksi high-performance steel in the bottom flange and 50-ksi steel in the top flanges and webs. The use of high-performance steel combined with the simple for dead–continuous for live load system allows eliminating the need for section transitions through the length of the structure and using constant cross-section throughout the length of the girders. Long-term monitoring of the structure was performed and showed the system performed as intended.

Keywords: steel bridges, steel girders, SDCL, simple for dead load–continuous for live load.

INTRODUCTION

This paper provides description of the development and implementation of the simple for dead–continuous for live loads (SDCL) bridge system for steel girders, a method well suited for accelerated bridge construction (ABC). The SDCL bridge system employs a joint detail at the interior supports that does not become continuous until after the dead loads have been applied. Prior to attaining this final continuity, the girders within the individual spans are simply supported. General information regarding the behavior and design of the SDCL system can be found in a companion series paper by Azizinamini (2014).

A current trend in bridge construction is the adoption of accelerated construction practices that reduce onsite construction time to mitigate extended disruptions to traffic. The inherently modular nature of the SDCL system makes it a natural fit for the accelerated construction paradigm. Therefore, the research being presented in this paper extends the simple-made-continuous system to address modular bridge construction methods. In addition to accelerating the bridge construction process, the system presented also greatly enhances worker safety.

Saeed Javidi, Ph.D., P.Eng., Structural Engineer, Associated Engineering Ltd., Burnaby, BC, Canada. Email: sjavidin@gmail.com

Aaron Yakel, Ph.D., Research Associate, Civil and Environmental Engineering Department, Florida International University, Miami, FL. Email: ayakel@fiu.edu

Atorod Azizinamini, Ph.D., P.E., Professor and Chair, Civil and Environmental Engineering Department, Florida International University, Miami, FL (corresponding). Email: aazizina@fiu.edu

RESEARCH OBJECTIVES AND SCOPE

The simple for dead–continuous for live load concept has been used with prestressed concrete bridges for many years. Research conducted at the University of Nebraska–Lincoln extends the application of this system to steel girder bridges.

The key component in the simple for dead load made continuous for live load system is the continuity connection over the interior supports. For the purpose of extending the application of SDCL system to bridges constructed using principles of accelerated bridge construction, detail capable of connecting the pre-topped girders over the middle supports is developed and described in this paper. To evaluate the performance of the proposed connection, a full-scale specimen was built and various tests conducted. The specimen was representative of the negative flexure region of a

two-span bridge having 94-ft span lengths with four girders, spaced at 8 ft 4 in. The tests carried out included static and cyclic loading to comprehend the strength and fatigue performance of the detail and development of appropriate design provisions. The results of the cyclic and ultimate test are described, and the load-resistance mechanism of the connection is examined. Following the completion of the experimental testing, the detail was utilized in the construction of the 262nd Street Bridge over I-80 in Nebraska. Several innovative concepts were used in the construction of this bridge. The bridge was instrumented and monitored during service for more than 2 years. Design and construction of the 262nd Street Bridge demonstrated the feasibility of using the developed detail in practice.

SYSTEM DESCRIPTION

Continuous steel bridges are usually constructed so that the system provides continuity for all loading, both dead and live. However, in SDCL steel bridge systems, girders behave as simply supported under their own self-weight and during casting of the concrete deck. The interior support connection detail is such that once the deck has been cast and allowed to cure, the system then becomes continuous for subsequent loading. The continuity for live loads is provided for by providing steel reinforcement over the interior support, before the casting deck.

Modular Concept

One of the objectives in using modular bridge systems is to minimize the interruption to traffic. This objective is achieved by casting the concrete deck over the girder, prior to placement over the supports. Pre-topped girders are then placed side by side and connected using narrow longitudinal joints. Figure 1 shows the system used for the 262nd Street Bridge, which incorporates SDCL, pre-topped and adjacent girder concepts.

The concept of pre-topped, adjacent girder system for ABC applications is also used with concrete girders. However, using steel girders provides two main advantages. First, the concrete girder with a pre-topped deck could weigh several times more than steel alternates. Second, concrete girders experience creep and shrinkage displacement, which creates challenges during construction. The creep and shrinkage displacement of pre-topped concrete girders results in pre-topped units to assume different elevations, which is difficult to correct in the field. This problem becomes more significant as girder length increases. Use of steel girders in a pre-topped, adjacent system, in large part, eliminates this challenging field problem, especially when a full-depth pre-topped deck system is used.

Pier Connection Detail

In the conventional SDCL system, continuous longitudinal reinforcement is placed over the interior support that is then

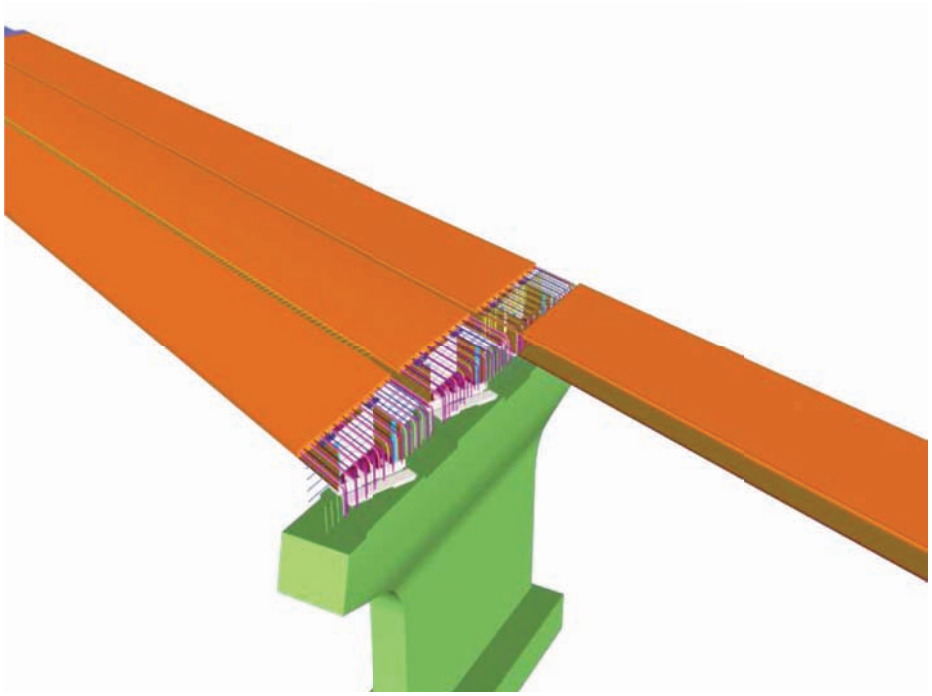

Fig. 1. Conceptual drawing of SDCL system using pre-topped and adjacent girder concepts.

cast into the deck. This is clearly not possible in the modular system because the concrete deck is already cast. Somehow the reinforcement from one span must be spliced with the reinforcement from the next span. The solution was to allow the longitudinal reinforcement to extend out of the concrete deck at the interior support. The reinforcement bars over the pier are then developed by hooking them in the concrete diaphragm. This detail can be seen in Figure 2. The compressive component of the connection is identical to that used in conventional use of SDCL system.

EXPERIMENTAL PROGRAM

The experimental testing performed on the connection detail was identical to that used in the development of the SDCL system. Additional details of the original specimen design can be found elsewhere (Lampe et al., 2014; Azizinamini, Lampe and Yakel, 2003; Azizinamini et al., 2005).

Specimen Geometry

The test specimens represented a full-scale model of a portion of a bridge in service. The prototype bridge consists of two 95-ft continuous spans with four steel I-girders.

The test specimen represents the interior pier region of the two-span bridge, from inflection point to inflection point, as shown in Figure 3. Loads applied at the ends of the cantilevers allow simulation of the loading the structure would be subjected to in the field and result in similar shear and moment profiles.

The basic deck reinforcement was based on the empirical deck design provisions. The longitudinal steel includes #5 bars at 12-in. on center in the top layer and #4 bars at 12-in. on center in the bottom layer. The transverse reinforcement consists of #5 bars at 12-in. on center in the bottom layer and #4 bars at 12-in. on center in the top layer.

The negative moment produced by the live loads and superimposed dead loads is resisted by additional slab reinforcement at the pier location. The additional reinforcement required in the top layer is comprised of two #8 bars centered between adjacent #4 bars. Similarly, one #7 bar is centered between adjacent #5 bars in the bottom longitudinal

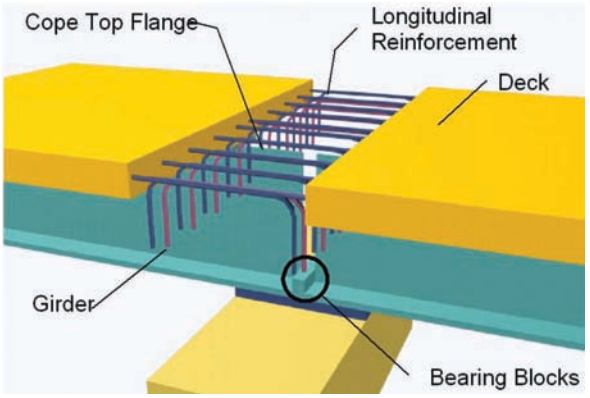

Fig. 2. Pier connection detail for modular system.

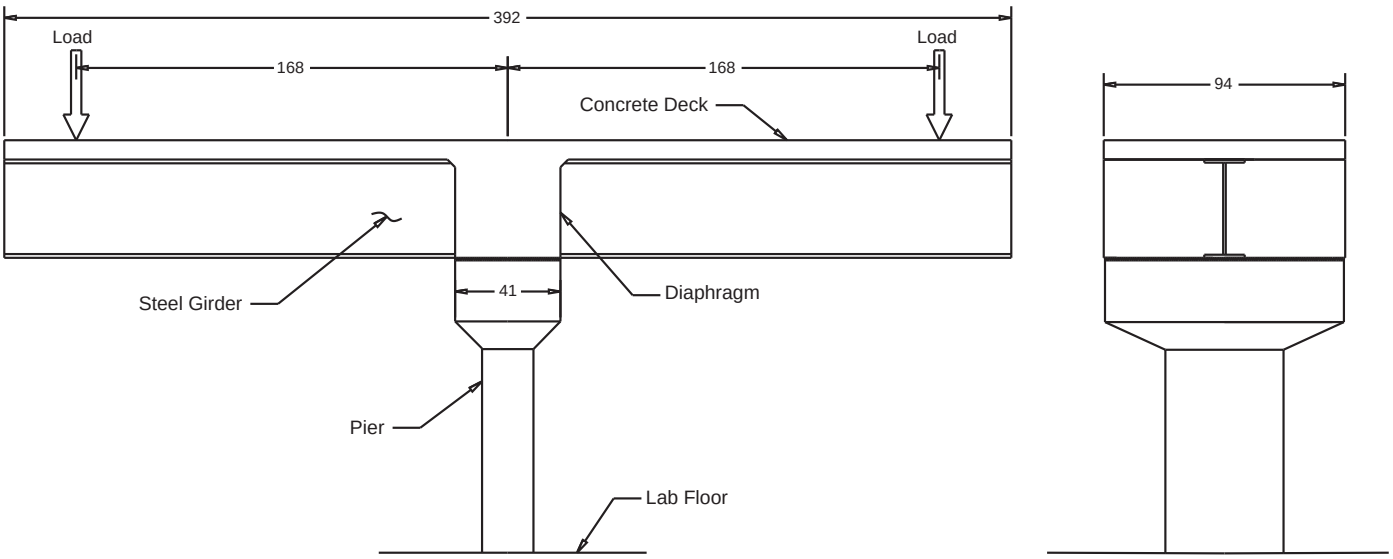

Fig. 3. Test specimen, dimensions in inches.

layer. This follows the typical two-thirds of the reinforcing steel in the top layer and one-third of the total area in the bottom layer. The details of the final slab reinforcement are shown in Figure 4. The L1, L2 and L3 notations indicate instrumentation locations and are discussed later.

To provide an additional resistance element in the connection, several high-strength bolts were attached to a region of the web located inside of the diaphragm. These bolts are shown in Figure 5. The results were inconclusive regarding the effectiveness of this detail. However, there is a need to prevent slippage of the girder web from the concrete diaphragm. The use of bolts as shown in Figure 5 is believed to accomplish this objective.

Because the test specimen is only a portion of the full bridge, it would have been unstable to cast the deck and then set the girders. Therefore, it was decided to build the specimen while the girders are in place on the pier. Although slightly different than the process to be used in the field, this change has no effect on the results of the study. Casting of the slab and diaphragm was completed in two stages. The first stage consisted of casting the diaphragm to half the total depth. This was done to add stability to the specimen during deck casting. The remainder of the diaphragm and the deck was cast 2 days later and was cured for 3 weeks.

Instrumentation

The specimen was monitored during the cyclic and ultimate tests using potentiometers, bonded electrical strain gages, welded and embedment vibrating wire strain gages, and a crack meter. Data were recorded through two data acquisition systems. Sixty-four resistance-based strain gages were mounted on the steel girders and longitudinal reinforcing bars to measure the strain variation during the test. Different parts of the girders, including top flange, bottom flange, web and bearing blocks, were instrumented by strain gages. Eleven vibrating wire embedment gages were used to monitor strain variations in the concrete diaphragm around the steel blocks in the longitudinal direction. A crack meter was installed between the girders' web at the centerline of the connection to measure the relative displacement of the two girders at both ends. Internal linear variable differential transformers (LVDTs) within the MTS rams measured the displacement of the specimen under the loading points during the cyclic test. Position transducers measured the displacement at two ends of the specimen during ultimate loading.

Materials

Twenty samples were cut from the steel rebar representing a sampling of all bar sizes. Figure 6 shows the engineering stress-strain curve for the #8 bars obtained from tensile tests. For the steel beam girders, samples were taken from near the end of the girder, which did not experience significant stress during testing. The average yield strength of the girder steel was determined to be 57 ksi, and the average ultimate stress was 72 ksi.

Concrete cylinders were prepared during the diaphragm and deck concrete casting. Based on the average compressive cylindrical test results, the 28-day compressive strength of the concrete was 5358 psi and 4947 psi for the deck and diaphragm, respectively.

Cyclic Testing

The bridge structure is expected to endure millions of cycles of repeated axle loads from vehicles during the design life. The available data show that the number of trucks on a bridge can reach more than 180 million vehicle load cycles during

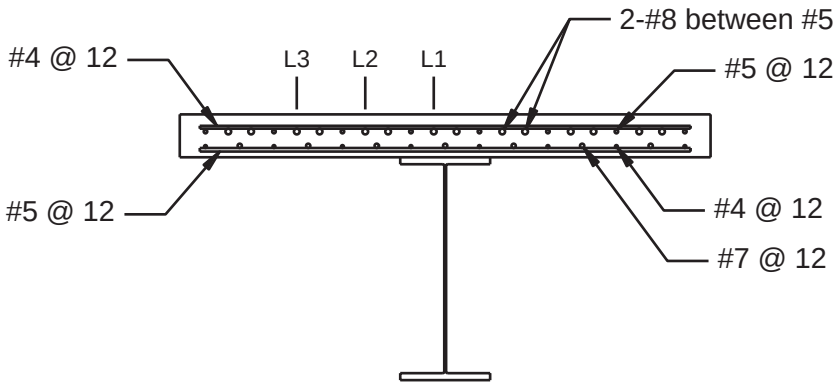

Fig. 4. Concrete slab section.

Fig. 5. Test specimen end detail.

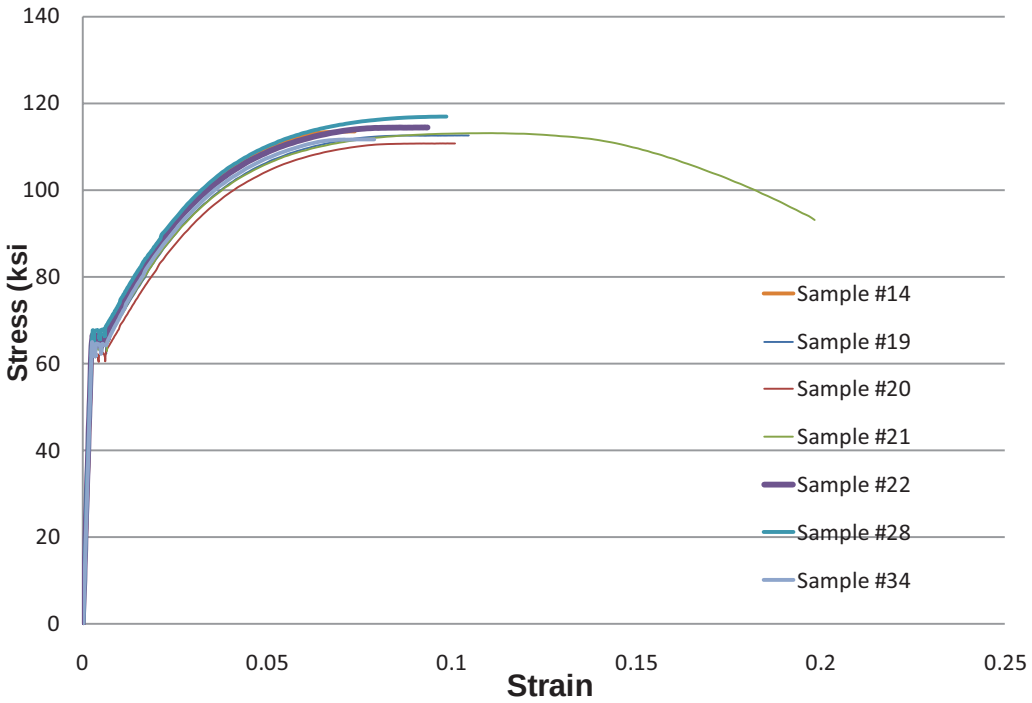

Fig. 6. Tensile test results for the #8 reinforcing bars.

the life time of 100 years (Szerszen and Nowak, 2000). The proposed connection should be able to operate and survive when subjected to cyclic loading generated by truck traffic. The specific goal of the cyclic testing performed was not intended to determine the fatigue strength or limit of the details, but rather as a proof loading to investigate whether the proposed details are capable of surviving a loading regimen equivalent to the cyclic loading anticipated over the design life of the bridge.

Procedure

The AASHTO *LRFD Bridge Design Specifications* (2007) were used to determine the fatigue resistance stress range based on the 75 years of service life for the bridge. During this period, the connection was expected to experience 135 million cycles. Applying this number of cycles would require an inordinate amount of time at a rate of two cycles per second. Therefore, the applied stress range was increased in order to reduce the number of cycles required to carry out the test. Four million cycles was chosen for the fatigue test. The applied moment for 4 million cycles to cause the same damage as 135 million cycles can be found by using the relationship developed herein and further explained in Lampe et al. (2014).

The fatigue limit state load combination was used to calculate the shear and moment envelope to which the prototype bridge would be subjected to. According to AASHTO-LRFD Specifications (1998), the prototype bridge, during its 75 year design life, and consequently, the connection of the two girders at the pier location, will experience 135,000,000 cycles of truck loadings. The simulation of this number of cycles in the laboratory would have taken a prohibitively long time. Therefore, there was a need to develop a procedure that could simulate 75 years of traffic in a reasonable time frame. This was accomplished by amplifying the level of load that was applied, as described later. Complete details of the procedure are provided in Lampe, Mossahebi, Yakel and Azizinamini (2013).

Equation 1 provides a relation between the loads and number of cycles under two conditions. Condition 1 represents the loading and number of cycles applied during the service life of the real structure as assumed for design. Condition 2 represents the structure under amplified loading.

$$\frac{M_1}{M_2} = \left(\frac{N_2}{N_1}\right)^{1/3} \quad (1)$$

where

M_1 = actual load
N_1 = cycles for actual structure corresponding to load of M_1
M_2 = amplified load (desired quantity)
M_2 = number of test cycles at load of M_1

From the bridge design calculations, the governing fatigue moment, M_1, is 352 kip-ft at an N_1 equal to 1.35 million cycles. With M_1 and N_1 known and having a desire to apply only 4 million cycles to reduce testing period (N_2 = 4,000,000 cycles), the applied moment needs to be increased to 1137 kip-ft as compared to 352 kip-ft. Given that the moment arm is 14 ft means 81 kips load must be applied to achieve the required moment (1137 ft-kips). In the laboratory, a 5-kip initial load was applied to the specimen and then the cyclic load was changed between 5 and 86 kips.

Two 1000-kN (220 kips) MTS actuators were used to apply the cyclic loading at 2 Hz (two cycles per seconds).

General Behavior of the Connection

Load-displacement curves for five periods during the cyclic test are generated at 1 million cycle intervals. Figures 7a and 7b show the load-displacement curves for the east and west side of the specimen, respectively.

Two observations can be made. First, there is a small difference between the stiffness of the west and east side of the connection. Second, it was observed that the initial load-displacement curve has a slightly greater slope than subsequent curves at later loading cycles. A 3.8% stiffness reduction was observed at the end of 4 million cycles.

Crack Pattern and Its Propagation on the Deck

No cracks were visible at the end of the curing period by visual inspection. After the initial application of load equivalent to the maximum fatigue load, the deck was again inspected and the initial cracks were mapped. During loading, the deck was inspected for cracking after each 1 million cycles. Figure 8 shows the crack map of the deck surface. The solid lines show the crack pattern after initial static load, while the dashed lines show the crack development during cycling. Note that the majority of crack growth occurred during the first 1 million cycles. No significant crack propagation was observed after 1 million cycles. As can be seen in the figure, little crack development occurred as a result of the cyclic loading. This would indicate that the connection performs well with regard to cracking of the concrete deck under repeated loading, which is important for the durability and service life of the structure.

Strain Profile in Longitudinal Direction

Six longitudinal reinforcing bars were instrumented to monitor the strain variation along the length of the bars. Figure 9 shows the strain variation along these six longitudinal bars, three on each side of the girder. Each figure is denoted by a name such as L1, which corresponds to the bar location as

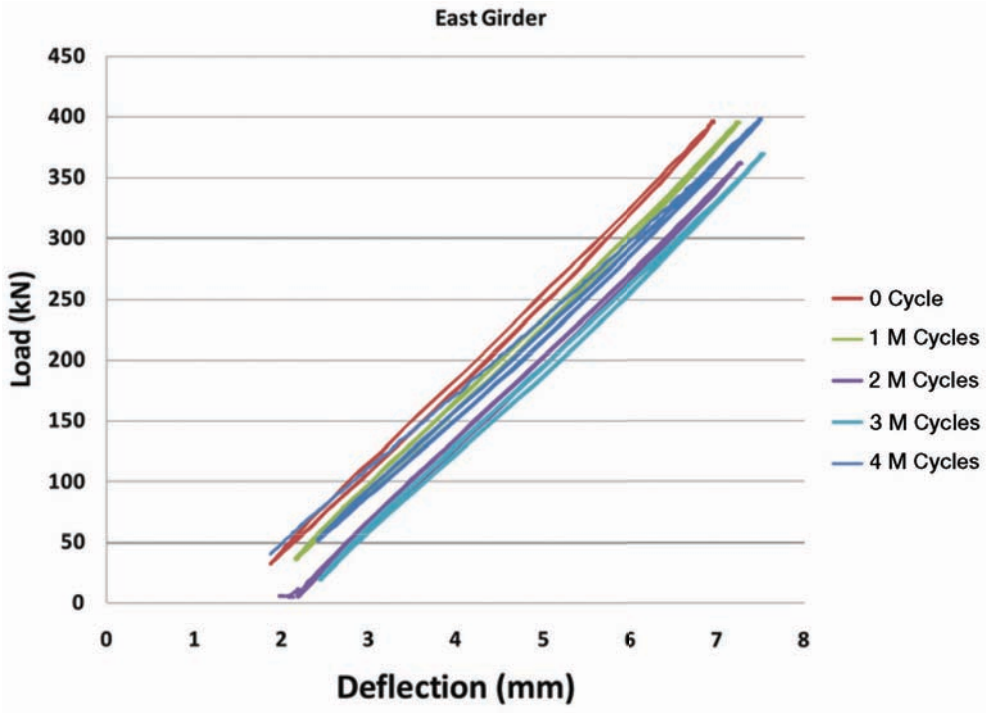

(a)

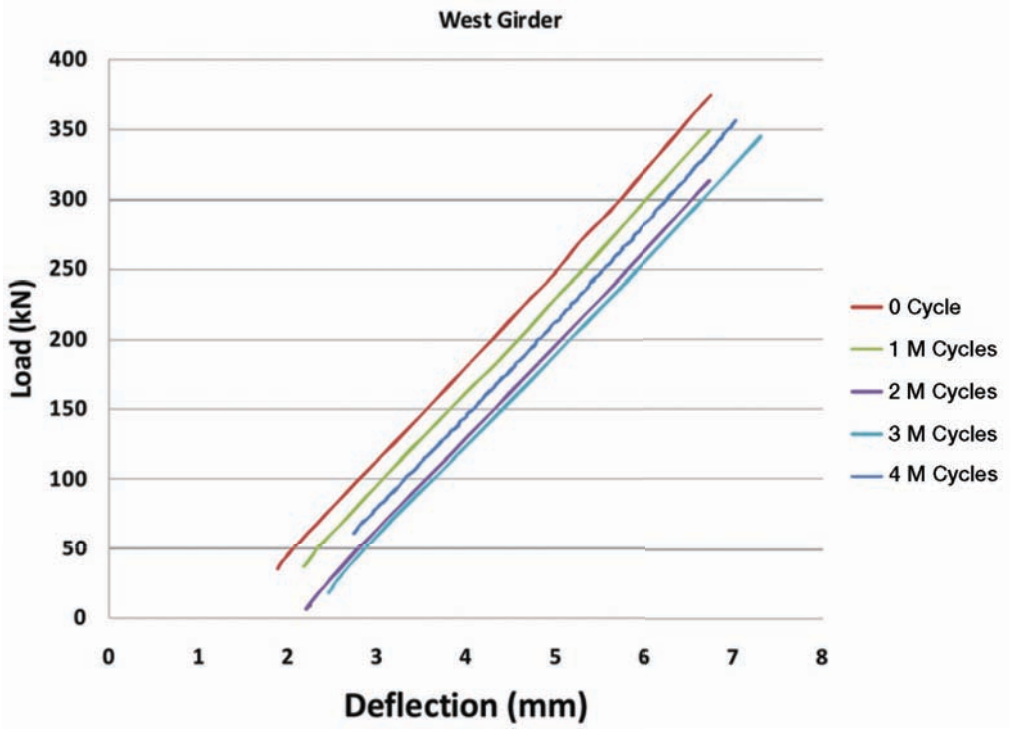

(b)

Fig. 7. Load-displacement curves for (a) the east side of the specimen and (b) the west side of the specimen.

shown in Figure 4. In all cases, the maximum strain occurs at point B, which is located just outside of the diaphragm. Longitudinal bars from each side lap each other in the diaphragm zone. Consequently, the area of longitudinal bars is doubled in this region, causing the bars to exhibit lower strain values than locations outside of the diaphragm region. The strain results in the longitudinal bars show that the bars are fully developed within the diaphragm region due in large part to presence of the hook.

The results show that the strain in the longitudinal bars increased slightly during the cyclic test. This change is more significant in the portion of deck outside of the diaphragm. The majority of this change happened within the first 1 million cycles. The average strain increase is 30 με, which is very small. The increase can be cracking in the deck. It can be concluded that performance of the connection was satisfactory during the fatigue service life.

Ultimate Test

The ultimate load test was carried out to investigate the behavior of the specimen under the ultimate load and evaluate the strength of the system. Loading of the specimen was achieved by placing a spreader beam on the deck at each end of the specimen. Threaded rods extended from the spreader to the basement of the structures laboratory, where they connected to hydraulic actuators. The loading system for the second test is shown in Figure 10. The distance of the spreader beam center to the centerline of the pier was 15 ft. During testing, displacement was applied in small increments with pauses for observations and data acquisition.

General Behavior of the Connection

Displacement was applied to the specimen until the specimen could no longer support additional load. The load-displacement curves were generated for both the west and east side of the connection and are shown in Figures 11 and 12, respectively. There is a slight difference in stiffness between the two ends. This is attributable to slight asymmetry or perturbations favoring one side of the connection. Other factors contributing to this slight difference could be unsymmetrical cracking in the deck concrete. The load corresponding to the theoretical plastic moment is shown in Figures 11 and 12. This calculation is based on the actual material properties and assumes complete participation of the full steel section and reinforcement. The assumption provides a value for reference and is not necessarily a basis for strength calculation, which is discussed in more detail elsewhere (Farimani et al., 2014).

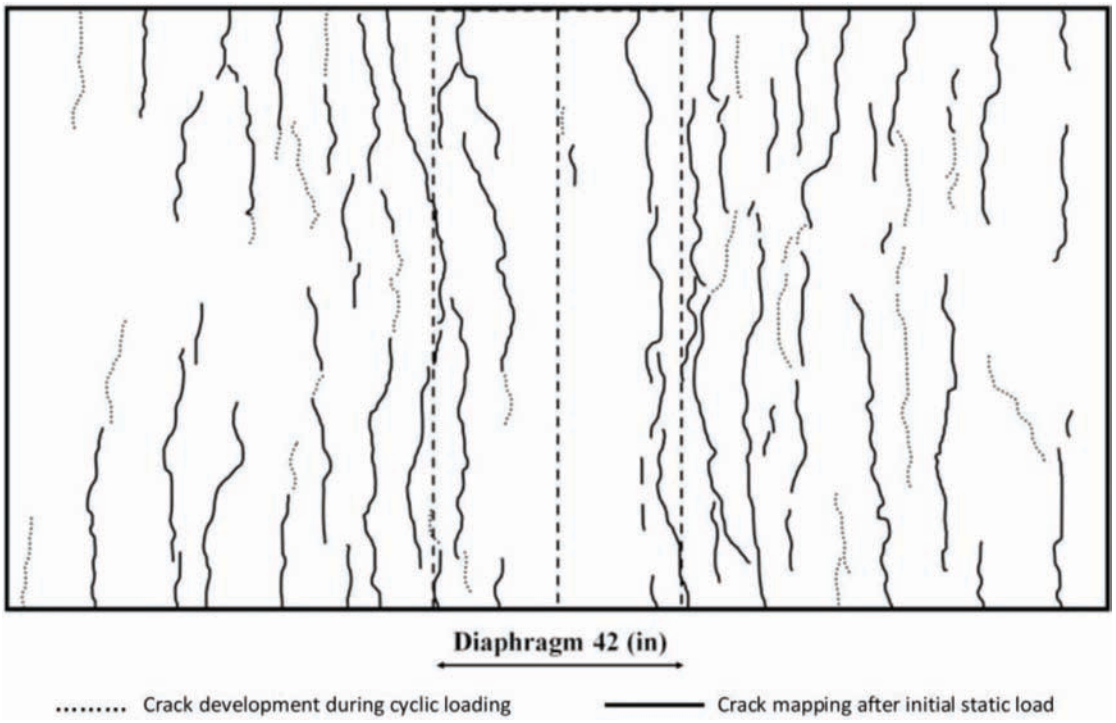

Fig. 8. Cracking on the slab deck surface.

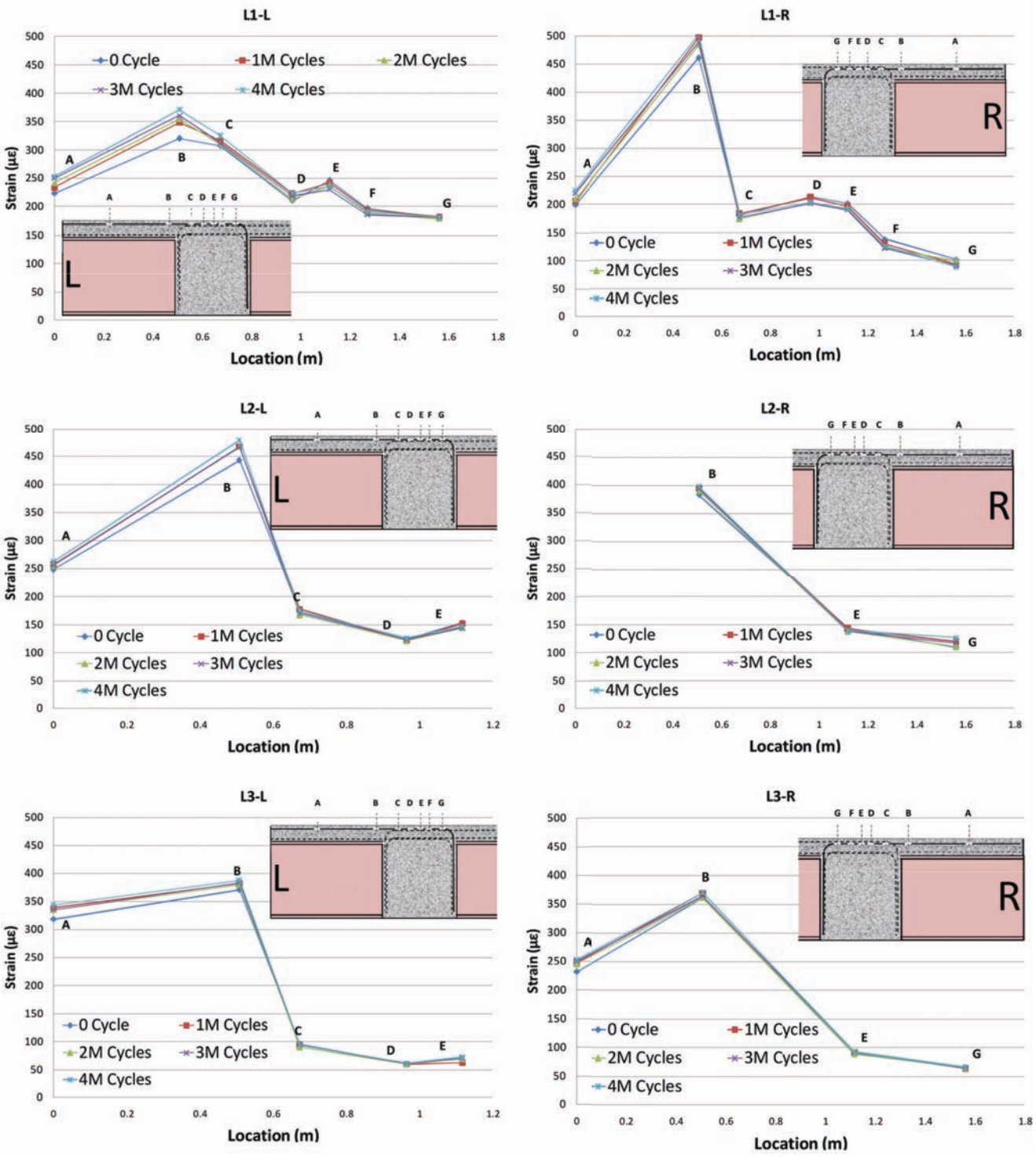

Fig. 9. Strain variation along the six longitudinal bars (L1-L, L1-R, L2-L, L2-R, L3-L, L3-R) during cyclic test.

The load-displacement behavior can be broken into four distinct regimens. At the outset of loading, there is a linear relation between the load and deflection. When the loading reached approximately 300 kips, this relation becomes nonlinear. This relationship can be seen in Figures 11 and 12 as a rounding of the load-displacement curve, corresponding to the initial yield of tension steel in the deck, over the pier. Once the majority of the tension steel over the pier has yielded, the behavior enters a plateau state, where there is little increase in load despite the application of large amounts of displacement. The small amount of load increase is mostly attributed to strain hardening of the tension steel. Note that the specimen was unloaded and reloaded several times during the test. Finally, at a load of approximately 415 kips and an applied displacement of 6.4 in., the load began dropping in response to the application of additional displacement, indicating the ultimate failure of the connection. Loading of the specimen continued until the end displacement of about 13 in. was achieved. The load corresponding to this displacement level (13 in.) was about 325 kips. This demonstrates the extreme ductility available from the connection. For the sake of clarity, the descending portions of the load displacement response of the test specimen are not shown in Figures 11 and 12.

Vertical Strain Profile in the Girders

Both girders were instrumented to monitor the strain variation during loading. The vertical strain profile was obtained at five locations, three locations in the west girder and two in the east girder. Figure 13 shows the vertical strain profile along the depth of the girder during ultimate loading for the various sections. The location of the strain gages and the section under the study are shown in each picture. The strain distribution along the depth of the girder is linear, and the location of the neutral axis based on the experimental results is in good agreement with that obtained theoretically. The strain distribution remained mostly linear through the test, the exceptions being the bottom flange on the west side just outside the diaphragm and the top flange on the east side just outside the diaphragm. It should be noted that these deviations from linearity were observed even at very low load levels and are, therefore, not a result of damage sustained during loading. However, the exact cause of these deviations was not identified.

Longitudinal Strain Profile in Continuity Reinforcement (Top Layer)

Longitudinal reinforcing bars were instrumented to monitor the strain variation along the length of the bars. Figure 14 shows the strain variation along bars at three different

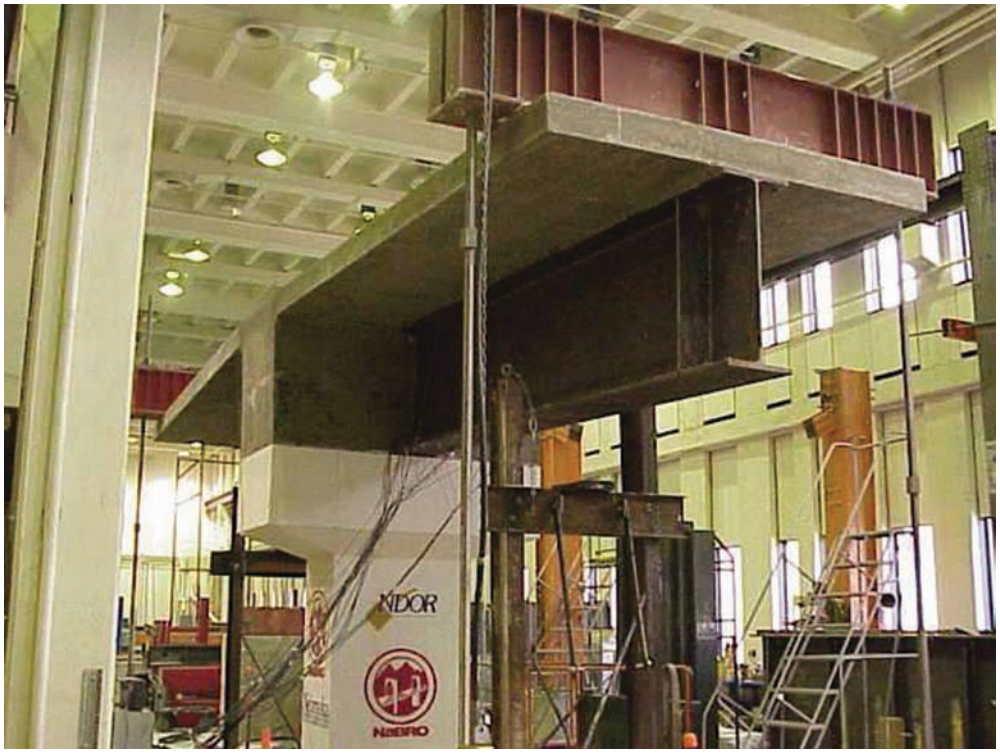

Fig. 10. Ultimate test setup for the second test.

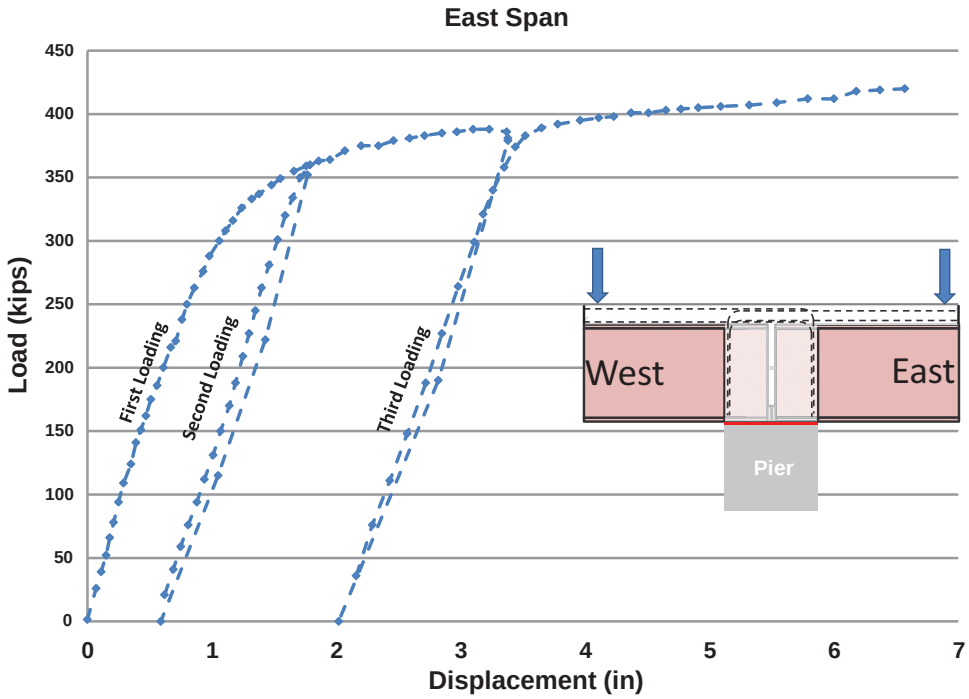

Fig. 11. Load displacement (east side).

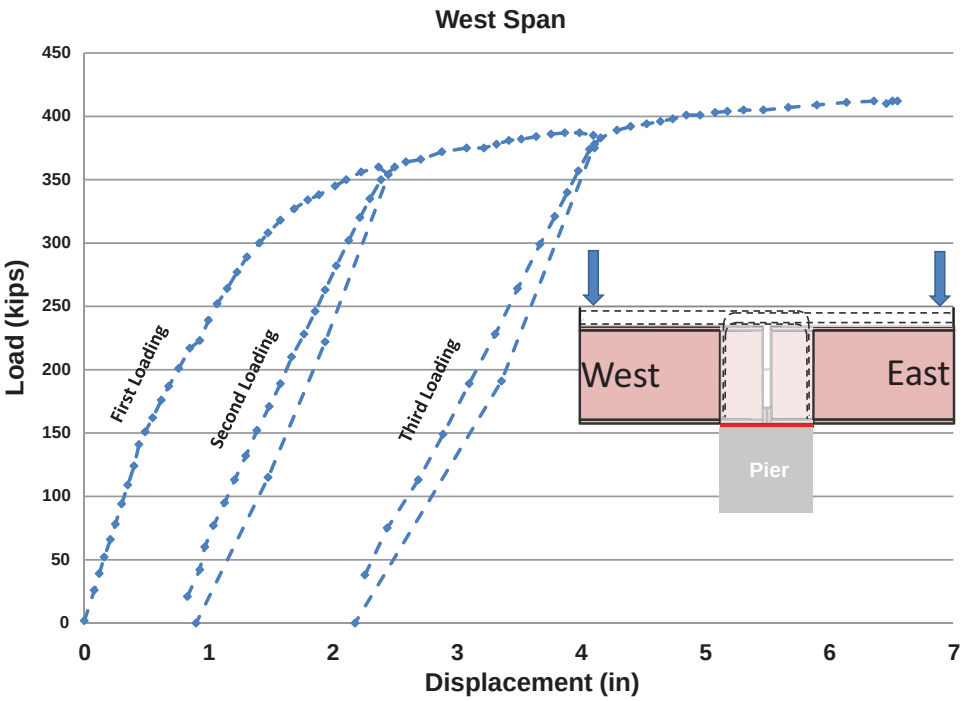

Fig. 12. Load displacement (west side).

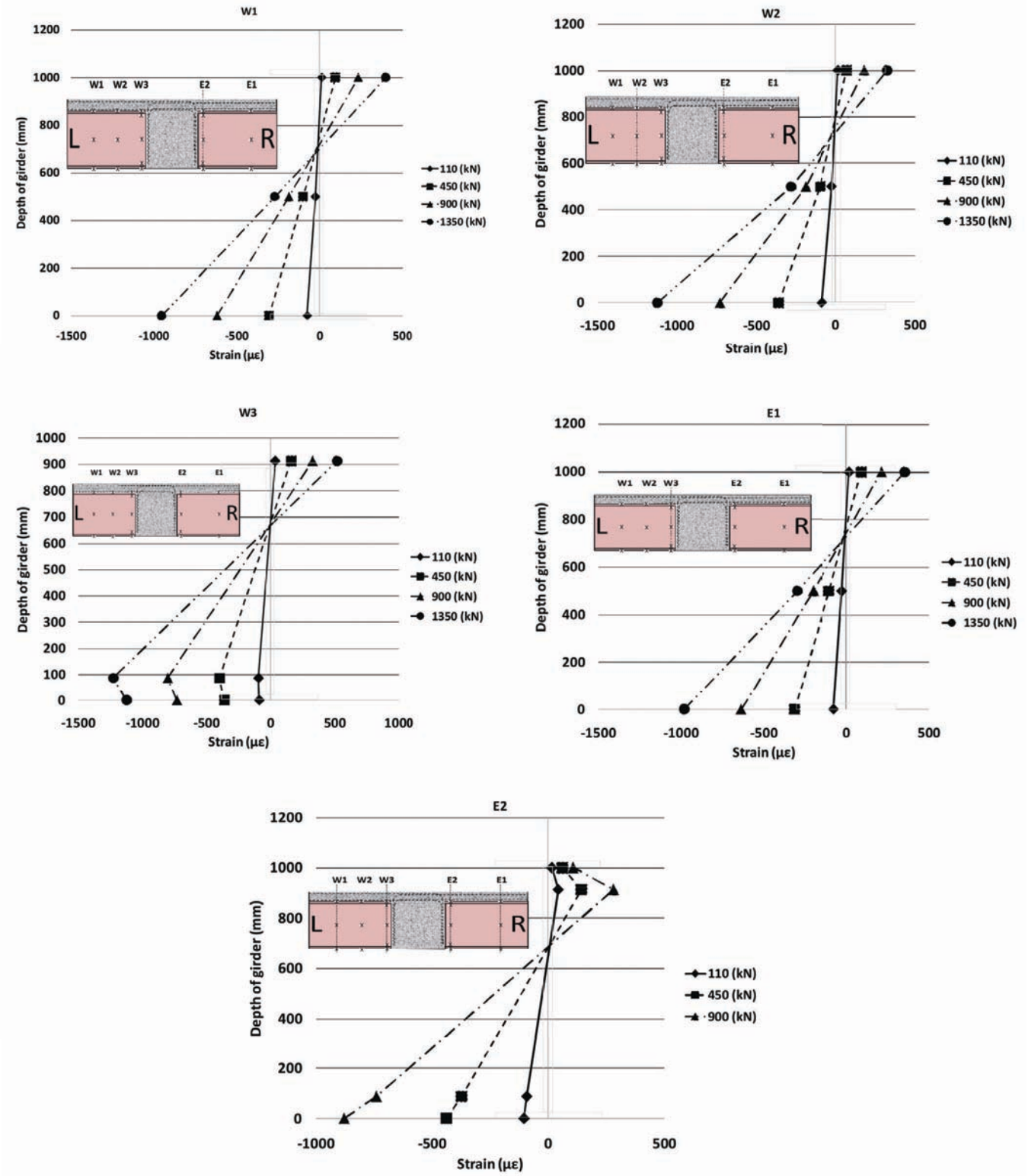

Fig. 13. Strain profile along the depth of the girder (W1, W2, W3, E1, E2) during ultimate load test.

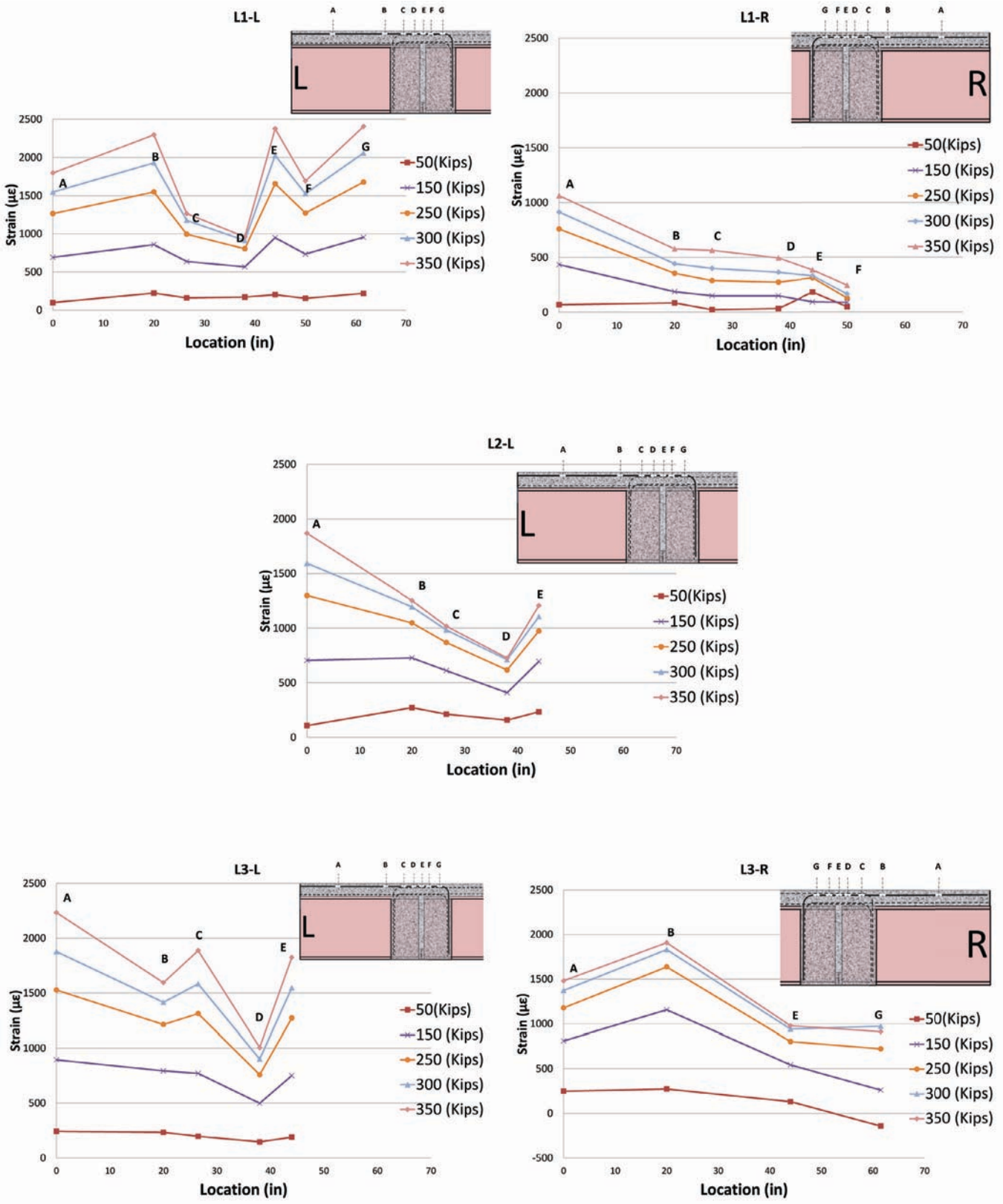

Fig. 14. Strain variation along the longitudinal bars (L1-L, L1-R, L2-L, L3-L, L3-R) during ultimate load test.

transverse positions. Because the bars are not continuous, each longitudinal rebar belongs to either the right or the left side of the specimen, which is indicated in the figure. Each figure is also denoted with a name such as L1, which corresponds to the bar location as shown in Figure 4. The strain variation observed in Figure 4 indicates that in general the strain decreases toward the hook end of each reinforcing bar developed using hooked end and splice. This behavior is mainly because the reinforcing bars over the pier are developed by splicing. This is a typical variation of strain over splice region (Azizinamini et al., 1999).

Separation at Centerline of Connection

A crack meter was installed between the girders to measure the separation during ultimate load. Figure 15 shows the displacement versus loading. As can be seen, no significant displacement was measured for loading up to 150 kips. A displacement equal to 0.2 in. was observed at the ultimate load.

Concrete Strain Variation in Diaphragm

The concrete strain variation in the region below the neutral axis and close to the steel blocks was monitored. Figure 16 shows the strain variation along the depth of the girder next to the web. The results show that there was no considerable strain at all monitored locations prior to 70 kips of applied load. Increasing the load beyond this value, the concrete began to exhibit some compressive strains in the lower region of the diaphragm. However, the gages indicate that the strains remained low, meaning the concrete was not significantly involved in the force transfer mechanism of this connection. For the most part, the compression force from one girder to another is transferred through the steel blocks welded to bottom portions of each girder.

Visual Inspection after Test Completion

Crack development was documented during the ultimate load test. The observation reported herein corresponds to condition of the test specimen at the conclusion of the testing. As mentioned earlier, the maximum load-carrying capacity of the test specimen was achieved when the end displacement was about 7 in. (see Figures 11 and 12), while loading was continued until end displacement of about 13 in. was achieved. This additional loading, beyond maximum loading capacity of the test specimen, resulted in significant additional damage to the test specimen.

Figure 17 shows the cracks that developed at test conclusion. The near side in the photograph is toward the east, which sustained much more damage than the west. As soon as one side begins to fail, the load drops; the other side may then never experience the same amount of damage.

APPLICATION OF THE SYSTEM

After the successful experimental test, this connection was used in construction of the 262nd Street Bridge over I-80 near Ashland, Nebraska. This type of connection can be employed in several different ways in conjunction with modular bridge construction. The adjacent beam concept used in the 262nd Street Bridge is one such example. The adjacent box concept utilizes prefabricated units consisting of an individual steel box girder topped by a portion of deck slab. These units are prefabricated and then shipped to the job site. Once on site, the individual units are set into place on two supports adjacent to one another. A longitudinal deck closure strip between the individual units is then cast, thereby joining them together. At the same time, the concrete diaphragm over the middle pier is cast, joining the adjacent pre-topped girders. The middle concrete diaphragm connects the adjacent spans and provides continuity between the spans for subsequent live loads.

This bridge incorporates several innovative concepts. The bridge uses a modular pre-topped steel box girder system, which allows much of the construction process to be performed prior to placing the girders. The bridge incorporates the simple for dead–continuous for live load system. The individual girders are simply supported while the pre-topped deck is placed. Once in place, the modular units are joined together such that resulting system is continuous for live load. The steel box girders utilize high-performance steel (HPS 70W) in a hybrid configuration, 70-ksi steel in the bottom flange and 50-ksi steel in the top flanges and webs. The use of high-performance steel combined with the simple for dead–continuous for live load system eliminates the need for section transitions through the length of the structure and uses constant cross-section throughout the length of the girders.

Figure 18 shows the cross-section of the bridge used for the 262nd Street Bridge. It consists of three pre-topped girders with vertical webs and two closure-pour regions, each 12 in. wide. The bottom flanges of the girder utilized 70-ksi high-performance steel with webs and top flanges using 50 ksi-steel.

Pre-topping the girder was performed on site, away from the final position of the girder. However, an alternative would be to pre-top the girder prior to shipping the girder to site. Figure 19 shows the layout of the pre-topped girder units.

Figure 20 shows the forming and casting of the deck for the pre-topped girders used for the 262nd Street Bridge, prior to placing them over the support.

A means was provided for lifting the pre-topped girders and placing them over the supports. Figure 21 shows the method used for lifting the pre-topped girders and placing them into their final positions; Figure 22 shows the lifting

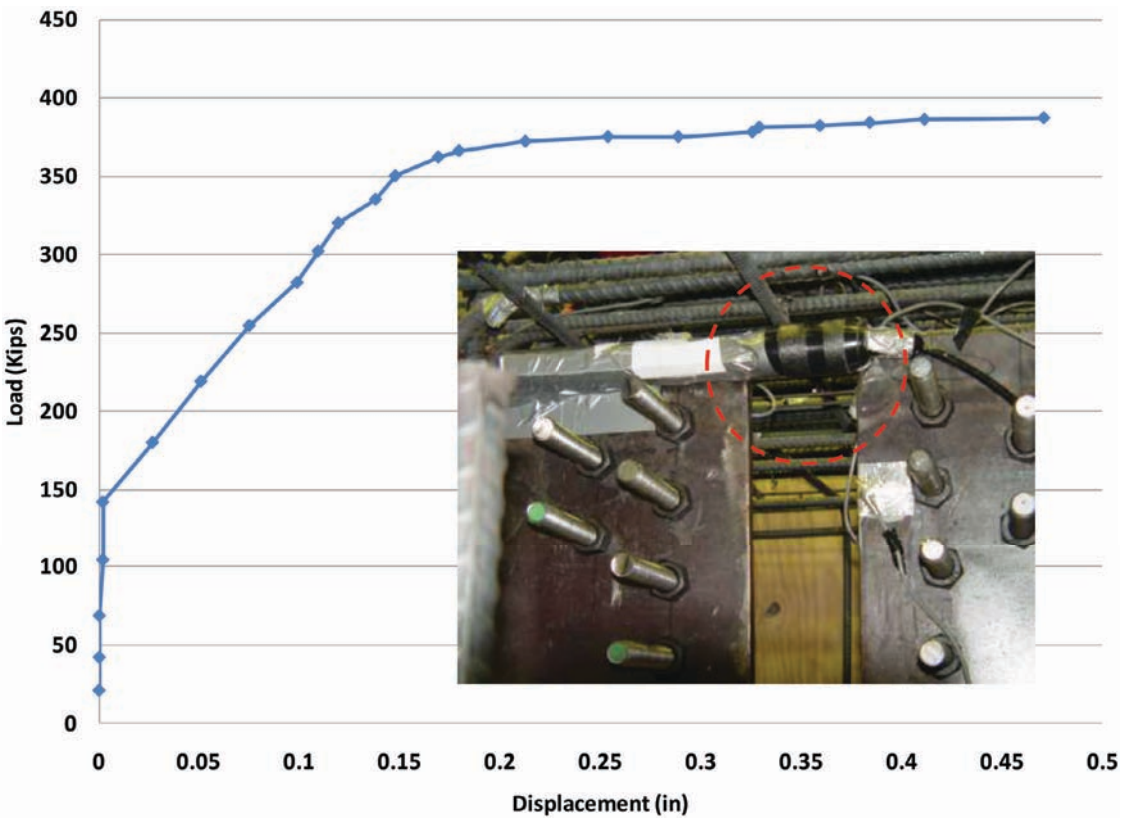

Fig. 15. Top flange separation.

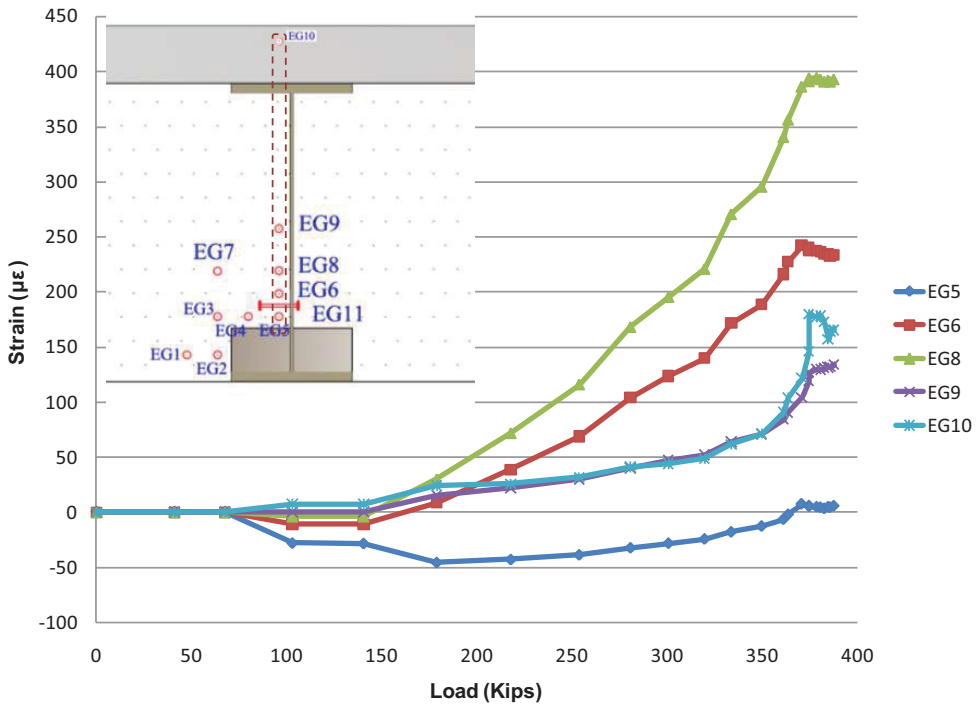

Fig. 16. Strain variation at concrete in vicinity of the steel blocks and web inside the diaphragm.

Fig. 17. Photo of specimen after conclusion of test.

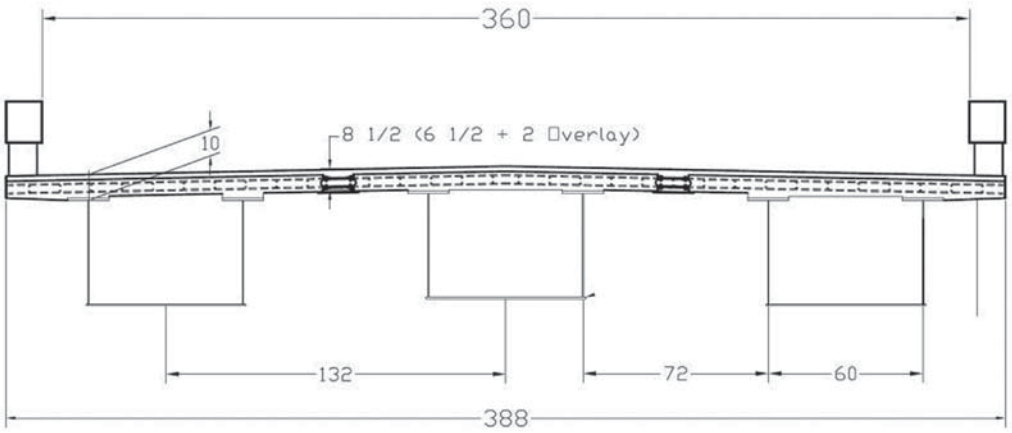

Fig. 18. Bridge cross-section consisting of three box girders.

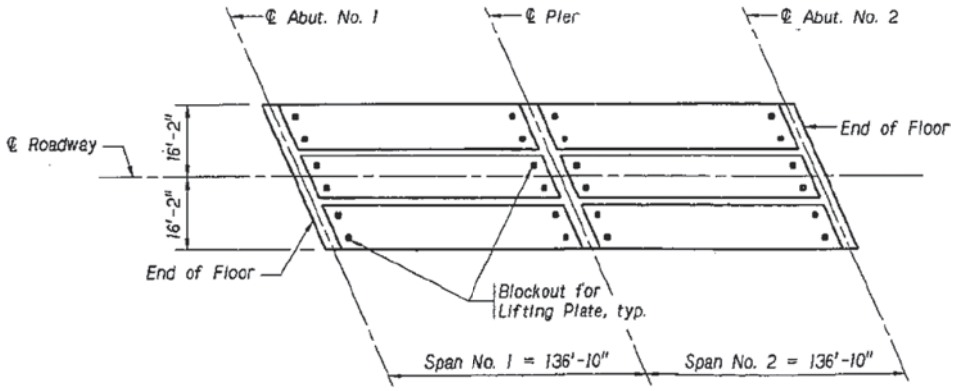

Fig. 19. Spanning and girder unit arrangement.

(a)

(b)

Fig. 20. Preparation of girder units for pre-topping operation: (a) forming; (b) reinforcement.

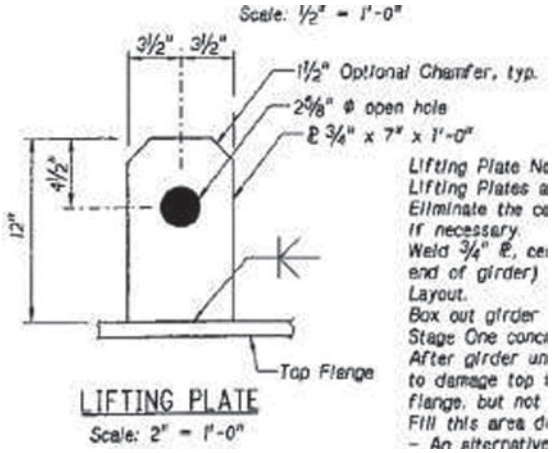

Fig. 21. Lifting of a single pre-topped girder for the 262nd Street Bridge.

Fig. 22. Second girder in second span of the 262nd Street Bridge.

operation of one of the girders, which was achieved using two cranes.

Adjacent girders have transverse reinforcement that extends beyond the slab edges. The adjacent pre-topped girders are connected through longitudinal closure pours. Figure 23 shows the alternative used for connecting the adjacent girders for the 262nd Street Bridge. The alternative shown in Figure 23, developed by the University of Texas (Thompson et al., 2003), consists of headed bars, which can provide development of the bars in short distances of only 8 in. Alternatively, ultra-high-performance concrete and regular reinforcing bars could be used in the longitudinal joint regions.

The chosen closure pour width was 12 in. Figure 24 shows the details of the closure pour and reinforcement. The detail over the pier used the detail described earlier in this paper (see Figures 1 and 2).

The sequence of completing the construction of the bridge depends on the depth of the pre-topped deck. There are two main alternatives. The pre-topped deck could be full or partial depth. The partial-depth alternative is attractive from the viewpoint of ensuring that the finished deck has the desired profile. When the partial-depth option is used, the construction sequence after placing the pre-topped deck units consists of casting the closure pour, casting the railing and finally placing the overlay. Because the 262nd Street Bridge was the first application where a modular steel bridge system was used incorporating several new ideas, the partial-deck option was selected as precautionary measure to allow minor adjustment, if needed. Figure 25 shows the view of

Fig. 23. Headed bar detail.

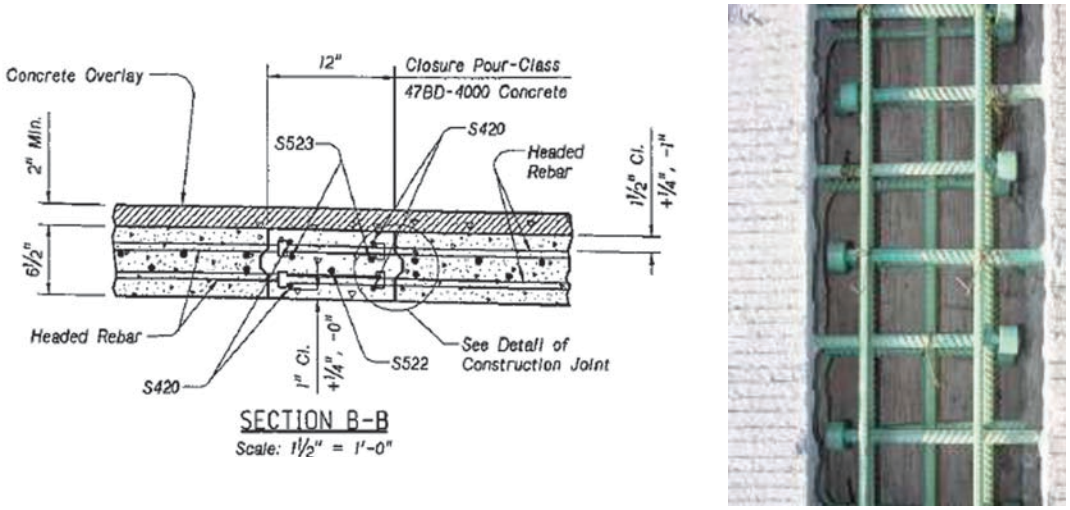

Fig. 24. Closure region details.

the 262nd Street Bridge after all of the pre-topped girders had been placed. The remaining operations were to cast the closure regions and then to apply the silica fume overlay.

MONITORING DATA

The instrumentation and monitoring of the 262nd Street Bridge was much more modest than the two previously reported bridge construction projects using the conventional SDCL system (Yakel and Azizinamini, 2014). With the basic performance of the SDCL system having been demonstrated, the focus was on the closure region performance. Figure 26 shows the representative instrumentation placed in the closure region. Additional gages were attached to the steel girders at the same location as the closure-pour instrumentation.

Figures 27 and 28 show the strain values obtained from the gages shown in Figure 26 both during the first 8 days of monitoring and also the full 21-month, long-term monitoring period. The results obtained indicate that the range of data is very limited, with no one gage showing a short-term variation greater than 100 με. The seasonal variation is also on the order of 100 με. These values are quite insignificant and indicate that the closure-pour region of the structure is not undergoing any long-term changes.

SUMMARY AND CONCLUSIONS

This paper presents a connection for use over the interior support of a continuous structure capable of extending the application of the simple for dead–continuous for live load steel bridge system (SDCL) to the case of accelerated bridge construction. The detail is intended to provide for use of the SDCL steel bridge system in conjunction with span-by-span construction of an adjacent pre-topped girder system. An experimental investigation was carried out to comprehend its performance followed by a field application, which was monitored for period of about 2 years.

The experimental investigation first examined the behavior of the detail under cyclic service-level loading. The performance of the connection was very good during the cyclic test. A 4% reduction of the connection stiffness was observed after simulating 100 years of truck traffic. This exceeds the typical design life of 70 years as specified by the AASHTO *LRFD Bridge Design Specifications* (2007). Specific observations through the testing include:

- Crack propagation was negligible through the cyclic test.
- No considerable change in the amount of strain in the longitudinal reinforcement was observed.

Fig. 25. Before casting the closure regions.

These observations demonstrate the capability of the system to develop the continuity reinforcement over the pier and maintain its integrity for 100 years of service life.

Following completion of the cyclic loading, the detail was monotonically loaded to failure. Specific observations made during the ultimate load test include:

- The connection displayed linear behavior until the applied load was sufficient to cause yielding of the longitudinal reinforcement.
- The connection reached its ultimate capacity after full yielding of longitudinal reinforcement had occurred.
- After yield, the connection demonstrated large displacement ductility before failure.

Further, examination of sensor data obtained from full-scale test indicated:

- The main element of the connection resisting the compression force was the steel block welded to the bottom portion of the end bearing plate.
- The contribution of the concrete in the vicinity of the steel block was small.
- The main element of the connection detail resisting the tension was the longitudinal continuity reinforcement within the deck.
- The connection failure coincided with tensile yielding of all longitudinal reinforcement within the full width of the deck.

The presented detail was used in the construction of the 262nd Street Bridge over I-80, near Ashland, Nebraska, which opened to traffic in October 2009. This bridge utilized adjacent, pre-topped, steel box-girders and the SDCL bridge system. The bridge consisted of two spans of three pre-topped steel-box units placed side by side. The side-by-side girders were connected using a longitudinal closure pour that developed headed reinforcement from the adjacent girders. The span-to-span connection over the pier was made using the details presented in this paper. After construction, the behavior of the structure was monitored continuously for a period of approximately 2 years, during which time it was observed that the behavior of the structure was essentially uniform, with only small seasonal fluctuations.

Based on the results of the experimental investigation and field trial, the SDCL steel bridge system using pre-topped adjacent girder units and the presented detail provide an economical and practical alternative bridge system suitable for accelerated bridge construction applications.

Fig. 26. Strain gages of closure in region 1.

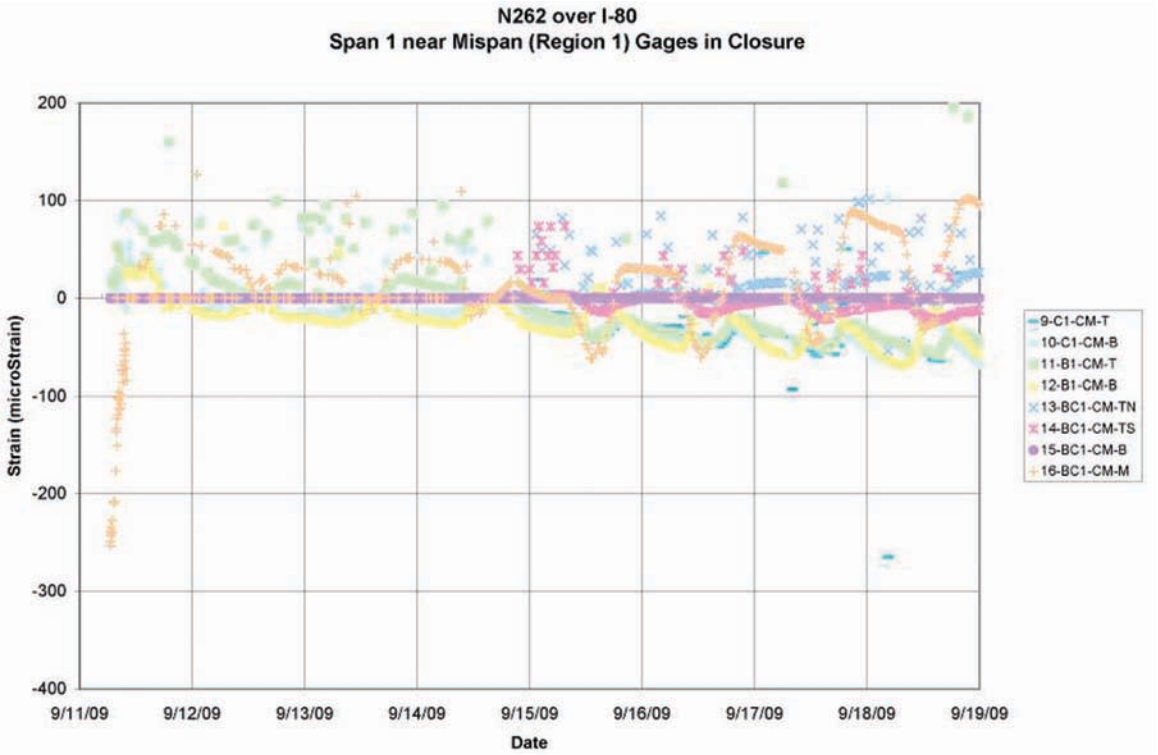

Fig. 27. Region 1 strains from closure gages (first 8 days).

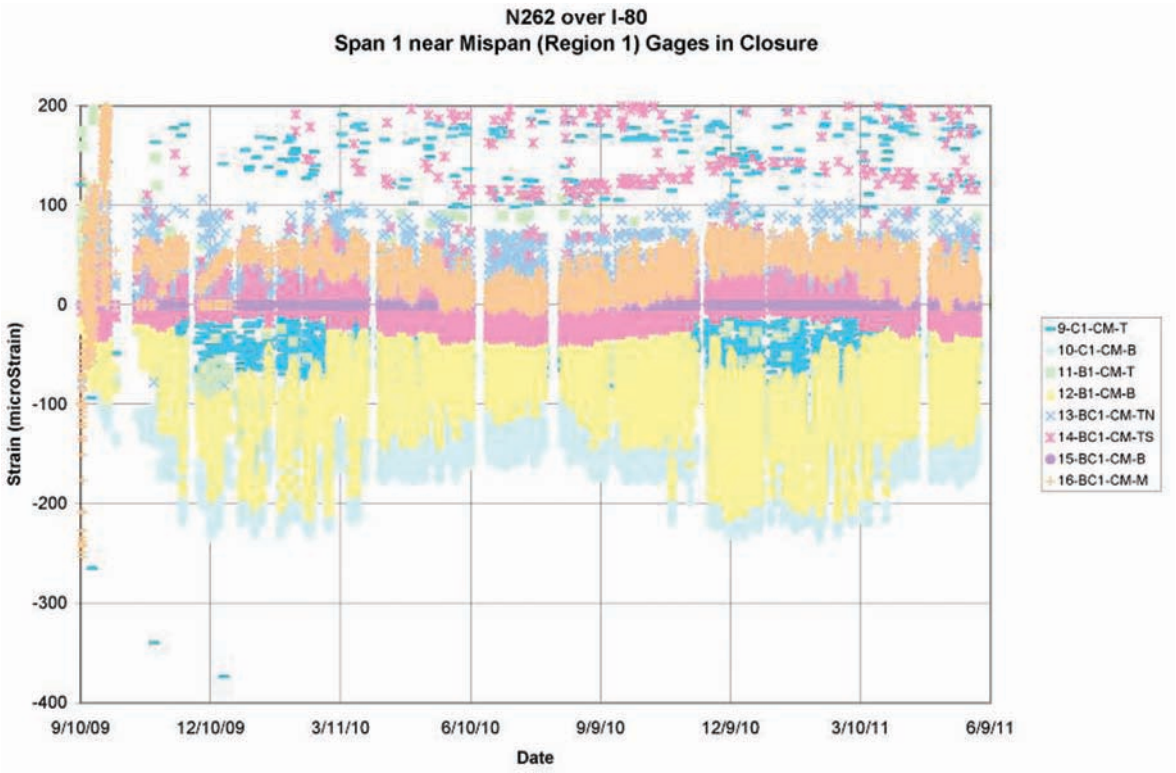

Fig. 28. Region 1 strains from closure gages (21 months).

ACKNOWLEDGMENTS

This paper presents details of a major undertaking to develop an economical steel bridge system. The investigation was directed by Dr. Atorod Azizinamini, Professor and Chair at Florida International University, and was made possible by contributions from many current and former graduate students and research associates, as well as input from many in the bridge community. In particular, the contributions of the following individuals are acknowledged.

Graduate students earning degrees from the project were Nick Lampe, Nazanin Mahasebi, Reza Farimani, Saeed Javidi, Derek Kowalski and Mark Otte. The research study was conducted at the University of Nebraska–Lincoln. Dr. Aaron Yakel was the research associate assisting the project. Laboratory technicians Jeff Boettcher, John Dageford, and Peter Hilsabeck assisted in conducting the experimental portion of the study. Graduate students who assisted with experimental testing include John Swendroski, J. Brian Hash, Patrick Mans, Luke Glaser and Nima Ala. The study was supported by the Federal Highway Administration and the Nebraska Department of Roads (NDOR). Several visionary engineers at NDOR were critical to the successful completion of the project: Mr. Lyman Freeman, Mr. Moe Jamshdi and Mr. Hussam "Sam" Fallaha. Steel fabrication and assistance during specimen preparation was provided by Capitol Contractors of Lincoln, Nebraska.

The opinions and conclusions presented in this paper are those of the authors and do not necessarily represent the viewpoints of the project sponsors.

REFERENCES

AASHTO (2007), *LRFD Bridge Design Specifications*, 4th ed., American Association of State Highway and Transportation Officials, Washington, DC.

Azizinamini, A. (2014), "Simple for Dead Load–Continuous for Live Load Steel Bridge Systems," AISC, *Engineering Journal*, Second Quarter, pp. 59–81.

Azizinamini, A., Lampe, N.J. and Yakel, A.J. (2003), *Toward Development of a Steel Bridge System—Simple for Dead Load and Continuous for Live Load*, A Final Report Submitted to the Nebraska Department of Roads, National Bridge Research Organization: http://www.nlc.state.ne.us/epubs/r6000/b016.0088-2003.pdf.

Azizinamini, A., Pavel, R., Hatfield, E., Ghosh, S.K. (1999), "Behavior of Lap-Spliced Reinforcing Bars Embedded in High-Strength Concrete," *ACI Structural Journal*, September–October, pp 826–835.

Azizinamini, A., Yakel, A.J., Lampe N.J., Mossahebi, N. and Otte, M. (2005), *Development of a Steel Bridge System—Simple for Dead Load and Continuous for Live Load, Volume 2: Experimental Results*, Final Report NDOR P542, Nebraska Department of Roads, Lincoln, NE, November.

Farimani, M.R., Javidi, S.N., Kowalski, D.T., Azizinamini, A. (2014), "Numerical Analysis and Design Provision Development for the Simple for Dead Load–Continuous for Live Load Steel Bridge System," AISC, *Engineering Journal*, Second Quarter, pp. 109–126.

Lampe, N.J., Mossahebi, N., Yakel, A.J., Farimani, M.R., and Azizinamini, A. (2014), "Development and Experimental Testing of Connections for the Simple for Dead Load–Continuous for Live Load Steel Bridge System," AISC, *Engineering Journal*, Second Quarter, pp. 83–108.

Szerszen, M.M. and Nowak, A. (2000), "Fatigue Evaluation of Steel and Concrete Bridges," *Transportation Research Record,* 1696.

Thompson, M.K., Ledesma, A.L., Jirsa, J.O., Breen, J.E. and Klingner, R.E. (2003), *Anchorage Behavior of Headed Reinforcement,* Center for Transportation Research Report 1855-3, Austin, Texas, May.

Yakel, A. J., and Azizinamini, A. (2014), "Field Application Case Studies and Long Term Monitoring of Bridges Utilizing the Simple for Dead–Continuous for Live Bridge System," *Engineering Journal*, AISC, Third Quarter, pp. 155–175.

Existing Simple Steel Spans Made Continuous: A Retrofit Scheme for the I-476 Bridge over the Schuylkill River

DANIEL GRIFFITH and JOHN A. MILIUS

Abstract

The rehabilitation of the SR 476 Bridge over the Schuylkill River near Philadelphia, Pennsylvania, converted existing steel multigirder simple spans into three- and four-span continuous units. Employing a design method typically used for construction of new simple-span-made-continuous (SSMC) steel girder bridges, it is believed to be the first bridge rehabilitation project in Pennsylvania to use such a scheme. The rehabilitation design upgraded load capacity of the girders to meet current LRFD code requirements. The SSMC design, coupled with other deck joint elimination techniques, was able to reduce the combined number of deck joints on the northbound and southbound structures from 25 to 8. With nearly all previous steel deterioration occurring at deck joints, this substantial reduction in deck joints will aid in extending the remaining life of the bridge. This paper will illustrate the construction methods employed for conversion of the bridge from multiple simple spans to continuous spans. The paper will also provide detailed insight into the many design requirements for this structural conversion, from substructure retrofits and sequential bearing replacements to superstructure continuity and full-depth concrete diaphragm details.

Keywords: simple-span-made-continuous (SSMC), bridge rehabilitation, modified fixity conditions, steel wedge plates, bolted steel splice plates, full-depth concrete diaphragm, staged construction, sequential bearing replacement, steel bolsters.

INTRODUCTION

AECOM was tasked by the Pennsylvania Department of Transportation (PENNDOT) District 6-0 to perform the rehabilitation design for the Schuylkill River Bridge (Figure 1) as part of the SR 476, Section RES Project. The bridge rehabilitation included the removal of the existing noncomposite concrete deck and replacement with a new composite concrete deck (see Figure 2). The rehabilitation also included the repainting of all structural steel and structural steel repairs required to upgrade the structure to meet current design code requirements. The rehabilitation of the southern approach spans of both the northbound and southbound structures is the focus of this paper.

DESIGN REQUIREMENTS

PENNDOT District 6-0 requested that AECOM investigate eliminating deck joints by providing continuity in the steel multistringer approach spans on the northbound and southbound structures. Several state bridge departments have begun utilizing SSMC construction techniques for new steel bridges over the past several years. The techniques were developed in an effort to make medium-span (100-ft to 140-ft) steel bridge designs cost competitive against prestressed concrete simple-made-continuous bridges. The cost advantage for SSMC construction is often realized in the speed and simplicity of girder erection (Azizinamini, 2004; Talbot, 2005; NSBA, 2006).

The techniques developed simplify the formation of continuous structures by eliminating the need for conventional bolted field splices, but also work to improve structural efficiency and long-term durability as compared to simple-span construction with numerous deck joints. While the SSMC concept has been used for the design of new steel bridges, its use as a rehabilitation strategy is a relatively new concept to the bridge industry. While the concepts may appear to be relatively simple on the surface, numerous design checks were required to accomplish this bridge rehabilitation scheme.

SUBSTRUCTURE ANALYSIS AND REVISED FIXITY CONSIDERATIONS

The first step in assessing the feasibility of making the simple-span approach spans continuous was to perform an analysis of the existing substructures and foundations to determine their capacity to resist the new loading and fixity conditions created by making the simple spans continuous.

The southern approach spans for the northbound bridge include three 119-ft simple spans, and the southbound

Daniel Griffith, P.E., Senior Project Engineer, AECOM, Philadelphia, PA (corresponding). E-mail: daniel.griffith@aecom.com

John A. Milius, P.E., Structures Department Manager, AECOM, Philadelphia, PA. E-mail: john.milius@aecom.com

southern approach spans include four 103-ft simple spans in their existing configuration (see Figure 3). In an effort to eliminate as many deck joints as possible, AECOM began by investigating a four-span-continuous unit and a three-span-continuous unit for the southbound and northbound approach spans, respectively. In each case, an arrangement that restrained the superstructure in the longitudinal direction at a single "fixed" pier was analyzed: pier 1 southbound and pier 1 northbound. Note that pier 1 southbound is actually the second interior support within the southernmost proposed four-span unit.

Analysis of the existing piers and foundations was

Fig. 1. I-476 northbound and southbound over the Schuylkill River.

Fig. 2. Approach spans: seven-stringer cross-section during half-width redecking.

performed using AASHTO design criteria (AASHTO, 2004). Seismic analysis and retrofits were not part of the scope of this project; therefore, load cases III through VI were the critical load combinations for verifying the structural adequacy of the existing piers under the new proposed loading conditions. Continuity resulted in redistributed longitudinal braking forces to the fixed piers and new thermal loading conditions to all of the substructure units. These increased longitudinal forces, combined with increased vertical loads at the interior supports of the continuous units, were used for the analysis of the existing piers.

Analysis of the piers proved to be an iterative process between bearing design and pier analysis. Because the proposed northbound fixed pier was not centered within its multispan unit, unequal thermal forces induced at the ahead-station and back-station expansion bearings were resolved at the fixed pier. Elastomeric bearings were designed for all of the supports along the three-span northbound unit. In order to reduce the thermal forces to an acceptable level at the fixed piers, low friction bearings were provided at pier 3 northbound. Elastomeric bearings equipped with PTFE/stainless steel sliding surfaces were utilized for this application. Standard reinforced elastomeric bearings were designed for the remaining substructure units. Once the bearings were designed, substructure analysis was then begun; the analysis demonstrated that the existing substructures and foundations could support the new load conditions.

STEEL STRINGER ANALYSIS AND CONTINUITY DESIGN

The analysis of the existing stringers and the continuity design also required a multistep process. The first step included investigating various alternatives for continuity details over the interior supports for the bridge rehabilitation project. The design requirements associated with making simple steel beams continuous are similar to the design requirements associated with field-splice design—moments and shears must be carried through the detail. The SSMC design must ensure that forces can be adequately carried through the joint without overstressing elements, particularly the concrete elements. Three alternatives for achieving these design requirements were investigated.

The first alternative investigated a Colorado Department of Transportation detail. In this detail, the compressive forces in the stringer bottom flanges are taken by two mated trapezoidal plates, called wedge plates, through the joint between the bottom flanges of the two adjacent beams (see Figure 4). The wedge plates are at least the thickness of the stringer bottom flanges and are installed in the gap to

Fig. 3. Southbound approach spans: existing simple-span condition.

provide a tight fit connection between the bottom compression flanges of the adjacent-span stringers. As dead loads are added to the bridge, bottom flange compression is transmitted through the wedge plates, locking the system in place and establishing a continuous steel bottom flange.

The longitudinal reinforcing bars in the deck slab are then designed to take the tensile forces, similar to the practice used for prestressed concrete bridges designed for continuity. If additional tensile capacity is required, a bolted top flange plate joining the adjacent beams is provided. For this detail, the deck slab must be designed to carry any net shear force across the gap in the beams. The net shear force is any shear that is not directly transferred from the webs of the steel girders into the bearings.

The second alternative was a variation of a continuity detail used by the Tennessee and Nebraska Departments of Transportation. The detail is similar to alternative 1, but includes the addition of a full-depth concrete diaphragm closing the open gap between the webs of the two adjacent stringers. The concrete diaphragm aids in providing additional rigidity in the detail, as well as transferring net shear through the joint. Similar to alternative 1, steel wedge plates are installed between the bottom compressive flanges of the adjacent beams. The thickness of the wedge plates is sized to carry the steel-beam, bottom-flange compression. The wedge plates also serve to minimize compressive stress in the concrete diaphragm, thereby preventing crushing of the concrete between the girders. Similar to alternative 1, the longitudinal reinforcing bars in the deck slab, or a bolted top flange plate, would be designed to transfer the tensile force through the continuity detail.

The third alternative considered the use of steel flange and web connection plates to splice over the gap, similar to a conventional steel-field splice. This alternative would require a large number of field-drilled bolt holes, making this alternative very labor intensive and cost prohibitive. This alternative would also require the removal and replacement of the existing bearing stiffeners. The fact that the existing girders are kinked at the centerline of the interior supports would only add to the cost of fabricating and installing this continuity detail alternative. For these reasons, this alternative was eliminated from the investigation early on in the design process.

Based on the results of the alternatives study, AECOM proposed alternative 2 as the continuity detail for final design. Alternative 2 was ultimately selected by PENNDOT due to the inclusion of a full-depth concrete diaphragm, particularly for ensuring the long-term durability and structural performance for this interstate highway bridge. See Figure 5.

Once the continuity detail was selected, the next step in the superstructure design was to analyze the existing stringers for the SSMC condition. This analysis was performed

Fig. 4. Wedge plates between bottom flanges of adjacent-span stringers (Section RES construction photo).

by superimposing noncomposite moments and shears with composite dead load and live load moments and shears. The results of our analysis showed that the stringer flanges alone were inadequate to support negative moments over the interior supports.

The stringers—noncomposite in their existing condition—are proposed to be composite as part of the bridge rehabilitation. The composite girders provided ample positive moment capacity but were insufficient in the negative moment region for the proposed loading condition. AECOM, therefore, proposed the installation of a bottom-flange cover plate between the bottom flange of the existing stringers and new bearing assemblies.

The design for this project required that a top-flange splice plate be used with the longitudinal reinforcing bars in the deck slab to transfer the tensile forces through the continuity detail. The top-flange splice plate used a single-shear, bolted connection to join the stringer from the adjacent span. Similar to the bottom-flange cover plates, the top-flange splice plates were extended as required to function as bolted cover plates. The detailing of the flange splice plates required another unique design for this project. The approach spans lie within a curved horizontal alignment, with the existing straight stringers chorded to frame the stringer around the curve. The chorded framing results in the stringers having a slight kink at their interior supports. In an effort to reduce fabrication costs, the splice plates were detailed as oversized rectangular plates with skewed lines of bolts, eliminating the need for fabrication of unique splice plates for each stringer support location, as shown in Figure 6.

The final continuity elements designed were the full-depth concrete diaphragms over the piers. A combination of transverse reinforcing steel passing through field drilled holes in the girder webs and shear studs welded to each side of the webs provided the way of locking the full-depth diaphragm and stringer together, enhancing continuity, as well as providing the means for transferring shear through the joint, as shown in Figure 7.

BEARING REPLACEMENT

Another unique aspect of this SSMC rehabilitation design was determining the feasibility of bearing replacement, particularly for staged deck reconstruction. This rehabilitation involved half-width re-decking for each direction. The construction specifications required the contractor to replace all bearings prior to first stage deck demolition. This requirement was so that all bearings along any given bearing line would all have the same capacities for load, translation and rotation.

Fig. 5. Formwork for full-depth concrete diaphragm (Section RES construction photo).

Fig. 6. Bottom-flange cover plate with skewed bolt lines.

Fig. 7. Reinforcing and shear studs on stringer webs for full-depth concrete diaphragm.

Another important design consideration is the sequence in which the bearings are replaced. The designer must consider temporary construction conditions, such as the changes in fixity conditions and thermal movement range for the new and existing bearings during sequential replacement of all the bearings within the multispan units, and the contract documents need to include a scheme outlining the order in which each support line would be replaced. This scheme ensured that all bearings would stay within their functional range for stresses and thermal translation during each step of replacement, as shown in Figure 8.

Steel bolsters were designed to maintain the same girder profile as the structure transitions from high-profile rocker bearings to elastomeric bearings, as shown in Figure 9. The use of steel bolsters was selected over reconstruction of the concrete bearing pedestals, enabling the contractor to replace all seven bearings within a given line in one overnight bridge jacking operation.

Steel bolsters also provided an efficient means for transitioning from two bearing lines to one bearing line at interior supports of the multispan units, while maintaining traffic over the structure during construction. The bolsters were designed for upward reactions from the new bearings, as well as for maximum downward shear from each side of the new interior support. This design was accomplished by detailing the steel bolsters to transmit bearing reaction from the new elastomeric bearing into the girder's existing bearing stiffeners. The bolster was also designed to transmit maximum shear forces from the existing girder-bearing stiffeners (offset from the centerline of the new bearing) into the new bearings, as shown in Figure 10.

CONCLUSIONS

The rehabilitation of the SR 476 Bridge over the Schuylkill River near Philadelphia, Pennsylvania, converted existing steel multigirder simple spans into three- and four-span-continuous units. Employing a design method typically used for construction of new SSMC steel girder bridges, this rehabilitation design upgraded load capacity of the girders to meet current LRFD code requirements.

The SSMC design, coupled with other deck joint elimination techniques, was also able to reduce the combined number of deck joints on the northbound and southbound structures from 25 to 8, as shown in Figures 11 and 12. With nearly all previous steel deterioration occurring at deck joints, this substantial reduction in deck joints will work to significantly extend the remaining life of the bridge.

Fig. 8. Jacking and temporary support of bridge for bearing replacement.

Fig. 9. Elastomeric bearings with steel bolsters.

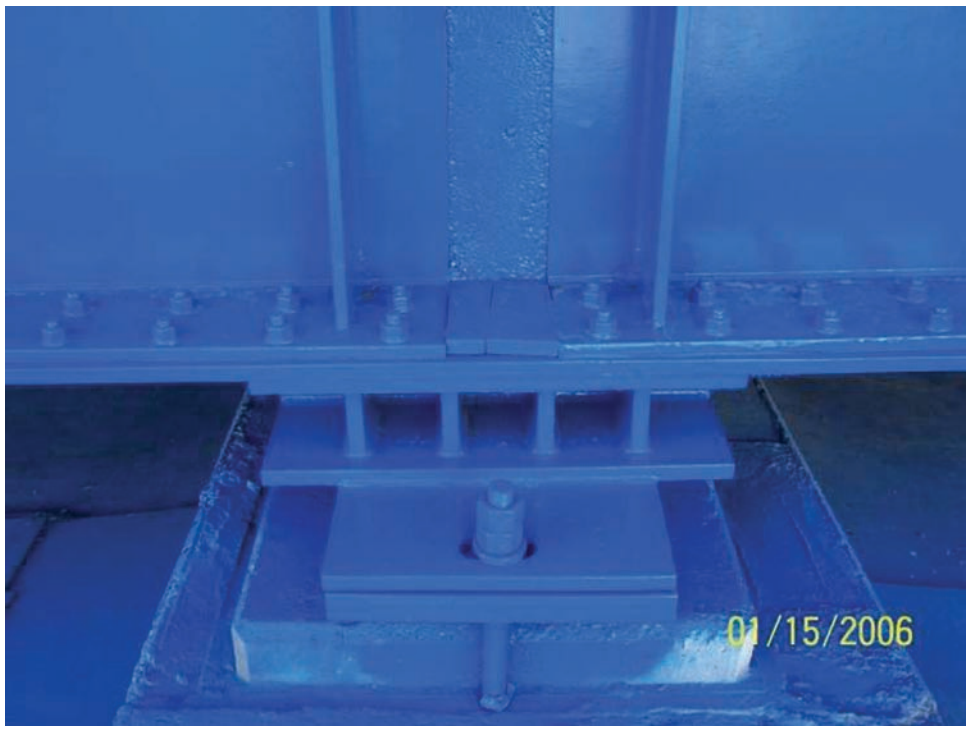

Fig. 10. Bolsters and concrete diaphragms transmit reactions to bearings.

Fig. 11. Completed northbound three-span structure.

Fig. 12. Reduced number of deck joints.

ACKNOWLEDGMENTS

The authors are grateful for the leadership of Tom Cushman of AECOM and Henry Berman and John Markus of PENNDOT District 6-0. Most importantly, the authors acknowledge all the project team members PENNDOT, AECOM and the contractor, J.D. Eckman; their efforts were essential for the success of this project.

REFERENCES

AASHTO (2004), *LRFD Bridge Design Specification*, 3rd ed., American Association of State Highway and Transportation Officials, Washington, DC.

Azizinamini, A. (October 2004), "Simple-Made-Continuous," *Steel Bridge News,* Vol. 5, No. 4, pp. 6–7, National Steel Bridge Alliance.

NSBA (September 2006), "Steel Bridge Uses Simple-Span-Made-Continuous Construction," *Steel Bridge News,* National Steel Bridge Alliance*, Modern Steel Construction*.

Talbot, J. (October 2005), "Simple Made Continuous," *Steel Bridge News,* Vol. 6, No. 4, pp. 1, 4–5, National Steel Bridge Alliance.

ERRATA

Elastic Buckling of a Column under Varying Axial Force

Paper by SURESH C. SHRIVASTAVA

(1st Quarter, 1980)

Equation 4 should be replaced with the following:

$$a_n = \alpha_n + \left(\frac{1}{2\pi}\right)\sin\left(2\pi\alpha_n\right)$$

$$b_n = \alpha_n + \left(\frac{1}{4\pi}\right)\sin\left(4\pi\alpha_n\right)$$

$$c_n = \left(\frac{1}{\pi}\right)\sin\left(\pi\alpha_n\right) + \left(\frac{1}{3\pi}\right)\sin\left(3\pi\alpha_n\right)$$

The table in the Numerical Example section on p. 20 should read as follows:

n	α_n	a_n	b_n	c_n	P_n kips	a_nP_n kips	b_nP_n kips	c_nP_n kips
1	1.0	1.0	1.0	0.0	–1.56	–1.560	–1.560	0.0
2	0.68	0.536	0.741	0.282	6.23	3.339	4.616	1.757
3	0.54	0.500	0.578	0.217	6.33	3.165	3.658	1.373
4	0.28	0.436	0.251	0.296	8.05	3.509	2.020	2.383
					19.05	8.453	8.734	5.513
					P_T	A	B	C

Equation 7 should be replaced with the following:

$$\frac{\pi^2 EI}{\lambda l^2} = 9.50$$

Finally, the buckling load factor, λ, should be 1.657.

GUIDE FOR AUTHORS

SCOPE: The ENGINEERING JOURNAL is dedicated to the improvement and advancement of steel construction. Its pages are open to all who wish to report on new developments or techniques in steel design, research, the design and/or construction of new projects, steel fabrication methods, or new products of significance to the uses of steel in construction. Only original papers should be submitted.

GENERAL: Papers intended for publication may be submitted by mail to the Editor, Keith Grubb, ENGINEERING JOURNAL, AMERICAN INSTITUTE OF STEEL CONSTRUCTION, One East Wacker Drive, Suite 700, Chicago, IL, 60601, or by email to grubb@aisc.org.

The articles published in the *Engineering Journal* undergo peer review before publication for (1) originality of contribution; (2) technical value to the steel construction community; (3) proper credit to others working in the same area; (4) prior publication of the material; and (5) justification of the conclusion based on the report.

All papers within the scope outlined above will be reviewed by engineers selected from among AISC, industry, design firms, and universities. The standard review process includes outside review by an average of three reviewers, who are experts in their respective technical area, and volunteers in the program. Papers not accepted will not be returned to the author. Published papers become the property of the American Institute of Steel Construction and are protected by appropriate copyrights. No proofs will be sent to authors. Each author receives three copies of the issue in which his contribution appears.

MANUSCRIPT PREPARATION: Manuscripts must be provided in Microsoft Word format. Include a PDF with your submittal. View our complete author guidelines at **www.aisc.org/ej**.

There's always a solution in steel.

ENGINEERING JOURNAL
American Institute of Steel Construction
One East Wacker Drive, Suite 700
Chicago, IL 60601

312.670.2400 www.aisc.org